Vienna Doctoral Programme on Water Resource Systems

Doctoral Thesis

The estimation of source and flowpath dynamics of water and solutes in an Austrian headwater agricultural catchment

submitted in satisfaction of the requirements for the degree of
"Doctor of Science in Civil Engineering"

as part of the
Vienna Doctoral Programme on Water Resource Systems

by

MSc. Michael Exner-Kittridge
Franz Hochedlingergasse 17/16
1020 Vienna

Examiners

Ao.Univ.Prof. Dipl.-Ing. Dr.techn. Matthias Zessner
Institute for Water Quality, Resources and Wastemanagement
Technische Universität Wien

Univ.Prof. Dipl.-Ing. Dr.techn. Günter Blöschl
Institute for Hydraulic and Water Resource Engineering
Technische Universität Wien

Dr. Adrienne Clement, PhD
Department of Sanitary and Environmental Engineering
Budapest University of Technology and Economics

Vienna, February 2016

Abstract

The difficulty in reducing diffuse pollution is inherently due to the distributed nature of diffuse pollution as compared to clearly defined point sources like waste water treatment plants (WWTPs), but also because the nutrients that are stored in the soil and transmitted to the surface waters are controlled by many complicated and heterogeneous natural processes which is much more difficult to control as compared to WWTPs. By understanding the natural mechanisms that control the storage and transmittance of nutrients and the water that carries them in typical agricultural catchments, better nutrient transport models can be made and subsequently better solutions can be found to help reduce the discharge of nutrients from agricultural lands to surface waters. The goals of the thesis are to develop the methodology to measure and analyze the data associated with solute transport, to identify the source reservoirs and the flowpaths of water and solutes, and ultimately to develop a qualitative and quantitative understanding of the interacting source and flowpath dynamics in an Austrian headwater agricultural catchment.

With many flowpath inputs to the stream (e.g. tile drainages and springs) and some with little to no baseflow during periods of the year, the ability to continuously measure solute concentrations required a unique solution. In Chapter 2, a new device to house water monitoring devices is presented and successfully deployed in the Hydrologic Open Air Laboratory (HOAL) catchment. The device was called the Water Monitoring Enclosure (WME) and it ensures a minimum internal water level which ensures that the enclosed water monitoring devices remain submerged even when there is no flow into the WME. The limited diameter of the inflow pipe buffers the flow velocity within the WME as some devices are sensitive to dramatic changes in flow velocity. The WME also conveys sediment through the system to ensure that the aggregation of sediment would not interfere with the internal water monitoring devices.

Clearly visible point inputs to the stream can be directly measured using water monitoring devices, but the truly diffuse water that enters the stream via groundwater must be estimated in a more indirect way. The continuous exchange of stream water and groundwater requires a more advanced methodology to estimate the fluxes as well as the groundwater solute concentrations. Chapter 3 presents a new methodology to estimate the stream to groundwater fluxes and associated groundwater solute concentrations, and a comparison to existing methodologies. The newly developed method assumes that the inflowing and outflowing fluxes occur simultaneously and uniformly along the entire stream reach. Through the use of artificial stream simulations, the new method had

the highest performance compared to the other methods and that all methods produced significantly different results depending on the flux distribution assumptions.

In the HOAL catchment, baseflow contributes the majority of the water and solute load throughout the year. Nitrate concentration was found to be seasonally variable throughout the year with higher concentrations in the winter and spring periods. Chapter 4 specifically addresses the question of the seasonal variability of the nitrate concentration by analyzing the seasonal source and flowpath dynamics in addition to other seasonal biochemical explanations. The cause of the seasonal nitrate concentration was due to the alternating source aquifer contributions throughout the year with the deep aquifer typically contributing 75% of the water during the summer and 50% in the winter. The shallow aquifer supplied the vast majority of the nitrate load with the perennial tile drainages acting as the dominant flowpath to the stream for the shallow aquifer water.

Runoff events play an important role in the transport of many substances in addition to the water, but are significantly more difficult to estimate compared to baseflow due to additional processes that occur during runoff events. Using the developments from the work in the previous chapters, Chapter 5 determines the representative source and flowpath dynamics of water and solute load during runoff events in the HOAL. Two large runoff events contributed over 50% to the total event runoff flow and nitrate load. The shallow aquifer and the rain water contributed equally to the event flow and combined contributed over 80% of the total event runoff flow with the top soil contributing the remainder. Large runoff events had different source and hydrograph responses as compared to smaller events. Small events had little top soil water with most of the nitrate load originating from the shallow aquifer, while the large events had a significant contribution from the top soil water with the soil water and the shallow aquifer contributing equally to the nitrate load.

The thesis has advanced the knowledge of the source and flowpath dynamics of water and solutes in a typical Austrian headwater agricultural catchment. This thesis has improved the collection of solutes in headwater catchments, improved source separation models and associated analysis methods, and provided additional knowledge for the development of large comprehensive transport models which will better identify and target significant pollutant sources and flowpaths that contribute to pollutant loads of surface waters.

Acknowledgements

I would like to thank the Austrian Science Foundation for funding our work as part of the Vienna Doctoral Programme on Water Resource Systems (DK Plus W1219-N22).

I would like to show my great appreciation and respect for my supervisor, Prof. Matthias Zessner, who has always supported me and given me constructive feedback on my research over the years. He always found time for discussions of my research.

I would also like to deeply thank my colleagues in Petzenkirchen, especially Peter Strauss, Alexander Eder, and Carmen Krammer. Without their help amongst many others in Petzenkirchen, my research would have been much more difficult and without the joy I gained from their rich character.

I would like to give my appreciation to both Prof. Günter Blöschl and Prof. Alfred Paul Blaschke. Even with his very busy schedule, Prof. Blöschl always found time to discuss details of my research and my manuscripts. Even though not my direct supervisor for my PhD, Prof. Blaschke has frequently supported me both academically and morally which I greatly appreciate.

I would like to thank Ernis Saracevic very much for all of the time that he spent helping me with my research. I always enjoyed my discussions with Ernis and the insight that I gained from his practical knowledge.

I would also like to thank my colleagues at the TU Wien and especially Jose Luis Salinas for creating a healthy and stimulating work environment. I always enjoyed the interesting conversations amongst my peers. I also thoroughly enjoyed the social activities outside of work that provided the occasional respite from the daily grind.

Last but certainly not least, I would like to give my love to my parents and my wife for their steadfast and unconditional support and love both personally and academically.

Contents

List of Figures

List of Tables

Chapter 1

Introduction

Excessive discharges of nutrients to the aquatic environment have been found to adversely affect human health and aquatic ecosystems (*Romstad et al.*, 1997; *Walling et al.*, 2002). Mass algal blooms in rivers and lakes from an abundance of nitrogen and phosphorous can produce harmful toxins and encourage bacteria that subsequently reduce oxygen levels for fish stocks. This eutrophication of lakes, rivers, and coastal zones is currently one of the primary issues facing surface water environmental policy (*Clercq*, 2001). As the regulation and technology of point source pollution associated with waste water treatment plants (WWTPs) have been greatly improved over the last decades to promote the removal of nutrients, diffuse agricultural discharges have become the dominant source of excess nutrients entering surface waters.

Reducing diffuse pollution is inherently difficult due to the distributed nature of diffuse pollution as compared to clearly defined point sources like waste water treatment plants (WWTPs), but also because the nutrients that are stored in the soil and transmitted to the surface waters are controlled by many complicated and heterogeneous natural processes which is much more difficult to control as compared to WWTPs. By understanding the natural mechanisms that control the storage and transmittance of nutrients and the water that carries them in typical agricultural catchments, better nutrient transport models can be made and subsequently better solutions can be found to help reduce the discharge of nutrients from agricultural lands to surface waters. The research was carried out at the Hydrologic Open Air Laboratory (HOAL) which is a typical catchment of the prealpine area alongside the eastern Alps with intensive agriculture associated with the seasonality of rainfall, runoff, and drainage density (*Merz and Blöschl*, 2007).

The estimation of yearly baseflow in typical monitoring procedures of weekly or biweekly sampling can accurately estimate the cumulative water and solute loads. On the other hand, runoff events are both unpredictable in occurrence and in the flow and solute load response, and periodic sampling is not sufficient to accurately estimate the flow and solute loads (*Aulenbach*, 2013). Much work has been performed to optimize the sample collection for runoff events (*Aulenbach and Hooper*, 2006; *Aulenbach*, 2013), but for those who require a high temporal resolution in addition to longer monitoring programs

spanning months or years the costs for both the laboratory analyses and labor become prohibitive. In situ sensors for continuous monitoring have become increasingly popular within the last couple decades for both wastewater and non-wastewater applications (*Newman*, 2001; *Kaelin et al.*, 2008; *Kim et al.*, 2009; *Kestel et al.*, 2010). Hydrologists have been using similar devices for many decades to measure physical water parameters (i.e. water level, temperature, electrical conductivity, etc), and now with in situ ion sensitive electrodes (ISE) solute concentrations can be continuously monitored at a reasonable cost and accuracy. Water sensors require an adequate place to be installed to monitor a discharge point. This can be especially difficult in locations with low flows, steep gradients, and high sediment loads like tile drainages. In these circumstances, a special enclosure to house the water monitoring devices would be necessary to both ensure the proper functioning of the devices and representative measurements of the parameters.

Point flows like tile drainages can be measured directly using specialized water monitoring devices, but distributed diffuse inputs to streams like groundwater flow cannot be measured directly to obtain a representative aggregate estimate. Simple aggregate methods can be applied along a stream reach by measuring the upstream and downstream discharge and solute loads to estimate the amount of diffuse groundwater entering the stream. Although this may be a relatively simple procedure to accomplish, the assumption that all flow within a stream reach must be either flowing into the stream or flowing out of the stream is in many cases an over simplification (*Castro and Hornberger*, 1991; *Harvey and Bencala*, 1993). Depending on local topography, geology, and the groundwater table, gains and losses into and out of the stream can be very dynamic even over short distances (*Harvey and Bencala*, 1993; *Anderson et al.*, 2005; *Payn et al.*, 2009). There are a number of methods to estimate gross stream gains and losses from stream to groundwater exchange (SGE), but the usage of solute tracers provides a representative aggregate estimate of the SGE and the tracers themselves are inexpensive (*Kalbus et al.*, 2006). When tracers are applied during baseflow (i.e. steady-state) conditions, analytical methods can be used to analyze the collected flow and tracer concentration data, but certain assumptions about the spatial distribution of the gain and loss fluxes must be made. Several assumptions have been made in the past, but no study has determined which spatial distribution assumption is the most accurate and if a better assumption could be made.

With sufficient monitoring and estimates of the flowpaths entering the stream, questions arise regarding the cause of the seasonality of important solutes. One of these recurring seasonal patterns over several years that many researchers have observed is the seasonal pattern of nitrate concentration in streams that increases in winter and decreases in summer (*Martin et al.*, 2004). There are several explanations in the scientific literature for the apparent seasonality of nitrate loads and concentrations and include higher summer in-stream nitrogen uptake and denitrification rates (*Mulholland et al.*, 2008; *Peterson et al.*, 2001; *Alexander et al.*, 2009), increased leaching from seasonal biochemical changes in the vegetation and soil microorganisms (*Holloway and Dahlgren*, 2001; *Ocampo et al.*, 2006; *Molenat et al.*, 2008; *Arheimer et al.*, 1996; *Burns et al.*, 2009),

and changes in the relative source water contributions throughout the year not associated with seasonal biochemical reactions (*Martin et al.*, 2004; *Grimaldi et al.*, 2004; *Pionke et al.*, 1999). A thorough examination of the source and flowpath dynamics of the nitrate and the seasonal biochemical reactions during baseflow conditions would be required to determine the dominant mechanism causing the seasonal nitrate concentration.

Runoff events contribute significant quantities of flow and solute load to surface waters, but are significantly more difficult to estimate and have additional sources and flowpaths that add to the complexity to the understanding of the hydrologic system compared to baseflow conditions (*Aulenbach*, 2013). Hydrograph separation through end-member mixing analysis (EMMA) has been applied by many researchers to understand the source water contribution dynamics of runoff events, but are almost always applied on a small number of runoff events (*Klaus and McDonnell*, 2013). If the source and flowpath contribution dynamics are to be representative for a full year rather than a couple runoff events, then source separation and flowpath analysis would need to be performed on a large representative sample of runoff events over a few years. EMMA can be applied to separate the contributing sources from any flow location when sufficient discharge and solute concentrations are continuously monitored during runoff events (*Christophersen et al.*, 1990). As tile drainages have been found to contribute significant amounts of solute load to surface waters, applying EMMA to input flowpaths to the stream like tile drainages in addition to the catchment surface water outlet will provide insight into the flowpath contributions and dynamics as well as the source contribution dynamics (*Schilling and Helmers*, 2008; *Tan et al.*, 2002a).

1.1 Thesis research questions and goals

The overall goals of the thesis are to determine the major sources and flowpaths of water and solutes as well as the processes involved with the water and solute transport dynamics in the HOAL catchment. The following research questions and associated chapters will be addressed to further the overall research goals:

- What housing device could be used for water monitoring sensors at discharge locations with significant hydrological constraints? (Chapter 2)
- What is the most accurate tracer method to estimate stream to groundwater exchange in small streams? (Chapter 3)
- Does the deep aquifer have a constant inflow to the stream throughout the year? (Chapter 4)
- Do the alternating source water contributions to the outlet cause the nitrate concentration seasonality? (Chapter 4)
- Do large events have different source water contribution dynamics as compared to small events? (Chapter 5)

- Does the shallow aquifer contribute most of the nitrate load to event runoff throughout the year? (Chapter 5)

The thesis is organized by chapters, and each chapter is a manuscript that has been published by or has been submitted to a scientific peer-reviewed journal. Chapter 2 will describe a new device to house water monitoring devices which was successfully deployed in the Hydrologic Open Air Laboratory (HOAL) catchment. Chapter 2 has been published in the journal Water Science and Technology (*Exner-Kittridge et al.*, 2013). Chapter 3 presents a new methodology to estimate the SGE and associated groundwater solute concentrations, and a comparison to existing methodologies. Chapter 3 has been published in the journal Hydrologic Earth System Sciences (*Exner-Kittridge et al.*, 2014). Chapter 4 addresses the question of the seasonal variability of the nitrate concentration by analyzing the seasonal source and flowpath dynamics in additional to other seasonal biochemical explanations. Chapter 4 has been published in the journal Science of the Total Environment (*Exner-Kittridge et al.*, 2016). Chapter 5 will determine the representative source and flowpath dynamics of water and solute load during runoff events in the HOAL. Chapter 5 has been submitted to the journal Water Resources Research. The knowledge gained from the thesis will help improve the development of large comprehensive transport models which will better identify and target significant pollutant sources and flowpaths that contribute to pollutant loads of surface waters.

Chapter 2

A simple and flexible field-tested device for housing water monitoring sensors at point discharges

2.1 Abstract

The Water Monitoring Enclosure (WME) provides a simple and flexible housing for many types of sensors for continuous measurements of water parameters (physical, chemical, or biological) and provides the opportunity of representative sampling for external analyses. The WME ensures a minimum internal water level and this ensures that the internal monitoring equipment remains submerged even when there is no flow into the enclosure. The limited diameter of the inflow pipe and water volume in the WME buffers the flow velocity from dramatic changes. The device ensures that the sediment entering the enclosure from the inflow will be conveyed through the enclosure with minimal sediment accumulation. The device is powered purely from natural hydraulic forces, so it requires no power source, and requires little additional maintenance beyond periodic cleaning. If desired, the WME can also measure discharge entering the device through additional modifications. Water samples were taken throughout the year to validate the effectiveness of the WME. The comparisons of the influent water to the water in the WME for all parameters were below the laboratory analysis standard error or below the limit of quantification indicating that the water in the WME is representative of the influent water.

2.2 Introduction

Measurements and samples of water parameters are a fundamental aspect of all water related research and monitoring aside from purely theoretical research. As technology

improves and scientific questions plunge deeper into the finer scales of time and space, water measurements have been migrating from grab measurements and samples taken personally at a field site to permanently or temporarily installed instrumentation continuously collecting data. This type of instrumentation has clear advantages. Researchers can acquire data at a high frequency and during periods or at locations that might be difficult to capture (i.e. short duration rainfall events, distant or temporarily inaccessible field sites, etc). Unfortunately, continuous monitoring equipment also tend to be much more complex and subsequently more maintenance prone than simple grab measurements or samples.

Direct laboratory analysis is still the most accurate method to analyze water chemistry as the equipment is regularly maintained, calibrated, and validated to ensure a specific level of data quality. Researchers who only require a couple dozen samples for periodic field tests have used automatic samplers to take samples remotely at a high temporal frequency (*Tan et al.*, 1998; *Burns et al.*, 2001; *Roser et al.*, 2002; *Ensign and Paerl*, 2006). But for those who require a high temporal resolution in addition to longer monitoring programs spanning months or years, the costs for both the laboratory analyses and labor become prohibitive.

Researchers have recognized that if long duration high temporal resolution measurements of water chemistry are to be performed then the laboratory would need to be mostly divorced from the actual measurement process. Currently, there are two overarching methods to remotely collect high temporal resolution water chemistry using temporary or permanent installations. The first is typically known as on-line measurement devices. These devices effectively miniaturize and automate aspects of the laboratory analysis (i.e. filtration, addition of chemical additives, etc.) at a fixed location directly at the water body for sampling. The second is to use an in situ sensor as a proxy for the measurement of the chemical compound. The former method has been used extensively in wastewater monitoring (*Legnerová et al.*, 2002; *Carrasco et al.*, 2007; *Stenholm et al.*, 2008). The ability of an automated on-line device to draw in a sample and prepare the sample through filtration or chemical additives is useful when the sample may have high concentrations of many toxic substances. The primary trade-off of such a highly complex device with automated pumping and filtration systems is that it requires a great deal of maintenance to upkeep the device.

In situ sensors have become increasingly popular within the last couple decades for both wastewater and non-wastewater applications (*Newman*, 2001; *Kaelin et al.*, 2008; *Kim et al.*, 2009; *Kestel et al.*, 2010). Hydrologists have been using similar devices for many decades to measure physical water parameters (i.e. water level, temperature, electrical conductivity, etc). The advantages of in situ sensors include a very small size relative to the on-line devices, simpler construction and operation, lower cost, and temporal resolution that can be finer than on-line devices. The primary disadvantage is a lower accuracy and higher detection limit to the on-line devices.

Both the on-line devices and the in situ sensors have physical measurement constraints that must be taken into account before installation to ensure proper measurement quality. The constraints become especially problematic when measuring in natural

environments with low discharges (¡5l/s). Both types of devices require a water depth of at least 20-30cm depending on the type of measurement device. The water could either be a free flowing stream or an intermediate pool of water. For sensors with polymer membranes, the water level must not drop below the measurement device as the sensors must always stay wet. Additionally for in situ sensors, large ranges in the water velocity can significantly affect electrochemical signals. If parameters associated with suspended solids are to be measured (i.e. turbidity, phosphate, etc), then resuspension during storm flow events should be greatly limited to ensure that the sampling is representative of the influent water. Suspended solids sampling are generally more difficult to be representative of the influent water than dissolved solids. *Harmel et al.* (2006) found that while sampling uncertainty for dissolved solids were ±25%, the uncertainty for suspended solids were over 50%. Finally, continuously deposited sediments into the measurement pool could reduce the optimal water depth and in the worst case bury the measurement device.

Given the above constraints for the installation conditions for water measurement devices, researchers traditionally have had two general options when installing equipment in natural environments. The first is to simply excavate a pool directly below the influent water and place the measurement devices (or pump tubing) directly into the pool. The main drawback of the pool is that it requires frequent excavation of the sediment deposited into the pool. Due to the reduction in the flow velocity from the influent water to the pool, sediment will inherently deposit into the pool and not be naturally transmitted through the system. Additionally, the flow velocity in the pool could vary dramatically depending on the volatility of the influent water. The second option is also to excavate a pool, albeit a smaller one to that of the first option, and use a tube with a pump to draw up the water into an external container where the measurement devices are housed. The pump-container option is advantageous in that the excavated pool can be much smaller than the first option and subsequently reduce the sediment deposition. The pump-container option would ensure both a minimum water level and a consistent flow velocity for the measurement devices. The key disadvantage for the pump-container option is the pump itself. Additional mechanical moving parts like a pumping system increases the likelihood of malfunction and breakdown especially during winter months where freezing can be an issue. An ideal option would have the relative simplicity of the first option, the consistent flow velocity of the pump-container option, and the ability to continuously transmit sediment through the measurement system.

We have designed, built, and tested a measurement system with all of the above constraints. The Water Monitoring Enclosure (WME) provides a simple and flexible housing for sensors for continuous measurements of many types of water parameters (physical, chemical, or biological) and provides the opportunity of representative sampling for external analyses (e.g. remote mini-laboratories or automatic samplers) . The WME ensures a minimum internal water level and this ensures that the internal monitoring equipment remains submerged even when there is no flow into the enclosure. The limited diameter of the inflow pipe and water volume in the WME buffers the flow

velocity from dramatic changes. The device ensures that the sediment entering the enclosure from the inflow will be conveyed through the enclosure with minimal sediment accumulation. The device is powered purely from natural hydraulic forces, so it requires no power source, and requires little additional maintenance beyond periodic cleaning. If desired, the WME can also measure discharge entering the device through additional modifications.

2.3 Test site

The test site chosen for the WME was the Hydrologic Open Air Laboratory (HOAL) catchment located in Petzenkirchen in Lower Austria approximately 100km west of Vienna. The catchment has an area of 67 hectares and the land cover is characterized as 90% agriculture, 5% impermeable surface, and 3% forest. There are twelve point discharges that drain into the catchment stream. These include seven subsurface tile drains, two springs, and four surface tributaries. Baseflow can range from 0.00l/s at some of the subsurface drains and surface tributaries to 5 l/s at the catchment outlet. Average baseflow at the subsurface drains and surface tributaries is 0.1-0.2l/s with a maximum measured discharge of approximately 13l/s. In total, four WMEs were installed within the catchment.

2.4 Design and construction

Figure 2.1 illustrates the individual components of the WME. There are five primary components: (1) center shaft, (2) plunger, (3) bladder, (4) outer enclosure, and (5) outflow siphon.

Figures 2.2 represents the fully constructed WME. The WME is almost entirely composed of polyvinyl chloride (PVC). The only exception is the plunger rod, which is composed of stainless steel. This type of PVC was primarily used due to its low corrodibility and ultraviolet resistivity. The inflow piping to the WME is standard 50mm diameter PVC attached directly to WME. The overflow should be located directly opposite of the inflow with a 50mm diameter pipe. The outflow opening at the bottom of the center shaft is 40-45mm diameter. A 75mm diameter PVC pipe is subsequently attached to the bottom of the center shaft, which is ultimately reduced to 50mm once it connects to the siphon. The plunger is set within the center shaft with the bladder set around the center shaft. Both the plunger and the bladder should be of a diameter that would allow them to move freely within the center shaft with a changing water level. An adjustable screw fixed to the upper end of the plunger and set atop of the bladder ensures that when the bladder moves vertically the plunger will also move with it. The adjustable screw on the plunger rod can be raised or lowered to modify the minimum and maximum water level within the WME. The plunger should have a flexible rubber seal on the bottom end to facilitate a water tight seal when in the closed position. The total height of the WME without the center shaft should be determined by the instrumentation to be placed inside the WME. Our WME had a wall height of 30cm

and a total height to the bottom center of the WME (excluding the center shaft) of 35cm. An inverted siphon should be placed at the outflow piping of the WME and should not rise above the bottom of the center shaft where the plunger would be in the closed position. The overflow should be connected to the outflow piping directly after the siphon using a "T" joint PVC pipe as shown in Figure 2.2.

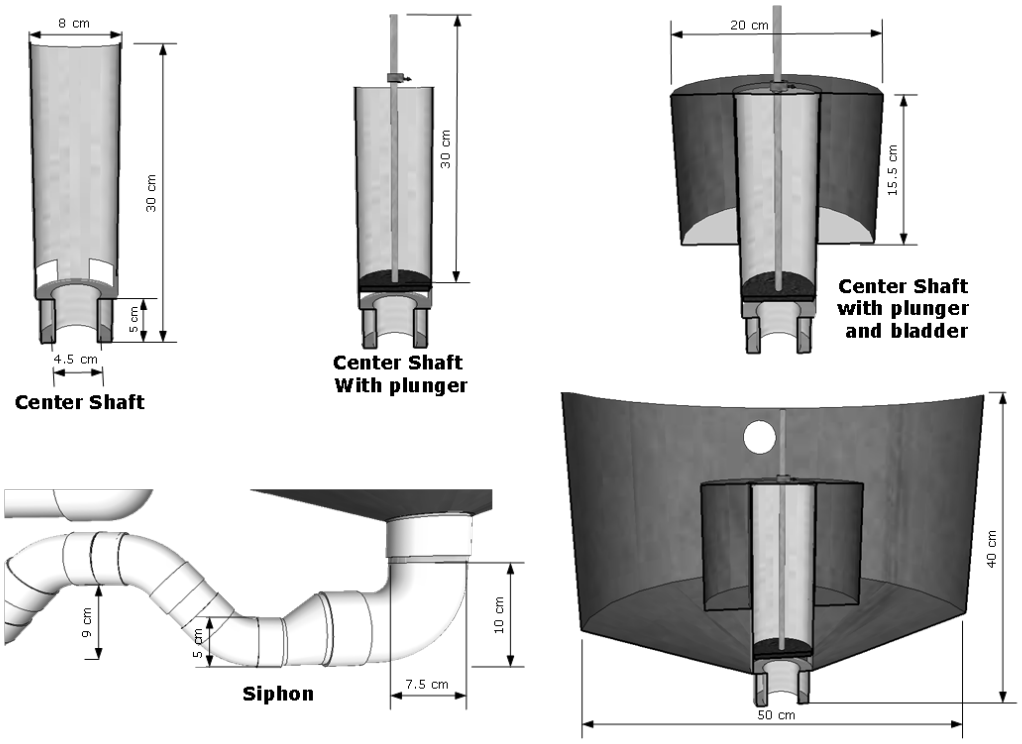

Figure 2.1: The individual components of the WME and associated dimensions: (1) center shaft, (2) plunger, (3) bladder, (4) outer enclosure, and (5) outflow siphon.

2.5 Function

The WME is designed to provide four key functions: (1) maintain a minimum water level to ensure that the measurement sensors do not become dry, (2) allow sediment to be continuously transmitted through the WME, (3) limit the flow velocity range, and (4) be simple and require little maintenance.

The 50mm diameter inflow restricts the amount of flow into the WME that can be readily discharged at the bottom of a 40-45mm diameter outlet (Figure 2.1). The inflow restriction removes the need for a large overflow in case of severe clogging of the outflow and limits the magnitude of the flow velocity in the WME. The inflowing water is directed perpendicularly into the WME to allow for proper circulation and mixing

Figure 2.2: Fully assembled and installed WME with foundation poles. The holes in the lid of the WME are for the placement of the measurement sensors.

within the WME. The sloped bottom funnel ensures that any sediment deposition will be gradually transported down towards the WME outlet during flushing and ultimately removed.

When a maximum water level threshold is reached within the WME, the bladder quickly lifts the plunger to allow a high velocity flow pulse through the outflow pipe. Following the initial opening of the plunger, the water level gradually drops since the outflow discharge is greater than the inflow discharge. Once the water level reaches a minimum threshold, the bladder lowers and the plunger closes the outflow. The mechanism is intended to always fully open regardless of the inflow rate to ensure proper sediment conveyance. In some instances with a long outflow pipe, the closing of the plunger to the outflow may bounce several times before completely closing due to natural water hammer.

The inverted siphon shape was configured to retain a volume and level of water directly below the outflow, but not as to exceed the height of the plunger inside the WME as this can cause poor sealing of the plunger. The closed volume of water in the siphon ensures that when the water level in the WME reaches the maximum threshold,

and the plunger is subsequently lifted by the bladder, the water exiting the outflow does not exert a counter force on the plunger potentially pulling the plunger back to a closed position. Without the siphon, the bladder and plunger mechanism would not open fully when the initial maximum threshold is reached, and consequently a steady state would be reached where the inflow would equal the outflow. Due to the high velocities in the siphon compared with the inflow and within the WME, no sediment accumulation occurs in the siphon.

2.5.1 Discharge measurements

When water is regularly entering the WME, the plunger opens and closes at a regular frequency relative to the incoming flow. With a consistent flushing frequency from the incoming flow, measuring the time between the flushings allows for the estimation of discharge from the WME. The mechanism functions similarly to a tipping bucket rain gauge and can be installed with similar instrumentation.

$$Q = \frac{t_2 - t_1}{V} \tag{2.1}$$

Where Q is the discharge, t_1 is the time of the initial opening of the plunger, t_2 is the time when the plunger closes, and V is the difference of the volume of water at the maximum water level and the minimum water level in the WME. In this situation, V is not equivalent to the volume of flushed water as the flushed water includes the inflow water during the flushing in addition to the V. For practical purposes, it may not be possible to measure both an opening time and a closing time, which could require two separate devices logging two separate time stamps. Measuring the time once per opening is more feasible, but a relationship must be derived between the times of the sequential openings of the plunger to the time between the opening and the closing of the plunger.

2.6 Functional assessment

Several tests were performed to verify the effectiveness of the WME. The tests included (1) a verification that the water chemistry in the WME is representative of the influent water and (2) a verification of the regularity of the flushings for use in estimating discharge.

2.6.1 Chemical assessment

For the chemical assessment, one sample was collected at the influent water (directly before the intake of the WME) and one sample was collected from within the WME at four separate times over a 1-year period. Table 1 summarizes the results from the chemical analysis of the samples. The sample representativeness error (SRE) was estimated with the following equation:

$$SRE = \frac{|\frac{C_{a1}}{C_{b1}} - 1| + |\frac{C_{a2}}{C_{b2}} - 1| + ... + |\frac{C_{an}}{C_{bn}} - 1|}{n} \tag{2.2}$$

Where SRE is the sample representativeness error, C_a is the concentration of the influent water, C_b is the concentration of the water in the WME, and n is the total number of sample sets. In our comparison, we had four sample sets.

In addition to the four sample sets that were taken over the course of a year, another set of 25 samples were taken on one day at the same WME to test the laboratory analytical error. These samples were taken in quick succession and with great diligence to ensure that minimal error could be attributed to the sample collection and sample transportation. The term laboratory analytical error includes both sample preparation and analytical error. Only three chemical parameters (e.g. phosphate, nitrate, and chloride) were analyzed due to cost limitations. The laboratory analytical error was calculated by the coefficient of variation (standard deviation divided by the mean) of all 25 samples. The results are shown at the bottom of Table 2.1 as lab analytical error.

The majority of the parameters had neither a consistent bias nor did they have an error greater than 2% of the original measurements. Although several parameters (e.g. DOC, TOC, phosphate, ammonium, and total phosphorus) had larger errors, these parameters were near or below the limit of quantification of the laboratory analytical techniques. Phosphate was close to the quantification limit of the laboratory analysis, while nitrate and chloride were well above the quantification limit. Nitrate and chloride with a concentration well above the detection limit had errors of approximately 0.01 and 0.05 respectively, while phosphate with a concentration near the detection limit had an error of approximately 0.30. Indeed, the error found between the influent water and the WME is well under the error for phosphate and at or below the error for nitrate and chloride. DOC and TOC had errors above 3%, and we were unfortunately not able to derive lab specific analytical errors. According to the DIN/EN 1484 standards for the laboratory analysis of DOC and TOC, the analytical error can be on average 1 to 2mg/l. As the average differences for the sample sets for DOC and TOC were 0.13 and 0.35mg/l respectively, the SRE can be attributed to the analytical error. During a normal sampling campaign, sample collection, sample transportation, sample preparation, and sample analysis all add error. *Harmel et al.* (2006) found that under typical conditions the cumulative probable uncertainty was 4% to 48% for sample collection, 2% to 16% for sample preservation/storage, and 5% to 21% for laboratory analysis. For this reason, it is surprising that our sample comparisons between the influent water and the WME had only a couple percent error for most of the parameters.

2.6.2 Discharge assessment

The data for the assessment of the consistency of the flushing frequency of the WME during constant discharge was collected at 10 separate times throughout the year and had a coefficient of variation of 0.01. The error in the WME estimation of discharge compared to the manual measurements of discharge during the previously mentioned 10 measurement times throughout the year was 0.05. The error was estimated using equation (2), but replacing concentrations with discharges. The flow ranges assessed ranged from 0.04 – 0.5l/s. Beyond approximately 0.7l/s the plunger remains opened continuously and therefore cannot be used to estimate discharge. If there is a need to

Location	Date	Dissolved Organic Carbon (mg/l)	Total Organic Carbon (mg/L)	Phosphate (mg/l)	Ammonium (mg/l)	Nitrate (mg/l)	Total Phosphorus (mg/l)	Total Nitrogen (mg/l)	Suspended solids (mg/l)	Hydrogen Carbonate (mg/L)	Chloride (mg/l)	Sulfate (mg/l)	pH	Electrical Conductivity (µs/cm)
Influent Water	2011-01-14	2.1	3.2	0.031	0.012	9.32	0.106	9.84	19.3	301	19.2	26.0	7.31	636
WME	2011-01-14	2.2	2.7	0.026	0.012	9.41	0.089	9.85	22.0	302	18.4	25.6	7.35	634
Influent Water	2011-02-23	2.1	2.1	0.008	0.010	13.79	0.015	13.70	0	325	23.7	39.8	7.64	770
WME	2011-02-23	2.4	2.4	0.007	0.020	13.94	0.020	14.17	0	331	23.8	39.4	7.63	770
Influent Water	2011-05-09	0.4	0.5	0.011	0.011	13.90	0.027	13.95	1	335	27.7	45.8	7.53	783
WME	2011-05-09	0.4	0.9	0.011	0.011	13.90	0.024	14.18	1	336	27.4	44.2	7.46	781
Influent Water	2012-01-11	1.0	1.3	0.007	0.017	10.85	0.021	11.14	0.0	356	24.4	35.7	7.67	780
WME	2012-01-11	0.9	1.1	0.006	0.021	10.92	0.018	11.33	0.5	347	23.8	35.1	7.56	772
Lab limit of quantification (mg/l)		0.3	0.3	0.014	0.029	0.10	0.070				1.5			
SRE		0.07	0.23	0.13	0.17	0.01	0.18	0.02	0.03	0.01	0.02	0.02	0.01	0.00
Lab analytical error				0.30		0.01					0.05			

Table 2.1: Chemical comparisons between the influent water and the WME taken at four times.

measure discharge with the WME, then a slight magnetic force between the plunger and the outflow pipe may be required to ensure a proper closing.

2.7 Design limitations

During the operation of the WME, we found two functional limitations and issues. The first occurred at a site with very low discharge (¡0.04l/s) combined with a heavy fine sediment load (up to 100mg/l of silt). In this situation, the WME did not flush frequently enough to continuously remove all of the sediment transported into the WME. The maximum sediment accumulation that we found was about 4cm of sediment deposited over a two week period.

The second issue was the accumulation of precipitated calcium carbonate within the WME. Normal agricultural practice in Austria (and many parts of the world) includes periodic spreading of lime on the agricultural fields to ensure that the soil does not become acidic. As with most chemicals that are spread onto agricultural fields, the calcium eventually makes its way through the various pathways and into the main water bodies. During our first 8 months of operation, we had only minimal accumulation of calcium carbonate that caused minimal functional issues for the WME. The first major rain storm after the farmers applied the calcium bicarbonate caused significant accumulations of calcium carbonate at nearly all of the WME stations. The primary issue with the build up of calcium carbonate is that the flushing mechanism of the plunger

within the center shaft seizes from the shrinking diameter in the center shaft and the additional friction. The seizing occurred on approximately a third of the devices and the others had some degree of problems opening properly from an incomplete plunger seal.

Both issues of the sediment accumulation at very low flows and calcium carbonate cementation are situational issues and should be dealt with as such. Periodic cleaning of the WME is necessary to ensure optimal performance and the frequency of cleanings will be unique for each installed WME due to the local environmental conditions. During the period when calcium carbonate was accumulating rapidly, our WMEs were cleaned once every two weeks. During the remainder of the year, the WMEs would only need to be cleaned once every couple months or in some cases not at all.

2.8 Conclusions

The WME has been shown to provide a simple, flexible, and effective housing for many types of water measurement devices. The WME can function in many environments that may be remote and without electricity for long periods of time at nearly any range of flow. The WME ensures a minimum internal water level and this ensures that the internal monitoring equipment remains submerged even when there is no flow into the enclosure. The limited diameter of the inflow pipe and water volume in the WME buffers the flow velocity from dramatic changes. The device ensures that the sediment entering the enclosure from the inflow will be conveyed through the enclosure with minimal sediment accumulation. The device is powered purely from natural hydraulic forces, so it requires no power source, and requires little additional maintenance beyond periodic cleaning.

The functional assessments have shown that the WME has a minimal effect on the chemistry of the water and with the addition of a small magnet the WME can also measure discharge accurately up to 0.5l/s. In certain environments, the WME must be cleaned regularly to ensure the proper functioning of the few moving parts within the WME. We cannot emphasize enough the importance of regular maintenance for any water monitoring device regardless of how simple and basic the device may be.

Chapter 3

An evaluation of analytical stream to groundwater exchange models: a comparison of gross exchanges based on different spatial flow distribution assumptions

3.1 Abstract

In this paper, a new method for estimating gross gains and losses between streams and groundwater is developed and evaluated against two existing approaches. These three stream to groundwater exchange (SGE) estimation methods are distinct in their assumptions on the spatial distribution of the inflowing and outflowing fluxes along the stream. The two existing methods assume that the fluxes are independent and in a specific sequence, while the third and newly derived method assumes that both fluxes occur simultaneously and uniformly throughout the stream. The analytic expressions in connection to the underlying assumptions are investigated through numerical stream simulations to evaluate the individual and mutual dynamics of the SGE estimation methods and to understand the causes for the different performances. The results show that the three methods produce significantly different results and that the mean absolute normalized error can have up to an order of magnitude difference between the methods. These differences between the SGE methods are entirely due to the assumptions of the SGE spatial dynamics of the methods, and the performances for a particular approach strongly decrease if its assumptions are not fulfilled. The assessment of the three methods through numerical simulations, representing a variety of SGE dynamics, shows that the method introduced, considering simultaneous stream gains and losses, presents overall the highest performance according to the simulations. As the existing methods provide the minimum and maximum realistic values of SGE within a stream reach, all three

methods could be used in conjunction for a full range of estimates. These SGE methods can also be used in conjunction with other end-member mixing models to acquire even more hydrologic information as both require the same type of input data.

3.2 Introduction

Groundwater and surface water interactions are an important process in hydrologic systems (*Winter*, 1998). These interactions within and around streams and rivers impact decisions on municipal water supply extractions, water pollution, riverine habitat, and many others. To make better decisions on these impacts, the stream to groundwater exchange (SGE) need to be accurately quantified as stream losses and gains can account for a substantial proportion of the total flow and chemical load of a stream.

In general, when people consider how to estimate the flow losses or gains along a stream reach they would take a discharge measurement upstream, a discharge measurement downstream, subtract the two values, and the result would be considered the gain or loss of flow within the stream reach. Although this may be a relatively simple procedure to accomplish, the assumption that all flow within a stream reach must be either flowing into the stream or flowing out of the stream is in many cases an over simplification (*Castro and Hornberger*, 1991; *Harvey and Bencala*, 1993). Depending on local topography, geology, and the groundwater table, gains and losses into and out of the stream can be very dynamic even over short distances (*Harvey and Bencala*, 1993; *Anderson et al.*, 2005; *Payn et al.*, 2009). Consequently, what might have originally been estimated as a small gain to the stream from simply subtracting the upstream and downstream discharges might end up becoming a small loss out of the stream and a large gain into the stream. Without a proper method to estimate SGE, any attempt at estimating a water or nutrient mass balance would be difficult and laced with errors.

Harvey and Wagner (2000) and many other researchers use a more realistic conceptual model of flow pathways within a stream (Figure 3.1). These major flow pathways include initial (or upstream) discharge (Q_{up}), final (or downstream) discharge (Q_{down}), stream gains from groundwater (Q_{gain}), stream losses to groundwater (Q_{loss}), and hyporheic flow (Q_{hyp}). In this conceptual model, Q_{gain} is considered to be pure groundwater entering the stream, and Q_{loss} is stream water permanently leaving the stream. Hyporheic flow occurs when stream water temporarily leaves the stream into the surrounding groundwater (or more specifically the hyporheic zone), but returns again to the stream at some downstream location. During this temporary departure from the stream, additional biochemical reactions may occur that would not necessarily have occurred while in the stream itself. The mass is still retained in the stream and not lost (permanently) to the groundwater. Although the hyporheic flow pathways do occur and can be very important for stream ecosystems (e.g. the movement of oxygen into the hyporheic zone, nitrogen cycling, etc.), hyporheic flow will not be directly addressed in this study as the authors are most interested on fluxes that are permanently adding or removing mass over a significant length of stream. As hyporheic flows only temporarily leave the stream, the mass of the water is still retained over sufficient distances.

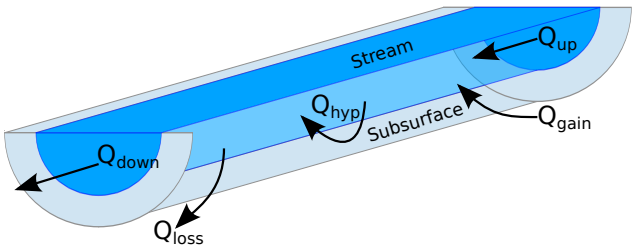

Figure 3.1: A conceptual overview of the major inflows and outflows within a stream reach. Q_{up} is the upstream discharge in volume per time, Q_{down} is the downstream discharge, Q_{gain} is the groundwater entering the stream, Q_{loss} is the stream water leaving the stream to the groundwater, and Q_{hyp} is the hyporheic flow water that is temporarily leaving the stream into the hyporheic zone. (Reproduced after *Harvey and Wagner* (2000))

There are a number of methods to estimate gross stream gains and losses (*Kalbus et al.*, 2006). The general categories are seepage meters, (heat or chemical) tracer tests, and hydraulic gradients derived from groundwater piezometers. Each has advantages and disadvantages. Seepage meters and groundwater piezometers are point measurements that can be accurate at a specific point, but in a heterogeneous system they may not represent the stream as a whole. On the other hand, chemical tracer tests are an aggregation of all fluxes along a stream reach, but do not represent any particular point along the stream. For this study, the focus is on the total aggregated flows over the stream reaches, so chemical tracer tests were found to be the most appropriate and inexpensive. *Kalbus et al.* (2006) and *Scanlon et al.* (2002) have a more thorough qualitative review of the different SGE methods.

Using chemical tracer tests for the source of data, the estimation of gross stream gains and losses is most frequently performed through numerical models like those similar to the OTIS model developed by the USGS (*Runkel*, 1998). While able to estimate fluxes in steady-state conditions, these types of models are primarily designed for non-steady-state conditions and provide many output parameters in addition to the inflow and outflow fluxes, and as a consequence require more input data than in steady-state conditions for estimating only SGE (e.g.stream cross-sectional area, flow advection, flow dispersion, etc). Additionally, the OTIS type models would require the estimation of parameters through a trial-and-error or an automated nonlinear least squares (NLS) procedure that are not directly measured. Under steady-state conditions, the data and parameter requirements for estimating only SGE are substantially lower requiring only discharge and tracer concentration measurements upstream and downstream. If steady-state is appropriate, then analytical methods are sufficient.

There are two existing analytical methods to estimate SGE under steady-state conditions ignoring hyporheic flowpaths. These methods use simple mass balance equations to estimate both gains and losses within a stream reach and assume that the fluxes are

independent and in a specific sequence. In this paper, a new analytical method has been developed using different assumptions on the spatial distribution of the inflowing and outflowing fluxes along the stream. The new spatial distribution assumption is simultaneous and uniform inflows and outflows over the entire stream reach.

The goal of our study is to quantitatively evaluate the accuracy and sensitivity of the new method against the existing steady-state SGE tracer methods. This evaluation is performed through a combination of analytical comparisons and numerical stream simulations as described in the following sections.

3.3 Methods

3.3.1 Theoretical basis of the SGE tracer methods

All tracer based methods designed to estimate SGE start with the conservation of mass equations under steady-state conditions for both the tracer and the water flux and assume complete mixing of the individual flows:

$$Q_{up}C_{up} + Q_{gain}C_{gain} = Q_{down}C_{down} + Q_{loss}C_{loss} \tag{3.1}$$

$$Q_{up} + Q_{gain} = Q_{down} + Q_{loss} \tag{3.2}$$

where Q_{down} is the downstream discharge (in volume per unit time), C_{down} is the downstream concentration (in mass per unit volume), Q_{up} is the upstream discharge, C_{up} is the upstream concentration, Q_{gain} is the discharge from the groundwater to the stream, C_{gain} is the concentration of Q_{gain}, Q_{loss} is the discharge from the stream to the groundwater, and C_{loss} is the concentration of Q_{loss}.

If we assume that C_{gain} will be estimated later from the tracer test, then there are three unknown variables (i.e. Q_{gain}, Q_{loss}, and C_{loss}) and two equations. As we want to solve for Q_{gain} and Q_{loss}, we must make some assumption about C_{loss} to make the derivation solvable. The two existing SGE estimation methods mentioned in the introduction make specific assumptions on the distribution of gains and losses throughout the reach (see Figure 3.2) to make appropriate assumptions about C_{loss}. The first method, we call "Loss–Gain", assumes $C_{loss} = C_{up}$, while the second method, we call "Gain–Loss", assumes $C_{loss} = C_{down}$. In both variants, the methods assume that the mixing of $Q_{gain}C_{gain}$ and $Q_{loss}C_{loss}$ are mixed separately and in a sequence defined by the above assumptions. The Loss–Gain variant assumes that the mixing sequence begins with Q_{loss} followed by Q_{gain}, while Gain–Loss is vice-versa.

Combining equations (3.1) and (3.2), the solution for Q_{loss} for Loss–Gain is:

$$Q_{loss,LG} = Q_{up} - Q_{down}\left(\frac{C_{down} - C_{gain}}{C_{up} - C_{gain}}\right) \tag{3.3}$$

Similarly, the equation for Q_{loss} for Gain–Loss is:

$$Q_{loss,GL} = Q_{up}\left(\frac{C_{up} - C_{gain}}{C_{down} - C_{gain}}\right) - Q_{down} \tag{3.4}$$

To get Q_{gain} for both methods, we need to include equation (3.2) into equations (3.3) and (3.4):

$$Q_{gain,LG} = Q_{down}\left(\frac{C_{down} - C_{up}}{C_{gain} - C_{up}}\right) \tag{3.5}$$

$$Q_{gain,GL} = Q_{up}\left(\frac{C_{down} - C_{up}}{C_{gain} - C_{down}}\right) \tag{3.6}$$

If we use an artificial tracer (e.g. Bromide salt), we can safely assume $C_{gain} \approx 0$ and the resulting equations are as follows:

$$Q_{loss,LG} = Q_{up} - Q_{down}\frac{C_{down}}{C_{up}} \tag{3.7}$$

$$Q_{loss,GL} = Q_{up}\frac{C_{up}}{C_{down}} - Q_{down} \tag{3.8}$$

and Q_{gain} becomes:

$$Q_{gain,LG} = Q_{down}\left(1 - \frac{C_{down}}{C_{up}}\right) \tag{3.9}$$

$$Q_{gain,GL} = Q_{up}\left(\frac{C_{up}}{C_{down}} - 1\right) \tag{3.10}$$

These methods can be applied conceptually along a stream length as illustrated in the A and B sections of Figure 3.2. Q_{up} is the upstream discharge and Q_{down} represents the downstream discharge. Depending on the equation variant, Q_{gain} is added or Q_{loss} is removed from Q_{up} at the beginning of the stream and Q_{loss} is removed or Q_{gain} is added at the end of the stream resulting in a downstream discharge of Q_{down}. As these methods make no assumptions about the exact location along the stream for Q_{gain} and Q_{loss}, they can occur over any length of the stream as long as they occur in sequence and independently.

If a stream reach has some amount of Q_{gain}, then there is a certain significance to the Loss–Gain and Gain–Loss methods. The concentration of the conservative tracer starting at the location of Q_{up} and ending at the location of Q_{down} will have a tracer concentration that starts at the value of C_{up}, changing towards the concentration of C_{gain} whenever Q_{gain} enters the stream, and finally ending downstream at a value of Q_{down} (which again is a value towards that of C_{gain}). As this occurs in every possible stream reach where $Q_{gain} > 0$ and $C_{gain} \neq C_{up} \neq C_{down}$, C_{up} and C_{down} represent the end point concentrations along a stream reach. Subsequently, the Loss–Gain (with

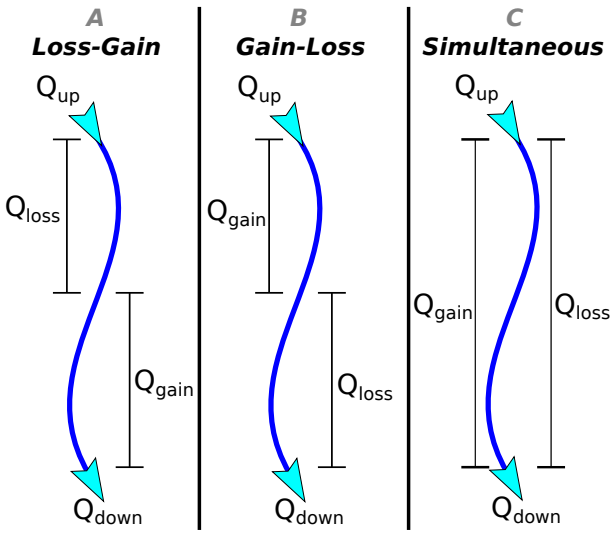

Figure 3.2: The conceptualizations of the three SGE methods. A) The LG(min) method assumes Q_{gain} occurs in the first section followed by Q_{loss} in the last section. B) The GL(max) method assumes Q_{loss} occurs in the first section followed by Q_{gain} in the last section. Both the LG(min) and GL(max) methods assume that Q_{gain} and Q_{loss} occur in sequence and independently, although the lengths of the first and last sections are arbitrary and can be of any length that when summed together equal the total length. C) The SIM method assumes that Q_{gain} and Q_{loss} are constant and occur simultaneously throughout the entire length of the stream reach.

the C_{up} assumption) and Gain–Loss (with the C_{down} assumption) methods represent the minimum and maximum possible SGE values given the initial mass balance assumptions from equations (3.1) and (3.2). This also means that any other SGE method must result in SGE values between the Loss–Gain and Gain–Loss methods. To provide the reader with an intuitive sense of both the underlying spatial distribution assumptions and the end point that these two methods represent, the Loss–Gain method will be called "LG(min)" and the Gain–Loss method will be called "GL(max)".

From studies that tested multiple stream reaches for SGE, almost every stream reach had both gains and losses regardless of the method and of the reach length (*Anderson et al.*, 2005; *Ruehl et al.*, 2006; *Payn et al.*, 2009; *Covino et al.*, 2011; *Szeftel et al.*, 2011). Additionally, studies that have tried to identify the spatial distribution of groundwater inflows and outflows to and from the stream have found a wide variety of diffuse flow locations throughout the stream and were not limited to one or two flow locations every several hundred meters (*Malard et al.*, 2002; *Wondzell*, 2005; *Schmidt et al.*, 2006; *Lowry et al.*, 2007; *Slater et al.*, 2010). This indicates that even short stream reaches typically have many instances of gains and losses to and from the stream and that limiting the flux instances to one flux each regardless of the stream length may not be the most

accurate assumption.

Following this rationale, this paper presents a new method based on a different assumption for the spatial distribution of SGE as compared to the GL(max) and LG(min) methods, namely that both Q_{gain} and Q_{loss} occur simultaneously and uniformly throughout the entire stream section. This new method is denoted as "SIM". Equations requiring the same input data as the GL(max) and LG(min) methods are derived in Sect. 3.3.2 and length is integrated into the mass balance equation (Figure 3.3).

3.3.2 Derivation of the method for simultaneous gains and losses

In this section, the fundamental equations of mass balance for the tracer and water flows will be applied on a control volume represented in Figure 3.3 under the assumption of simultaneous and uniform gains and losses throughout the stream reach and stationarity in time in order to obtain the expressions predicting Q_{gain} and Q_{loss} as functions of Q_{up}, C_{up}, Q_{down}, C_{down} and C_{gain}. First, applying mass balance for discharge:

$$Q(x) + q_{gain}dx = Q(x) + \frac{\partial Q(x)}{\partial x}dx + q_{loss}dx \tag{3.11}$$

where x is distance along the stream, $Q(x)$ is the discharge at length x, q_{gain} is the added discharge per unit length of stream, and q_{loss} is the lost discharge per unit of length. Both q_{gain} and q_{loss} are assumed constant for a given stream reach. In the one-dimensional and stationary case, we can write $\frac{\partial Q(x)}{\partial x}dx = dQ$. After rearranging and integrating from the beginning of the reach over an arbitrary length:

$$\int_{Q_{up}}^{Q(x)} dQ = \int_{0}^{x} (q_{gain} - q_{loss})dx \tag{3.12}$$

which becomes:

$$Q(x) = Q_{up} + (q_{gain} - q_{loss})x \tag{3.13}$$

Then, applying mass balance for the tracer:

$$\begin{aligned} &\dot{m}(x) + C_{gain}q_{gain}dx = \\ = \quad &\left(\dot{m}(x) + \frac{\partial \dot{m}(x)}{\partial x}dx\right) + C(x)q_{loss}dx \end{aligned} \tag{3.14}$$

where $\dot{m}(x)$ is the mass flow at length x, $C(x)$ is the concentration at length x, and C_{gain} is the concentration of q_{gain}. $\dot{m}(x)$ is defined as $\dot{m}(x) = Q(x) \cdot C(x)$. The inflowing concentration C_{gain} is assumed constant for a given stream reach. Again in the one-dimensional and stationary case, we can write $\frac{\partial \dot{m}(x)}{\partial x}dx = d\dot{m}$. Taking into account the

definition of $\dot{m}(x)$, we can write $d\dot{m} = d(C \cdot Q) = Q \cdot dC + C \cdot dQ$. Rearranging the equation we get:

$$Q(x)dC = C_{gain}q_{gain}dx - C(x)\left(dQ + q_{loss}dx\right) \tag{3.15}$$

Substituting equations (3.12) and (3.13) for $Q(x)$ and dQ respectively in equation (3.15), and rearranging:

$$dC = \frac{C_{gain}q_{gain}dx - C(x)\left[(q_{gain} - q_{loss})dx + q_{loss}dx\right]}{Q_{up} + (q_{gain} - q_{loss})x} \tag{3.16}$$

Simplifying and integrating from the beginning of the reach over an arbitrary length x:

$$\int_{C_{up}}^{C(x)} \frac{dC}{C(x) - C_{gain}} = -q_{gain} \int_{0}^{x} \frac{dx}{Q_{up} + (q_{gain} - q_{loss})x} \tag{3.17}$$

which becomes:

$$\ln \frac{C(x) - C_{gain}}{C_{up} - C_{gain}} = -\frac{q_{gain}}{q_{gain} - q_{loss}} \ln \frac{Q_{up} + (q_{gain} - q_{loss})x}{Q_{up}} \tag{3.18}$$

Evaluating equation (3.13) for $x = L$, where L represents the total length of the stream reach:

$$q_{gain} - q_{loss} = \frac{Q_{down} - Q_{up}}{L} \tag{3.19}$$

Substituting equation (3.19) in equation (3.18) and evaluating for $x = L$:

$$\ln \frac{C_{down} - C_{gain}}{C_{up} - C_{gain}} = -\frac{q_{gain}}{\frac{Q_{down} - Q_{up}}{L}} \ln \frac{Q_{down}}{Q_{up}} \tag{3.20}$$

Calling $Q_{gain} = q_{gain} \cdot L$ and rearranging:

$$Q_{gain,Sim} = (Q_{up} - Q_{down}) \frac{ln[\frac{C_{down} - C_{gain}}{C_{up} - C_{gain}}]}{ln[\frac{Q_{down}}{Q_{up}}]} \tag{3.21}$$

If we substitute equation (3.2) for $Q_{gain,Sim}$ in equation (3.21), the solution for Q_{loss} is:

$$Q_{loss,Sim} = (Q_{up} - Q_{down}) \frac{ln[\frac{Q_{down}(C_{down} - C_{gain})}{Q_{up}(C_{up} - C_{gain})}]}{ln[\frac{Q_{down}}{Q_{up}}]} \tag{3.22}$$

where $Q_{gain,Sim}$ and $Q_{loss,Sim}$ are the SIM equations for the SGE into and out of the stream, respectively.

As with the previous methods, if we use an artificial tracer (e.g. Bromide salt) we can safely assume $C_{gain} \approx 0$ and the resulting equations are as follows:

$$Q_{gain,Sim} = (Q_{up} - Q_{down}) \frac{ln[\frac{C_{down}}{C_{up}}]}{ln[\frac{Q_{down}}{Q_{up}}]} \tag{3.23}$$

and

$$Q_{loss,Sim} = (Q_{up} - Q_{down}) \frac{ln[\frac{Q_{down}C_{down}}{Q_{up}C_{up}}]}{ln[\frac{Q_{down}}{Q_{up}}]} \tag{3.24}$$

Equations (3.21)–(3.24) are discontinuous when $Q_{up} = Q_{down}$. Fortunately, this is a removable discontinuity and can be solved by applying *L'Hôpital*'s rule (*Arfken and Weber*, 2005). Applying *L'Hôpital*'s rule to equation (3.21) and differentiating for Q_{up} results in the following:

$$Q_{gain,Sim} = -Q_{up} \cdot ln[\frac{C_{down} - C_{gain}}{C_{up} - C_{gain}}] \tag{3.25}$$

Equation (3.25) is the solution for the condition that $Q_{up} = Q_{down}$ and applies to both $Q_{gain,Sim}$ and $Q_{loss,Sim}$ as they will produce the same result in that situation. This is only a mathematical exception and should not be needed in practice as Q_{up} and Q_{down} should not truly be equal when measuring in the natural environment due to the natural heterogeneity of streams and the inherent measurement error of the method to measure discharge.

Naturally occurring tracers (e.g. chloride salt) can also be applied to the SGE equations with additional information about C_{gain}. As long as a quasi-steady-state condition applies and that $Q_{gain} > 0$, the only additional information to be collected would be the C_{up} and C_{down} prior to the injection of the tracer. For the derivation, we can use any one of the three SGE methods (6 possible equations) and they all will produce the same final equation as the final equation is not reliant on spatial distribution assumptions. For a more thorough derivation starting from the initial mass balance equations, refer to Appendix A. For simplicity, we will use the $Q_{gain,LG}$ equation from equation (3.5). As the value of $Q_{gain,LG}$ will be the same before and after the tracer injection, we can make two versions of the $Q_{gain,LG}$ before and after the tracer injection with a different C_{up} and C_{down} prior to the injection of the tracer and post injection of the tracer.

$$\begin{aligned} & Q_{down}\left(\frac{C_{down,prior} - C_{up,prior}}{C_{gain} - C_{up,prior}}\right) = \\ = \quad & Q_{down}\left(\frac{C_{down,post} - C_{up,post}}{C_{gain} - C_{up,post}}\right) \end{aligned} \tag{3.26}$$

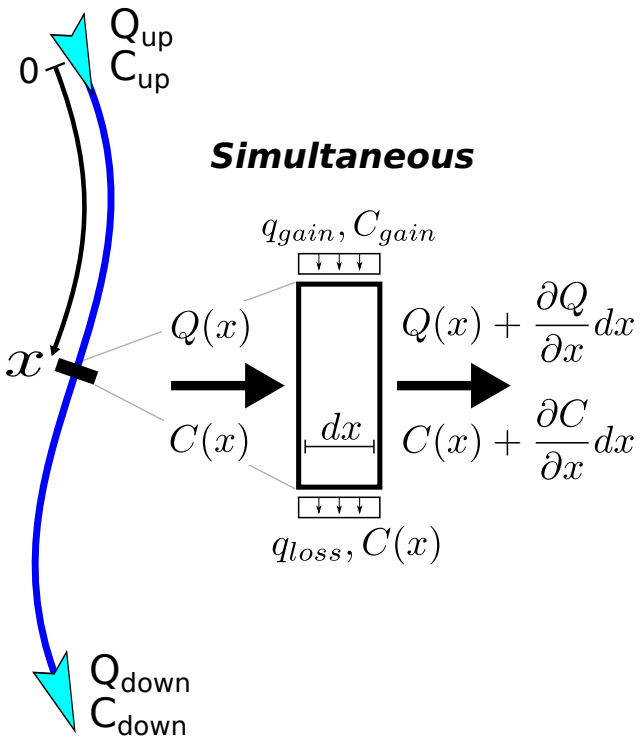

Figure 3.3: A conceptual representation of the analytical formulation of the SIM method.

With some rearrangement, we come to our final equation:

$$C_{gain} = \frac{C_{up,prior}C_{down,post} - C_{down,prior}C_{up,post}}{C_{up,prior} - C_{up,post} - C_{down,prior} + C_{down,post}} \tag{3.27}$$

where $C_{up,prior}$ is the upstream concentration prior to the tracer injection, $C_{up,post}$ is the upstream concentration from the tracer injection, $C_{down,prior}$ is the downstream concentration prior to the tracer injection, and $C_{down,post}$ is the downstream concentration from the tracer injection. The only main disclaimer to the application of this equation in the field is that the difference between $C_{up,prior}$ and $C_{down,prior}$ must be large enough to be statistically significant when estimated using available laboratory or field measurement techniques. The accuracy of the measurement techniques is a general problem for any chemical tracer test performed to estimate SGE. If the difference between the Q_{up} and Q_{down} is very small, much tracer may be needed to accurately measure a concentration difference between C_{up} and C_{down}. This issue will become more important with larger rivers as the proportion of the Q_{gain} and Q_{loss} to the Q_{up} is substantially reduced.

It would also be possible to estimate C_{gain} from groundwater piezometers adjacent to the bank of the stream. As the intent of our study was to determine integrated values over a stream reach rather than point values, we preferred to use equation (3.27) as it is an integrated value of C_{gain}.

The application of tracer methods to measure SGE in the field is typically performed by two different techniques: constant injection and slug injection. These two techniques have been well researched in the scientific community and will not be evaluated in this study (*Wagner and Harvey*, 1997; *Payn et al.*, 2008). Both techniques can be used with the above SGE methods and provide very similar results. As slug injections cause the C_{down} to not be in steady-state, C_{down} must be continuously measured and integrated over the measurable period of time. A more thorough explanation can be found in *Payn et al.* (2008, 2009); *Covino et al.* (2011). For simplicity, we will assume constant injection with steady-state conditions.

3.3.3 Evaluation methods

Analytics

All three SGE methods were broken down analytically to better understand the dynamics of the equations of the methods. We wanted to know what caused the differences in the results of the three SGE methods and how these differences were related. The relative differences between the methods were accomplished by the ratio of one method's equation to another both analytically and illustratively.

Numerical simulations

Perfect measurements or estimates of SGE are impossible using any existing method. Arbitrarily comparing results of different methods using field collected data will only indicate that the different methods produce different results, and it will not indicate if one method is more accurate than another. Consequently, we thought that it would be appropriate to simulate artificial streams with known SGE for comparisons. With SGE perfectly known, we could effectively evaluate the accuracy of the different methods.

We simulated the lateral inflows and outflows per unit length throughout a stream using an autoregressive integrated moving average (ARIMA) model performed using the arima.sim package in the R statistical computing environment (*R Development Core Team*, 2011). The routine generates a variety of artificial time series with both a randomness and memory component. To represent a small stream, the ARIMA model was designed to take a random discharge between 1-5 l/s as input discharge and a random input tracer concentration between 20-150 mg/l to represent practical tracer test concentrations.

In an attempt to create realistic simulations of the streams, we tuned the ARIMA model to have spatial flux dynamics based on studies using distributed temperature sensing (DTS) of groundwater inflows within streams (*Lowry et al.*, 2007; *Westhoff et al.*, 2007a; *Briggs et al.*, 2012; *Mwakanyamale et al.*, 2012). The quantitative surrogate we used for the spatial flux dynamics was the average length that the fluxes would switch from inflow to outflow or vice-versa within a stream reach. For example, if we simulate a stream with 1000m total length and the fluxes in this stream oscillates between inflows and outflows 10 times then the average length per switch would be 100m. For our

simulations, we used two different switch lengths of 100m and 200m and total stream lengths of 1000m and 2000m. The switch lengths had a strong linear relationship with the correlation lengths and resulted in correlation lengths of 40m and 70m for the switch lengths of 100m and 200m, respectively. Correlation length is commonly defined as the length at $1/e$ on the autocorrelation distribution (*Blöschl and Sivapalan*, 1995).

We used stream lengths of 1000m and 2000m in the simulations for two main reasons. First, the stream lengths of 1000m and 2000m scale well with the switching lengths of 100m and 200m and could easily be converted to non-dimensional values if needed. Second, the lengths fit within practical tracer test lengths that have been performed in the past to determine stream to groundwater exchange, albeit towards the upper end (*Covino et al.*, 2011). In practice, the appropriate stream lengths will be dependent on the discharge in the stream, the available mass of tracer, and the sensitivity and accuracy of the laboratory analytical methods.

The ARIMA model allowed us to create 5000 simulations of stream fluxes within a hypothetical stream. We ran four series of 5000 simulations. Series A had a 1000m stream length and a 100m average switch length, Series B had a 1000m and a 200m average switch length, Series C had a 2000m and a 100m average switch length, and Series D had a 2000m and a 200m average switch length. The spatial discretization of the model was 1m for all series and simulations. These four series of simulations were to test the effects of both length and intermittency on the stream flux methods. Without loss of generality, we defined $C_{gain} = 0$ for the simulations, which would be equivalent to the use of an artificial tracer (e.g. bromide salt) for the tracer test.

We tested two distinct assumptions when deciding on the appropriate SGE ARIMA model. One assumption was that both Q_{gain} and Q_{loss} can occur simultaneously at one point. For example, if the groundwater table is sloped perpendicular to the stream then water would be flowing into one side of the bank, while water would be flowing out of the other side of the bank. In this assumption, we created two separate and independent vectors of Q_{gain} and Q_{loss} along the stream. The second assumption was that both Q_{gain} and Q_{loss} cannot occur simultaneously at one point. In this assumption, only one vector of SGE was created that could oscillate between Q_{gain} and Q_{loss}. We decided to omit the option for simultaneity of Q_{gain} and Q_{loss} throughout the stream as this assumption coincided too closely with the assumption in the SIM method. To ensure a more rigorous evaluation against the SIM method, we decided to omit the ARIMA model assumption of simultaneity and only use the non-simultaneity assumption for the simulations.

We attempted to simulate the stream with realistic dynamics of SGE, but we also tried to keep the model complexity as simple as possible. Although we did attempt to cover a wide range of SGE conditions when creating the many simulations, undoubtedly we did not cover all possible SGE conditions that could exist in nature. Realistically, the scientific community does not even know the full range of possibilities for natural SGE. We have also likely created simulations of SGE that do not exist in nature. Both issues are unavoidable when creating hydrologic simulations, particularly with the stochastic generation approach used in this paper. The hope is that the flux distributions of the simulations do closely represent reality for the purpose of our evaluation.

The statistical evaluation consisted of several methods and procedures. First, we took all of the simulated scenarios (5000 in our case) within an individual series and averaged the inflows and outflows for each simulation. This gave us an average inflow to the stream and outflow from the stream over the entire length of the stream for each scenario and served as our "true" values of the fluxes that the other SGE methods would be compared to. Next, we calculated the SGE of each scenario using the three SGE methods from the starting and end values of the scenarios. We did not include additional randomness in the input values for the SGE methods, which would equate to measurement error. This is due to the large variety of measurement devices and techniques that could be used in a tracer test, and each device and technique would have different measurement errors associated with them. Additionally, we calculated the net flux (we will call "Net") simply by subtracting Q_{up} from Q_{down}. We considered the Net as the upper error benchmark for the evaluation as the estimation of Net requires less information and should therefore perform worse than the other three SGE methods that require more information.

Once the SGE was calculated for all of the methods to be evaluated, we used as a performance measure the absolute normalized error for method m and for each simulation i, defined as:

$$\varepsilon_i^m = \left| \frac{Q_{est,i}^m - Q_{true,i}}{Q_{true,i}} \right| ; i = 1, ..., 5000 \tag{3.28}$$

where $Q_{est,i}^m$ is the estimated gross gain or loss value from the SGE method m and simulation i and $Q_{true,i}$ is the average flux from the ARIMA model at simulation i. The results of ε_i^m are two vectors (one for gross gains and one for gross losses) for each of the four methods. Each vector contains 5000 elements, one for each scenario. To make an overall evaluation for each method, we simply took an average of all of the scenarios in each series for both vectors of gains and losses:

$$\bar{\varepsilon}^m = \frac{1}{n} \sum_{i=1}^{n} \varepsilon_i^m \tag{3.29}$$

where $\bar{\varepsilon}^m$ is the mean absolute normalized error (MANE) for each method m (either flux leaving the stream or entering the stream) and n is the total number of scenarios in each series (5000). This is a compound measure of relative bias and accuracy.

We also used the normalized root-mean-square error (NRMSE) as a supplement to the MANE:

$$NRMSE = \frac{\sqrt{\frac{1}{n} \sum_{i=1}^{n} (Q_{est,i}^m - Q_{true,i})^2}}{\frac{1}{n} \sum_{i=1}^{n} Q_{true,i}} \tag{3.30}$$

The use of the NRMSE to supplement the MANE is to provide a higher weight to larger errors and scatter as compared to the MANE.

In addition to calculating the $\overline{\varepsilon}^m$ for all of the SGE methods, we compared the ε_i^m within each of the SGE methods to determine how frequently one method outperformed another:

$$r_{m1,m2} = \frac{1}{n}\sum_{i=1}^{n}\begin{cases} 1 & \text{if } \varepsilon_i^{m1} < \varepsilon_i^{m2} \\ 0 & \text{if } \varepsilon_i^{m1} \geq \varepsilon_i^{m2} \end{cases} \tag{3.31}$$

where $r_{m1,m2}$ is the frequency of $m1$ SGE method outperforming $m2$ SGE method.

Once ε_i^m and $\overline{\varepsilon}^m$ were estimated, we wanted to determine the causes of the errors in the individual methods. This was accomplished through a correlation of the ε_i^m to various combinations of the input parameters.

3.4 Results

3.4.1 Analytics

When there is 0 flux of either Q_{gain} or Q_{loss} all three equations produce the same results. For example, if $Q_{loss} = 0$ then equation (3.2) becomes:

$$Q_{down} = Q_{up} + Q_{gain} \tag{3.32}$$

As Q_{down} and Q_{up} are previously known, there is only one solution for Q_{gain} regardless of the other equations. Similarly, as the ratio of Q_{gain} to Q_{loss} grows to infinity or to 0, the results for the three equations will converge.

Although somewhat obvious, if all of the assumptions are met for any of the SGE methods then the method will perfectly reproduce reality. For example, if there is only inflow to the stream from 1-100m followed by only flow out of the stream from 101-1000m then the GL(max) equation will estimate both fluxes perfectly.

If $Q_{gain} > 0$ and if $C_{gain} < C_{up}$ then $C_{down} < C_{up}$. Similarly, if $C_{gain} > C_{up}$ then $C_{down} > C_{up}$. This indicates that C_{up} and C_{down} are the concentration end points within the stream reach. As formulated in equations (3.7)–(3.10), the LG(min) and GL(max) equations are divided by the end point concentrations of the stream and will therefore represent the minimum and maximum values of fluxes within a stream reach. The LG(min) equations will always produce the minimum flux values, while the GL(max) equations will always produce the maximum flux values. Consequently, as LG(min) and GL(max) have the minimum and maximum flux values, the flux values for the SIM equations must be somewhere in between the two.

The GL(max) and LG(min) methods are very similar, and subsequently can be compared quite easily. Dividing the inflow and outflow equations for the two methods can show the rate of increase of one method over the other:

$$\frac{Q_{loss,GL}}{Q_{loss,LG}} = \frac{C_{up}}{C_{down}} \tag{3.33}$$

and

$$\frac{Q_{gain,GL}}{Q_{gain,LG}} = \frac{Q_{up}C_{up}}{Q_{down}C_{down}} \tag{3.34}$$

For both Q_{loss} and Q_{gain}, GL(max) grows from LG(min) at a rate proportional to the concentration ratio, and additionally Q_{gain} grows with load ratio. As Q_{loss} and Q_{gain} increase in a stream reach, Q_{down} will change and C_{down} will decrease. In the case of a lower C_{down} caused by higher SGE, the ratio between the results of GL(max) and LG(min) grows larger (Figure 3.4).

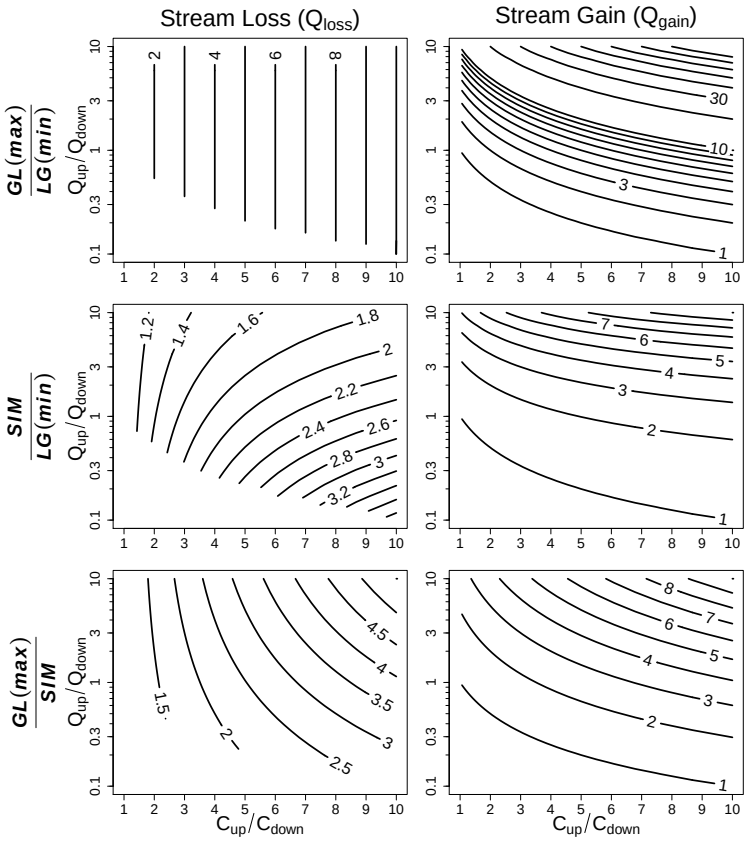

Figure 3.4: Relative comparisons between the different methods due to changes in the input ratios. The rows are the ratios of two of the SGE methods and the columns are the results for Q_{loss} and Q_{gain}. If we look at the two graphs in the second row for example, if the ratio of the input parameters C_{up} and C_{down} is 5 and the ratio of the input parameters Q_{up} and Q_{down} is 1 then the SIM method will result in Q_{loss} and Q_{gain} being approximately 2 times larger than the LG(min) method. The Y-axes of $\frac{Q_{up}}{Q_{down}}$ is on a logarithmic scale to ensure equal space weighting on the plot for Q_{up} and Q_{down}. The X-axes are plotted from 1 to 10 as $C_{up} \geq C_{down}$.

Unfortunately, the SIM method does not simplify nearly as well as the others due to the non-linearity of the SIM equations. For a better visual comparison, the three methods were plotted together with axes of concentration and discharge ratios (Figure 3.4). As shown analytically in equations (3.33) and (3.34), the ratio of GL(max) to LG(min) is insensitive to discharge for Q_{loss} and sensitive to both discharge and concentration for Q_{gain}. The ratios of SIM to the other methods illustrate the non-linearity of the method. The methods' ratios for Q_{gain} show a surprising similarity in the distribution of the contours even though the magnitudes are different.

3.4.2 Numerical simulations

Figure 3.5 presents the major input and output parameter density distributions created by the ARIMA simulations for the inflow and outflow profiles. The parameter distributions for Q_{loss}, Q_{gain}, and Q_{net} closely follow a normal distribution. As defined in the model, Q_{up} and C_{up} are equally distributed between 1-5 l/s and 20-150 mg/l, respectively.

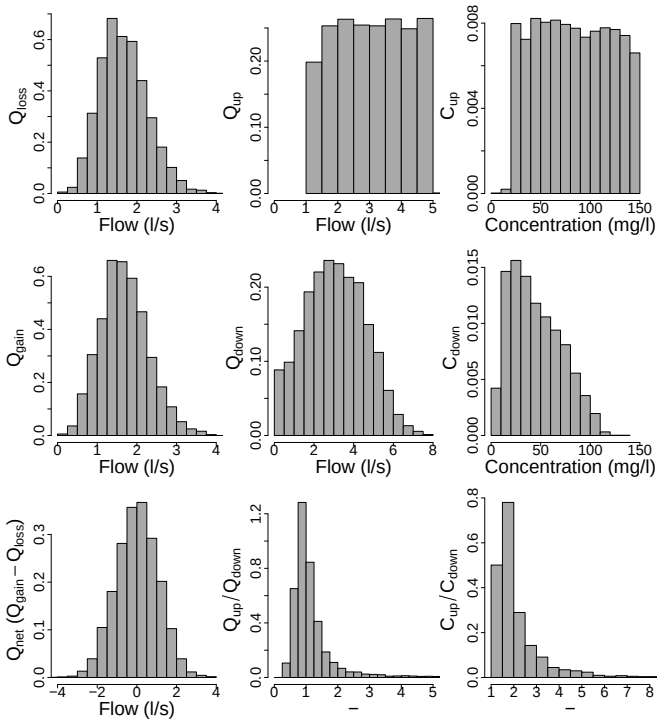

Figure 3.5: The major input and output parameter density distributions of the ARIMA numerical model for Series A (1000m with 100m average switch length).

The results of the numerical simulations are presented in Tables 3.1, 3.2, and 3.3.

Plots of the estimated gains and losses to the actual gains and losses for each of the methods for Series A are illustrated in Figure 3.6. The plots for the other scenarios have similar patterns only with a greater or lesser degree of spread. The numerical simulations indicate that the SIM SGE method is on average the best performer when compared to the other two SGE methods with a 1:1 slope to the true value, the lowest $\overline{\varepsilon}^m$ and the $NRMSE$ in every series, and the highest $r_{m1,m2}$ in nearly every series. However, the LG(min) method has a slightly higher $r_{m1,m2}$ to Net as compared to SIM. The LG(min) method also performed very well as compared to the SIM method according to the $NRMSE$. The LG(min) method had effectively the same error as SIM in Series B and is very close in Series D, both of which have the longer switch lengths. Interestingly, simply using the net discharge between upstream and downstream (Net) results in lower error values for $\overline{\varepsilon}^m$ as compared to GL(max) in both 2000m series and GL(max) performed poorer than Net in all Series according to the $NRMSE$. This is attributed to the fact that Net by definition cannot have an error of 1 or greater. Similarly, LG(min) also cannot have errors 1 or greater and must have errors less than those of Net. If 0 is used for all the values of Q_{gain} and Q_{loss} in the error assessment of $\overline{\varepsilon}^m$ then $\overline{\varepsilon}^m$ would be exactly 1. GL(max) and SIM can have errors greater than 1 as they can have values larger than the true value, which is clearly exemplified by the GL(max) equation's high $\overline{\varepsilon}^m$ and the $NRMSE$ in some series.

Figures 3.7 and 3.8 show the six simulations with the smallest ε_i^m for both LG(min) and GL(max). Not surprisingly, they performed best when the assumptions of the individual methods were met. Figure 3.9 shows the six simulations with the smallest ε_i^m for SIM. No obvious conclusion can be drawn from the simulations other than an evenly random spread between Q_{gain} and Q_{loss} with no clear spatial trend unlike the other methods.

The ratios of C_{up} to C_{down} and $Q_{up}C_{up}$ to $Q_{down}C_{down}$ show a strong correlation to the ε_i^m of the SGE methods (Figure 3.10). They are the same ratios that were found during the analytical evaluation described by equations (3.33) and (3.34). Both LG(min) and GL(max) have stronger correlations than SIM. SIM appears to have an error trend towards lower values rather than the full range of the correlation.

LG(min) and GL(max) also have a strong correlation to the midpoint concentrations and loads. GL(max) had a strong correlation to the ratios of C_{mid} (the midpoint of the concentration profile of the stream) to C_{down} and $Q_{up}C_{up}$ to $Q_{mid}C_{mid}$ (the midpoint of the load profile of the stream). LG(min) had a very strong correlation to the ratios of C_{mid} to C_{up} and $Q_{down}C_{down}$ to $Q_{mid}C_{mid}$.

3.5 Discussion

3.5.1 Stream to groundwater exchange methods evaluation

As described in earlier sections and shown by Figure 3.6, the LG(min) and GL(max) methods represent the minimum and maximum realistic SGE values and consequently will always produce SGE values below or above the true SGE values unless the individual

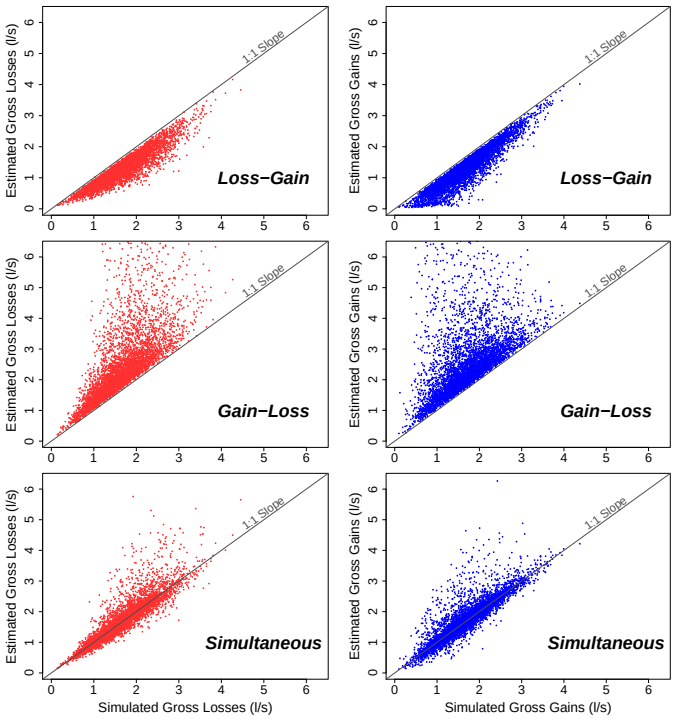

Figure 3.6: A plot of simulated inflow and outflow flux values by the estimated values from the three SGE methods using the Q_{up}, Q_{down}, C_{up}, and C_{down} from Series A simulations (1000m with 100m average switch length).

spatial flux assumptions are perfectly met. This does not mean, however, that the SGE estimates from LG(min) and GL(max) will be equidistant from the true SGE value as shown in Figure 3.6 and Tables 3.1 and 3.2.

LG(min) performed consistently better than GL(max) through all of the numerical simulation assessment measures (i.e. $\overline{\varepsilon}^m$, the $NRMSE$, and $r_{m1,m2}$). As described in the previous sections, the GL(max) equations can create results that can be many times larger than the other methods and consequently can be many times larger than the true value from the ARIMA model. Although these circumstance may account for a small proportion of the total simulations, they can cause the average error to be very high. These large deviations are exemplified in the $NRMSE$ measure due to the square of the difference. Net was clearly superior in Series C and D for the $\overline{\varepsilon}^m$ and for all Series for the $NRMSE$, but GL(max) had a solid majority over Net in the $r_{m1,m2}$. In the Series A, GL(max) and Net had a similar $\overline{\varepsilon}^m$, but according to $r_{m1,m2}$ GL(max) performed better almost 80% of the time. Indeed, if the top 10% of the simulations with the highest errors were removed from Series C then GL(max) and Net would have approximately the same $\overline{\varepsilon}^m$. Nevertheless, even with the help of removing 10% or 20% of the simulations with

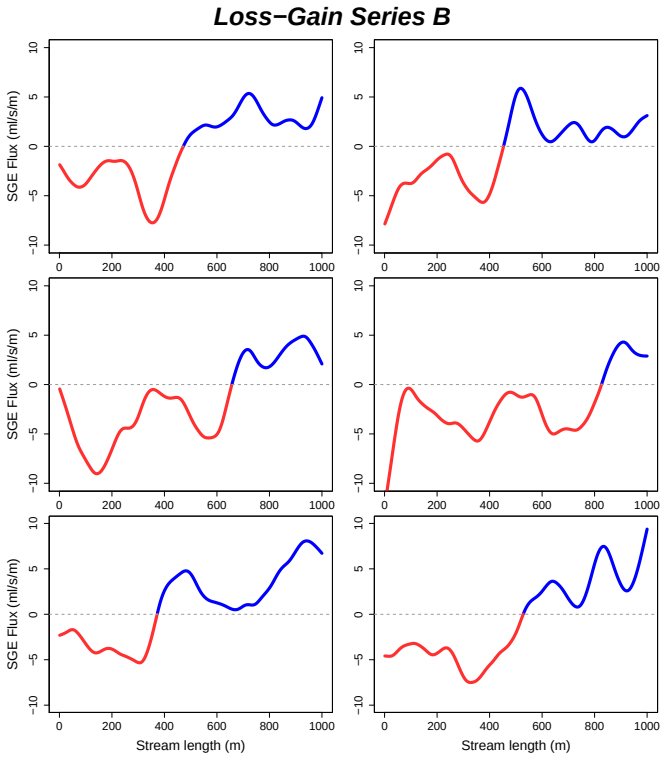

Figure 3.7: The simulated SGE profiles from Series B (1000m with 200m AVG switch length) of the six scenarios with the smallest normalized error (ε_i^m) for LG(min). A clear pattern can be seen according to the spatial assumption of the method. Predominant stream losses are at the beginning, while stream gains are towards the end of the reach. Red indicates losses, while blue indicates gains.

the highest errors, both LG(min) and SIM perform substantially better than GL(max).

Since the LG(min) and GL(max) methods bound the realistic values of SGE, any new method must have spatial flux distribution assumptions that cause the SGE estimate to be in between LG(min) and GL(max). The SIM method has such assumptions. The ARIMA stream simulation model randomly generated stream flows with a specific reach length and switching length, and this was to evaluate the effects of both reach length and intermittency on the three SGE methods. According to the $\overline{\varepsilon}^m$ and the $NRMSE$, LG(min) and GL(max) were affected by both the switch length and the stream length. SIM was affected by stream length, but was not significantly affected by switch length. As LG(min) and GL(max) are affected by switch and stream length, the reader can extrapolate from Table 3.1 that as the stream length decreases and the switch length increases the errors for LG(min) and GL(max) will continue to decrease and potentially below that of SIM.

No net emphasis on the Q_{gain} or Q_{loss} was programmed into the ARIMA model

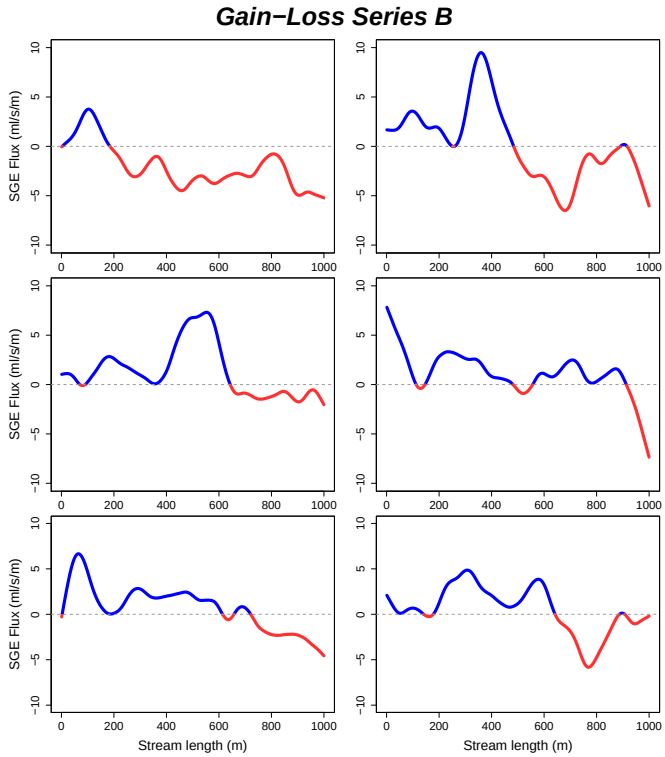

Figure 3.8: The simulated SGE profiles from Series B (1000m with 200m AVG switch length) of the six scenarios with the smallest normalized error (ε_i^m) for GL(max). A clear pattern can be seen according to the spatial assumption of the method. Predominant stream gains are at the beginning, while stream losses are towards the end of the reach. Red indicates losses, while blue indicates gains.

as shown by the normal distribution and mean of approximately 0 of Q_{net} in Figure 3.5. The introduction of a Q_{net} emphasis towards a higher Q_{gain} would cause the SGE estimates of Q_{loss} of the three methods to slightly decrease or stay the same and the SGE estimates of Q_{gain} to have significant improvement. A emphasis towards a higher Q_{loss} would cause the SGE estimates of Q_{loss} of the three methods to slightly improve or stay the same and the SGE estimates of Q_{gain} to have a significant reduction in accuracy. Nevertheless, the accuracy rankings would remain the same as those listed in Table 3.1. If a weight was introduced into the ARIMA model on one type of spatial flux distribution, then the SGE model (i.e. LG(min) or GL(max)) that most closely represented this weight would have a reduction in the error.

Most of the ε_i^m errors in LG(min) and GL(max) could be correlated by the ratio of the upstream and downstream concentrations for Q_{loss} and the ratio of the upstream and downstream loads for Q_{gain}. $Q_{loss,GL}$ had an especially strong correlation. LG(min) on the other hand had an especially strong correlation to the concentration and load

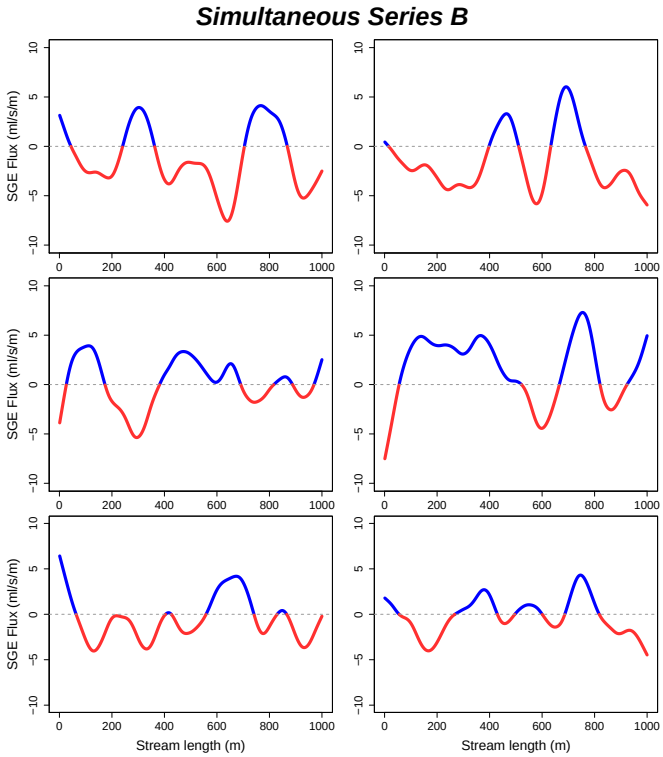

Figure 3.9: The simulated SGE profiles from Series B (1000m with 200m AVG switch length) of the six scenarios with the smallest normalized error (ε_i^m) for SIM. No consistent or obvious pattern can be seen within the scenarios. Red indicates losses, while blue indicates gains.

midpoints along the stream (not shown in figures). As with much of the previous results, the midpoint correlations follow precisely the assumptions of the methods. LG(min) assumes that the Q_{loss} occurs at the beginning and if the ratio of C_{mid} to C_{up} does not follow a relationship that the method assumes then it will produce a larger error. At least in LG(min), it appears that if the concentration ratio does not follow the predicted pattern by the time it reaches the midpoint then the method is more likely to create erroneous results. A similar pattern can be seen in GL(max), but not nearly as strong as the upstream and downstream ratios. Unfortunately, SIM did not have such clear correlations. There only appears to have an error trend towards smaller upstream and downstream ratios.

There is much scientific literature on the estimation of SGE from chemical tracers. Many have preferred to use the well established OTIS numerical model, which effectively solves the differential equations with a finite difference model with similar spatial flux assumptions to our SIM method. We found only one study that took the OTIS model and tested the three different assumptions that we also tested (*Szeftel et al.*, 2011).

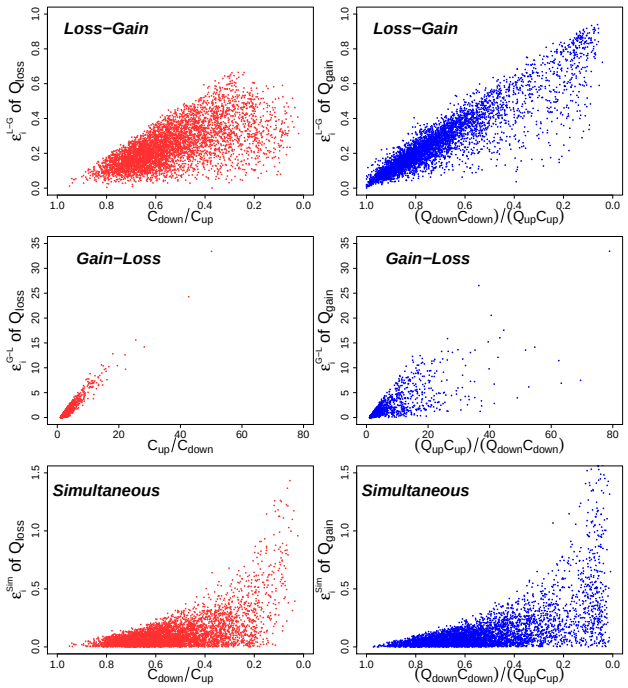

Figure 3.10: A correlation of various input parameters to the normalized error (ε_i^m) of the SGE methods for Series A. Both the LG(min) and GL(max) methods have strong correlations, while SIM only tends to have an error trend at lower ratios.

However, the reasoning behind their test appeared to be precisely the opposite of ours. As they stated in the methods, they assumed that simultaneous inflows and outflows at a single cell was unrealistic and implemented the LG(min) and GL(max) type scenarios to provide more realistic alternatives. Although they did not test the accuracy of the three methods, they concluded that the spatial flux distribution assumptions of the SGE methods have a significant impact on the SGE estimates and that breakthrough curve (BTC) analysis is not sufficient to determine the spatial variability.

Like us, others have instead preferred to use the more simple analytical equations to estimate SGE (*Harvey and Wagner*, 2000; *Payn et al.*, 2009; *Covino et al.*, 2011). One of the earliest to hint at using tracers with analytical equations to determine SGE was *Zellweger et al.* (1989). The use of tracers with dilution gauging to estimate SGE was only mentioned in passing as an explanation for the differences in the estimation of discharge from a flow meter and from dilution gauging. Later, *Harvey and Wagner* (2000) picked up on the idea of using dilution gauging with a current meter to estimate SGE. Their description for the procedure to estimate SGE was purely qualitative and did not fully explain the underlying assumptions in the method that they proposed (i.e. the spatial distribution of the fluxes). The dilution gauging method to estimate discharge was ref-

Table 3.1: $\bar{\varepsilon}^m$: The average value of ε_i^m for each series and for both Q_{loss} and Q_{gain}.

					SGE Method			
Series	Stream Length (m)	AVG Switch Length (m)	Corr. Length (m)	Flux Type	Net	LG (min)	GL (max)	SIM
A	1000	100	40	Q_{loss}	0.821	0.243	0.675	0.115
				Q_{gain}	0.821	0.264	0.849	0.135
B	1000	200	70	Q_{loss}	0.775	0.183	0.421	0.111
				Q_{gain}	0.763	0.204	0.591	0.143
C	2000	100	40	Q_{loss}	0.852	0.393	2.390	0.170
				Q_{gain}	0.855	0.422	2.949	0.194
D	2000	200	70	Q_{loss}	0.815	0.306	1.268	0.168
				Q_{gain}	0.821	0.339	1.652	0.202

erenced back to *Kilpatrick and Cobb* (1985). Based on the dilution gauging method and the description provided by *Harvey and Wagner* (2000), they effectively proposed the use of the GL(max) method. *Payn et al.* (2009) and *Ward et al.* (2013) estimated SGE using both the LG(min) and the GL(max) methods. They also found significant differences in the estimations between the two different methods and correctly identified that the LG(min) and the GL(max) methods produce the minimum and maximum values for SGE, respectively. Similar studies were also performed in sewer systems (*Rieckermann et al.*, 2005, 2007). Although in these studies, the conceptual model included only Q_{loss} and not Q_{gain} and subsequently did not need to use a spatial distribution of fluxes assumption to solve for Q_{loss}.

3.5.2 Connections with end-member mixing models

End-member mixing models or end-member mixing analysis (EMMA) as they tend to be known is a method to estimate the relative contributions of defined source waters at a specific downstream discharge measurement point. For example, EMMA can estimate the amount of groundwater contribution within a single hydrograph. EMMA is used extensively for this precise purpose.

Similarly to the SGE methods, EMMA uses the mass balance equations with distinct chemical tracers that represent the end-member sources to formulate the model. The EMMA equations start with the assumption that the discharge at a specific point along the stream (x) is composed of the source waters. We will name these sources Source 1 (S1) and Groundwater (GW):

$$Q(x) = Q_{S1}(x) + Q_{GW}(x) \tag{3.35}$$

where $Q(x)$ is the total discharge at location x along the stream, $Q_{S1}(x)$ is the part of $Q(x)$ from Source 1, and $Q_{GW}(x)$ is the part of $Q(x)$ from groundwater. The chemical

Table 3.2: $NRMSE$: The value of he $NRMSE$ for each series and for both Q_{loss} and Q_{gain}.

					SGE Method			
Series	Stream Length (m)	AVG Switch Length (m)	Corr. Length (m)	Flux Type	Net	LG (min)	GL (max)	SIM
A	1000	100	40	Q_{loss}	0.784	0.269	1.639	0.198
				Q_{gain}	0.776	0.267	1.624	0.196
B	1000	200	70	Q_{loss}	0.724	0.210	1.056	0.201
				Q_{gain}	0.705	0.205	1.029	0.196
C	2000	100	40	Q_{loss}	0.830	0.417	7.581	0.292
				Q_{gain}	0.834	0.419	7.617	0.294
D	2000	200	70	Q_{loss}	0.779	0.331	3.771	0.294
				Q_{gain}	0.786	0.334	3.807	0.297

load mass balance is the following:

$$Q(x)C(x) = Q_{S1}(x)C_{S1} + Q_{GW}(x)C_{GW} \tag{3.36}$$

where $C(x)$ is the concentration of $Q(x)$ at location x, C_{S1} is the concentration of Source 1, and C_{GW} is the concentration of the groundwater.

Unlike the SGE methods that apply the mass balance equations over the length of a stream reach, the EMMA equations only apply the mass balance equations at one specific point and as a result do not need the same spatial flux assumptions to solve the mass balance equations as the SGE methods (i.e. does not require a Q_{loss} term).

Combining equations (3.35) and (3.36) and solving for $Q_{GW}(x)$, we get the following:

$$Q_{GW}(x) = Q(x)\left(\frac{C(x) - C_{S1}}{C_{GW} - C_{S1}}\right) \tag{3.37}$$

Equation (3.37) will produce the same result regardless of the spatial flux assumptions associated with the SGE methods presented in this study.

Equation (3.37) is strikingly similar to equation (3.5). Indeed, if we apply the LG(min) method at an arbitrary discharge location (x) and use C_{up} as C_{S1}, then we would produce the same result for both EMMA and SGE (if we want to make the LG(min) spatial assumption). As described above, this is not due to shared assumptions. The LG(min) method assumes that all of the Q_{gain} enters the stream after the Q_{loss} and thus the Q_{gain} estimated by the LG(min) method must be the groundwater proportion of Q_{down}.

If EMMA can be applied to a single stream measurement location and produce the same results as the LG(min) SGE method, the next natural question would be could EMMA be applied on multiple downstream measurement locations and still produce the same results as LG(min)? If we estimate the groundwater proportions at two downstream

Table 3.3: $r_{m1,m2}$: The ratios of the frequency that the methods in the rows (*m1*) have a smaller ε_i^m than the methods in the columns (*m2*). In simpler terms, the table shows how often the methods in the rows outperform the methods in the columns.

			Denominator (*m2*)			
	Series	Method	Net	LG(min)	GL(max)	SIM
Numerator (*m1*)	A	Net	0.000	0.000	0.204	0.014
		LG(min)	1.000	0.000	0.711	0.149
		GL(max)	0.796	0.289	0.000	0.068
		SIM	0.985	0.851	0.931	0.000
	B	Net	0.000	0.000	0.143	0.022
		LG(min)	1.000	0.000	0.627	0.223
		GL(max)	0.857	0.373	0.000	0.163
		SIM	0.978	0.777	0.837	0.000
	C	Net	0.000	0.000	0.501	0.029
		LG(min)	1.000	0.000	0.869	0.109
		GL(max)	0.499	0.131	0.000	0.013
		SIM	0.971	0.891	0.987	0.000
	D	Net	0.000	0.000	0.352	0.037
		LG(min)	1.000	0.000	0.753	0.177
		GL(max)	0.648	0.247	0.000	0.067
		SIM	0.963	0.823	0.933	0.000

measurement locations using EMMA, could we subtract the two to get estimate gross gain of groundwater over that stream reach? Figure 3.11 illustrates the use of EMMA for estimating the groundwater proportions of the upstream ($Q_{GW,up}$) and downstream ($Q_{GW,down}$) measurement locations and the gross gains and losses from the two sources. In this scenario, we want to consider if $Q_{gain,EMMA} = Q_{GW,down} - Q_{GW,up}$. Using equation (3.37) at Q_{up} and Q_{down}, we get the following:

$$\begin{aligned} & Q_{gain,EMMA} = \\ = \; & Q_{down}\left(\frac{C_{down} - C_{S1}}{C_{GW} - C_{S1}}\right) - Q_{up}\left(\frac{C_{up} - C_{S1}}{C_{GW} - C_{S1}}\right) \end{aligned} \tag{3.38}$$

where $Q_{gain,EMMA}$ is the hypothetical Q_{gain} from the EMMA equations. To determine the underlying assumptions in the above equation, we must rearrange the equation back to the basic mass balance equation from equation (3.1) including both equation (3.38) and equation (3.2).

$$Q_{up}C_{up} + Q_{gain,EMMA}C_{GW} = Q_{down}C_{down} + Q_{loss}C_{S1} \tag{3.39}$$

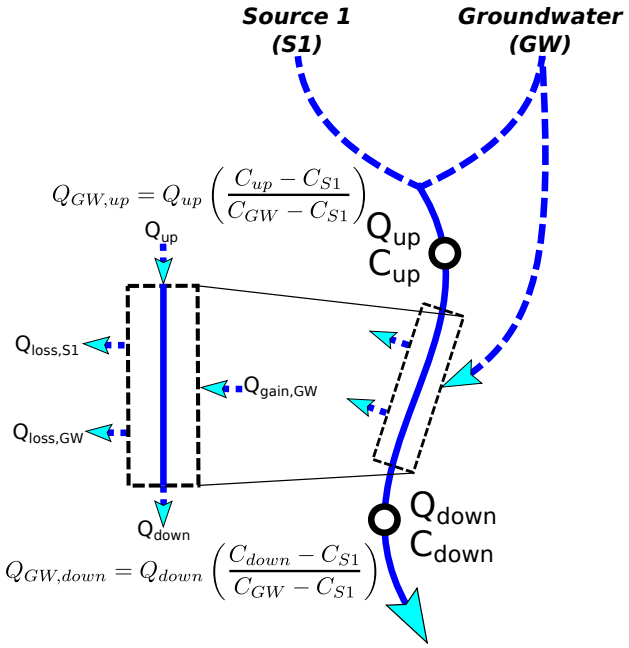

Figure 3.11: A conceptual illustration of the application of EMMA at two measurement locations along a stream reach and the associated gross gain and loss components between the two measurement locations. $Q_{GW,up}$ is the groundwater proportion of Q_{up} and $Q_{GW,down}$ is the groundwater proportion of Q_{down}. $Q_{loss,S1}$ is the gross loss specifically from Source 1, $Q_{loss,GW}$ is the gross loss specifically from the groundwater, and $Q_{gain,GW}$ is the gross gain from the groundwater (and the only gross gain). The SGE methods estimate the total gross loss ($Q_{loss,S1}+Q_{loss,GW}$) and gross gain ($Q_{gain,GW}$). Subtracting $Q_{GW,up}$ from $Q_{GW,down}$ estimates $Q_{loss,S1}$ and the net of the groundwater components ($Q_{gain,GW} - Q_{loss,GW}$).

As stated in Sec. (3.3.1), the LG(min) method assumes $C_{loss} = C_{up}$ and the GL(max) method assumes $C_{loss} = C_{down}$. C_{up} and C_{down} represent the end point concentrations within the stream and thus LG(min) and GL(max) represent the realistic minimum and maximum values for SGE. The use of EMMA according to equation (3.38) makes the final assumption of $C_{loss} = C_{S1}$ and represents a concentration end point potentially outside of C_{up} and C_{down}, which indicates that this is an unrealistic mass balance assumption for SGE models.

For the mass balance equation (3.39) to have physical meaning, we would have to redefine $Q_{gain,EMMA}$ and Q_{loss}. Q_{loss} would no longer be the gross loss from the SGE methods, but rather only the loss from Source 1 over the stream reach (we will rename $Q_{loss,S1}$). The other gross loss component is from the groundwater ($Q_{loss,GW}$). $Q_{gain,EMMA}$ would become the net groundwater components instead of only $Q_{gain,GW}$ (i.e. $Q_{gain,GW} - Q_{loss,GW}$). These flow components are shown in Figure 3.11. Conse-

quently, equation (3.39) can be rewritten with Q_{loss} replaced as $Q_{loss,S1}$ and $Q_{gain,EMMA}$ replaced with the appropriate net groundwater components:

$$\begin{aligned} & Q_{up}C_{up} + (Q_{gain,GW} - Q_{loss,GW})C_{GW} = \\ = \quad & Q_{down}C_{down} + Q_{loss,S1}C_{S1} \end{aligned} \tag{3.40}$$

Equation (3.40) is the solute mass balance for this scenario. The water mass balance would be the following (in the same form as equation (3.2)):

$$Q_{up} + Q_{gain,GW} = Q_{down} + Q_{loss,GW} + Q_{loss,S1} \tag{3.41}$$

If we combine equations (3.40) and (3.41) and solve for $Q_{loss,S1}$, we get the following equation:

$$Q_{loss,S1} = \frac{Q_{down}(C_{down} - C_{GW}) + Q_{up}(C_{GW} - C_{up})}{C_{GW} - C_{S1}} \tag{3.42}$$

The interesting aspect about equation (3.42) is that no spatial flux assumption is yet needed to solve the derivation unlike the SGE methods. $Q_{loss,S1}$ is independent of spatial flux assumptions and so is the result from equation (3.38) which represents $Q_{gain,GW} - Q_{loss,GW}$. Although both $Q_{gain,GW}$ and $Q_{loss,GW}$ must include a spatial flux assumption to be estimated individually, the difference will always be the same regardless of the spatial flux assumption. In this scenario, $Q_{gain,GW}$ can be estimated using the SGE methods described in Sect. 3.3 and subsequently the components of Q_{loss}. The additional information about Source 1 provides slightly more information about Q_{loss} without the necessity of a spatial flux assumption.

To take the EMMA and SGE combination to the final logical conclusion, we will include a scenario where there are two components inflows and outflows unlike the previous example with one inflow and two outflows. We will call the two sources "Source 1" and "Source 2" with variables names similar to those presented above. The mass balance for Q_{gain} for a stream reach is the following:

$$Q_{gain} = Q_{gain,S1} + Q_{gain,S1} \tag{3.43}$$

and

$$Q_{gain}C_{gain} = Q_{gain,S1}C_{S1} + Q_{gain,S2}C_{S2} \tag{3.44}$$

If we combine equations (3.43) and (3.44) and solve for $Q_{gain,S1}$, we get the following equation:

$$Q_{gain,S1} = Q_{gain}\left(\frac{C_{gain} - C_{S2}}{C_{S1} - C_{S2}}\right) \tag{3.45}$$

To estimate $Q_{loss,S1}$, we need to incorporate $Q_{gain,S1}$ into equations (3.40) and (3.41) and change the groundwater terms to Source 2. Combining the resulting equation and solving for $Q_{loss,S1}$ gives the following:

$$Q_{loss,S1} = \left(\frac{Q_{up}(C_{up} - C_{S2}) + Q_{down}(C_{S2} - C_{down})}{C_{S2} - C_{S1}} \right) - Q_{gain,S1} \tag{3.46}$$

Combining EMMA with SGE methods can provide valuable complimentary hydrologic information. They both require the same type of input data and as a consequence would be easy to apply together. They should not, however, be used interchangeably due to both conceptual and quantitative conflicts.

3.6 Conclusions

A new SGE estimation method is presented and derived analytically with the assumptions of constant, uniform, and simultaneous groundwater inflow and outflow throughout a given stream reach. This new method is compared to the two existing methods and presents the smallest error measures when applied to four different sets of artificially generated scenarios. The main control of the model performance for all three cases is the spatial dynamics of the actual SGE in relationship with the assumptions for each method. As the LG(min) and GL(max) methods bound the realistic values of SGE estimates, the SIM method, or any other new SGE method, produces SGE estimates between those two methods. Although this study found that the SIM method performed better against the numerical simulations, estimating SGE using all three methods would be very valuable as minimum and maximum SGE values can provide information on the full range of realistic SGE values. For the same inputs, the different assumptions of each method can lead to values of gross stream gains and losses differing up to one order of magnitude between approaches. Estimating SGE using the proposed simple analytical method over numerical models solving full hydrodynamic sets of partial differential equations has the clear advantages of much less complexity and less parametrization.

Although separate from the SGE methods, end-member mixing analysis can be used in conjunction with the SGE methods to acquire even more hydrologic information as both require the same type of input data. Nevertheless, these two approaches should not be used interchangeably as they estimate different stream variables and are based on distinct derivations and assumptions.

Chapter 4

The seasonal dynamics of the stream sources and input flowpaths of water and nitrogen of an Austrian headwater agricultural catchment

4.1 Abstract

Our study examines the source aquifers and stream inputs of the seasonal water and nitrogen dynamics of a headwater agricultural catchment to determine the dominant driving forces for the seasonal dynamics in the surface water nitrogen loads and concentrations. We found that the alternating aquifer contributions throughout the year of the deep and shallow aquifers were the main cause for the seasonality of the nitrate concentration. The deep aquifer water typically contributed 75% of the total outlet discharge in the summer and 50% in the winter when the shallow aquifer recharges due to low crop evapotranspiration. The shallow aquifer supplied the vast majority of the nitrogen load to the stream due to the significantly higher total nitrogen concentration (11 mg-N/l) compared to the deep aquifer (0.50 mg-N/l). The main stream input pathway for the shallow aquifer nitrogen load was from the perennial tile drainages providing 60% of the total load to the stream outlet, while only providing 26% of the total flow volume. The diffuse groundwater input to the stream was the largest input to the stream (39%), but only supplied 27% to the total nitrogen load as the diffuse water was mostly composed of deep aquifer water.

4.2 Introduction

Excessive discharges of nutrients to the aquatic environment have been found to adversely affect human health and aquatic ecosystems (*Romstad et al.*, 1997; *Walling et al.*, 2002). Mass algal blooms in rivers and lakes from an abundance of nitrogen and phosphorous can produce harmful toxins and encourage bacteria that subsequently reduce oxygen levels for fish stocks. This eutrophication of lakes, rivers, and coastal zones is currently one of the primary issues facing surface water environmental policy (*Clercq*, 2001). In response to public concern and scientific evidence over the hazards of water pollution, many developed countries, including the European countries and the European Union (EU) as a whole, have enacted environmental legislation to combat the growing problem of water pollution.

Agricultural management and catchment conditions regulate the nutrient conversions and release into the groundwater and surface water. These include fertilizer application rates and timing, crop type and growth periods, soil type and composition, precipitation rates and seasonality, the size of the riparian area, and many others. Improved knowledge on these important conditions and processes will improve the accuracy of nutrient transport models and ultimately better target those processes that can best reduce excessive nutrients to the water bodies. Natural systems are inherently difficult to isolate and test specific processes to determine the effect and sensitivity of those specific processes to the response of the entire system. Consequently, identifying and determining the causes of recurring changes in the nutrient concentrations and loads over several years in a single catchment where many of the catchment conditions are kept the same (e.g. soils, land management, etc.) may be more appropriate than comparing multiple different catchments with varying catchment conditions over the same period.

One of these recurring nutrient changes over several years that many researchers have observed is the seasonal pattern of nitrogen concentration in streams that increase in winter and decrease in summer. This phenomenon has been observed on all sizes of streams and rivers from headwater streams to major rivers. There are several explanations in the scientific literature for the apparent seasonality of nitrate loads and concentrations. One explanation is attributed to higher in-stream nitrogen uptake and denitrification rates during the summer as compared to the winter (*Mulholland et al.*, 2008; *Peterson et al.*, 2001; *Alexander et al.*, 2009). The second explanation is attributed to increased leaching from seasonal biochemical changes in the vegetation and soil microorganisms associated with certain source waters (*Holloway and Dahlgren*, 2001; *Ocampo et al.*, 2006; *Molenat et al.*, 2008; *Arheimer et al.*, 1996; *Burns et al.*, 2009). Many of these studies have attributed the riparian zone as the primary source of the seasonal biochemical changes and uptakes. Others have found that the seasonality is caused by changes in the relative source water contributions throughout the year without a clear impact from seasonal biochemical reactions (*Martin et al.*, 2004; *Grimaldi et al.*, 2004; *Pionke et al.*, 1999). A final possible candidate is the seasonal agricultural land management associated with fertilizer application timing and crop growth when direct surface runoff is significant.

There are wide varieties of catchments. Some have unique characteristics that only

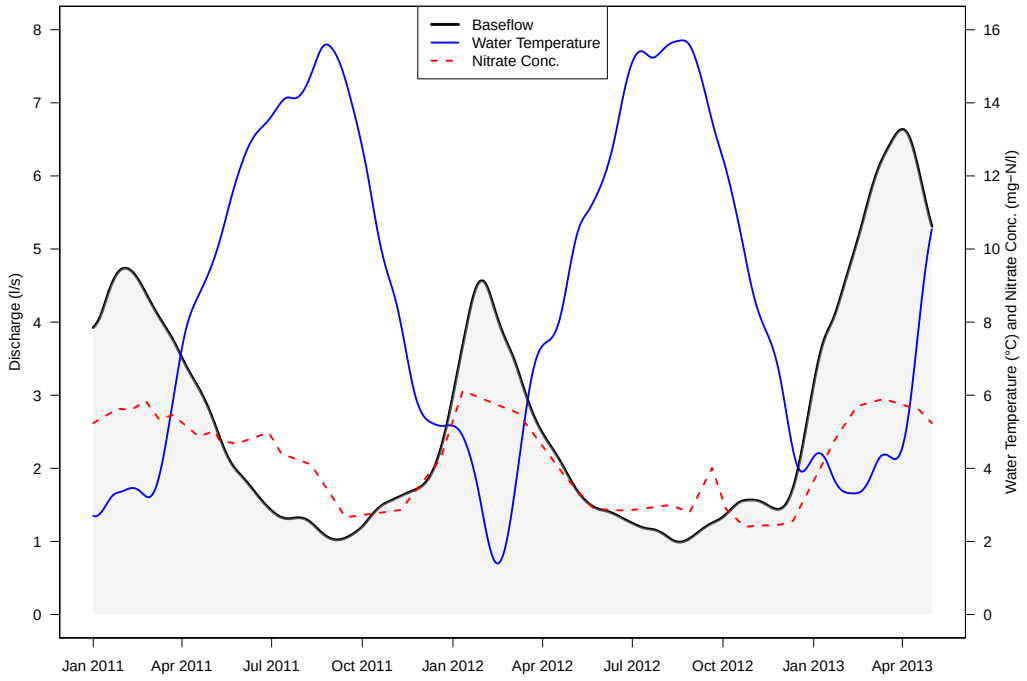

Figure 4.1: The baseflow discharge, nitrate concentration, and water temperature of the HOAL catchment surface water outlet from early 2011 to mid 2013.

exist in a few isolated locations, while others have typical catchment characteristics representative of broader regional catchments. We have chosen to investigate a headwater agricultural catchment that has typical characteristics of soils, land use, and precipitation for the region. These seasonal nitrate and total nitrogen concentrations have also been observed at our small headwater agricultural catchment called the Hydrologic Open Air Laboratory (HOAL) in Petzenkirchen, Austria (Figure 4.1).

The goal of our study is to determine the primary mechanisms that cause the seasonal dynamics of the nitrogen loads and concentrations at the surface water outlet of a headwater agricultural catchment. We accomplished this goal through analyses of monthly input and output totals of water and nitrogen loads entering and exiting the catchment, point and diffuse input contributions of water and nitrogen to the surface waters, and finally the source water contributions to the catchment outlet.

4.3 Field Site

The study was performed at the Hydrologic Open Air Laboratory (HOAL) catchment located in Petzenkirchen in Lower Austria, approximately 100km west of Vienna (Figure

4.2) (*Blöschl et al.*, 2016). The catchment is about 66 hectares in area with about 82% of arable land, 3% riparian forest, 5% planted trees with grass undergrowth, 8% grassland, and 2% impermeable surfaces (e.g. paved roads, buildings, etc.). It also has a first order stream that runs about 620m through the catchment (Figure 4.2).

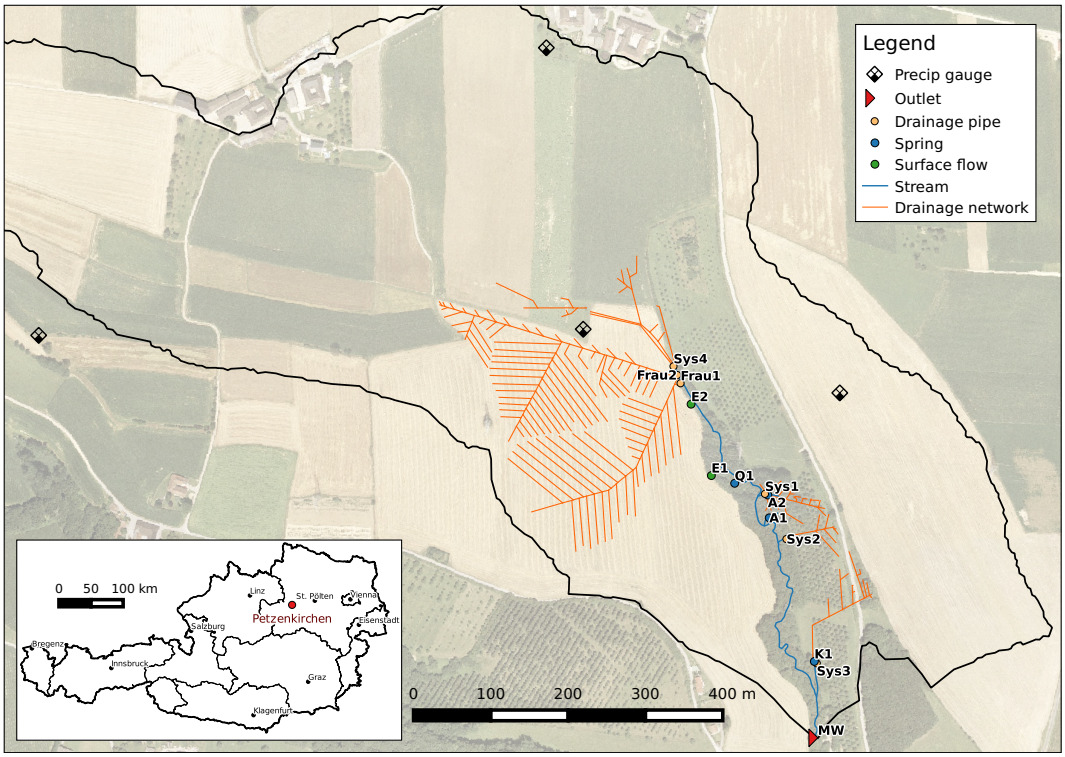

Figure 4.2: Overview map for the HOAL catchment in Petzenkirchen, Austria.

The catchment area of 66 hectares is defined as the topographic region where rainfall would flow over the surface and converge to the stream outlet gauge. The stream outlet gauge is named MW. 631 mm and 742 mm of precipitation fell during 2011 and 2012 respectively, while 133 mm and 124 mm left the catchment from surface waters for 2011 and 2012 respectively. The average discharge during these two years was 2.8 l/s and 2.6 l/s. There are six tile drainage systems along the stream named Sys1, Sys2, Sys3, Sys4, Frau1, and Frau2. Additionally, there are four known springs with two measured directly at the source (Q1 and K1) and two springs measured at a location 40 m down gradient of the actual springs before they enter the main stream (A1 and A2). There are also two locations on the edge of the riparian area that drain much of the overland flow during heavy rainfall events from the adjacent fields called erosion gullies (E1 and E2). Although the term spring may also refer to tile drainages that have perennial flow, springs in this study are defined as locations along the riparian area of the stream where water is visibly flowing out of the soil.

During normal baseflow conditions, water entering the stream at Sys4 will take approximately 3 to 4 hours to reach the catchment outlet. During this time, the riparian area provides almost continuous shading for the stream. The depth of the water in the stream ranges from 5 cm in the upper end to 20 cm at the outlet. The HOAL exhibits general properties which are typical throughout the range of catchments of the prealpine area alongside the eastern Alps with intensive agriculture associated with the seasonality of rainfall, runoff, and drainage density (*Merz and Blöschl*, 2007).

Based on a detailed soil survey conducted in 2010, the soils throughout the catchment are generally classified as silt loam or more specifically as Cambisols that have 7.2% sands (0.51 coefficient of variation (CV)), 68.7% silts (0.11 CV), and 24.1% clays (0.30 CV) (*Deckers et al.*, 2002). The Cambisols also have hydromorphic characteristics such as Stagnosols and Gleysols, and these types of soils cover almost 50% of the land of the federal province of Lower Austria. The soil survey found that the silt loam extends vertically at least 0.7 m below the surface throughout the catchment. A detailed geologic survey has not been performed in this catchment, but based on core samples from piezometers placed in and around the riparian area and production wells installed by the local farmers the silt loam extends down approximately 5 to 7 m below the surface where it meets a fractured siltstone unit. There is neither information about the thickness of the fractured siltstone unit nor what geologic units are below it. Due to the high clay and silt content of the soil, cracking of the soil occurs frequently during the dry summer months.

The deep aquifer is defined as the water contained within the fractured siltstone unit, while the shallow aquifer is associated with the water draining the shallow subsurface soil (i.e. the silt loam) (Figure 4.3). The origin of the Q1 spring can be seen visually as this fractured siltstone, and subsequently the water from Q1 is used to define the water from the fractured siltstone unit. The chemical and hydrologic dynamics of the deep aquifer are distinctly different from water draining the shallow aquifer. The shallow aquifer water is primarily identified by the baseflow water from the perennial tile drainages (i.e. Sys2 and Sys4) as most of the tile drainages were installed between 1 to 1.5 m below the surface. Distinct chemical characteristics of the deep aquifer as compared to the shallow aquifer include a much lower nitrate concentration, generally higher chloride concentration, much lower dissolved oxygen concentration, higher dissolved silica concentration, and higher ammonium concentration. The other distinct difference between the two aquifers is that the deep aquifer has a lack of hydrograph dynamics during rainfall events. At most discharge inputs to the stream, the associated hydrographs during rainfall events show clear increases associated with the rainfall event magnitude. The inputs to the stream that are purely deep aquifer water (e.g. Q1) show no such dynamics during rainfall events and only change gradually associated with monthly or seasonal hydrologic conditions.

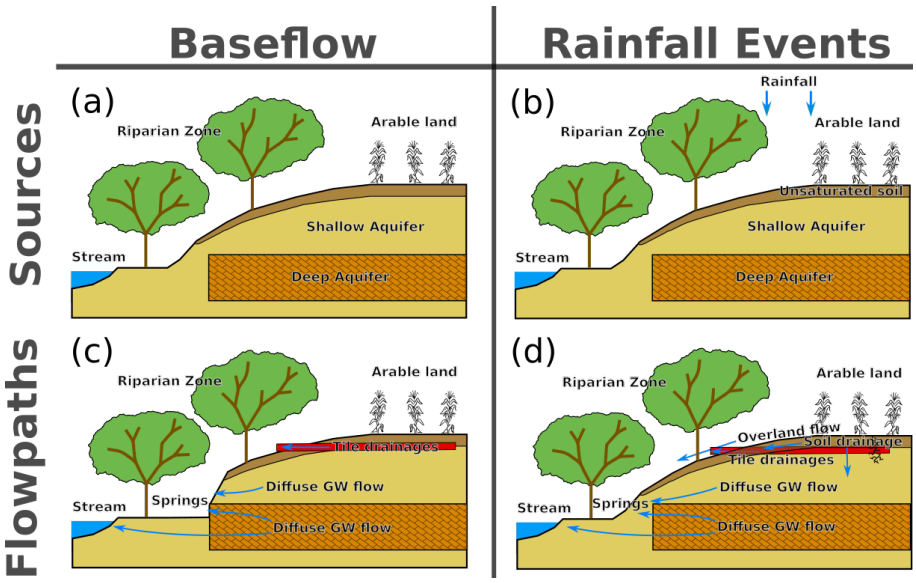

Figure 4.3: A schematic diagram of the sources and pathways of water and nitrogen during baseflow and rainfall conditions in the HOAL catchment. Diagrams (a) and (b) illustrate the source reservoirs during baseflow and rainfall event conditions, and diagrams (c) and (d) illustrate the flowpaths of the water and nitrogen from the reservoirs to the stream during baseflow and rainfall event conditions. The main reservoirs for stream baseflow are the shallow aquifer and the deep aquifer, and in addition to the previously mentioned aquifers the unsaturated soil and the rainfall are the source reservoirs during rainfall events. Diagram (c) illustrates a slightly different cross-section where the deep aquifer outcrops into the riparian zone and manifests as a spring. This cross-section is representative of the location of the Q1 spring found in Fig. 4.2. In both (c) and (d), diffuse groundwater (GW) flow through the soil matrix and macropores are important flowpaths in addition to tile drainage discharge.

4.4 Methods

4.4.1 Available data

Manual grab samples were collected at all point discharge inputs along the stream including MW (Figure 4.2). These water samples were collected once every 1-4 weeks during 2010-2013 and were analyzed for many physical and chemical parameters. The parameters used in this study include nitrate nitrogen (NO_3-N), total nitrogen (TN), total phosphorus (TP), dissolved silica, and discharge. Two 24-bottle autosamplers were installed at MW to collect samples of flow during rainfall events.

MW has all flow routed through an H-flume to capture both baseflow and runoff events. Water level was measured continuously using two independent devices that included a pressure sensor installed in a submerged pipe connected below the H-flume

and an ultrasonic water level sensor installed within the H-flume. Both were used to estimate discharge from calibrated water level to discharge relationships (*Shaw*, 2011). The two independent water level devices were used to assess the uncertainty in the discharge estimation associated with the water level measurements.

In addition to discharge, MW was measured continuously for nitrate using an Ion Sensitive Electrode (ISE). Other physical and chemical parameters were measured at MW and other sites, but are unrelated to this study. The ISE device had an offset calibration performed approximately once a month and a 2-point calibration was performed twice a year. Sys1, Sys2, Sys4, and Q1 flow at least 0.05 l/s throughout the year, while all of the other stations run dry or below 0.01 l/s for some time during the year. The piezometers installed along the riparian zone had water samples taken four times between 2011 and 2012 in addition to water samples in the stream in close proximity to the piezometer groups.

Three precipitation gauges located within the catchment used precision weighting systems to measure precipitation during 2011 and 2012. The precipitation gauges are distributed evenly throughout the catchment. The gauges measure near real-time (nRT) precipitation at 1 minute intervals. No post-processed corrections to the precipitation data were performed. A meteorological station is located within the town of Petzenkirchen less than 1 km from the catchment and is maintained by the Federal Agency for Water Management, Institute for Land and Water Management Research (IKT). From 2011 to 2012, this station measured incoming solar radiation, sunshine hours, minimum and maximum temperature, minimum and maximum relative humidity, wind speed, wind direction, and precipitation at daily intervals.

Detailed land management information from a survey of the land owners was obtained for 2011-2012 and this information included the plowing, fertilization, sowing, and harvesting schedules for all parcels within the catchment.

Missing data

Every continuous measurement device had some periods without measurements. This can be attributed to device failure, transmission failure, or data storage failure. Regardless of the type of failure, data are either completely missing or of such low quality that they are unusable. The missing data were estimated to complete the analyses for this study.

During the period from 2011-2012, there were 126 runoff event hydrographs captured at MW that exceeded a rise in discharge above baseflow of 2 l/s. There were 9 additional runoff events that were not captured at MW due to equipment failure and identified based on the rainfall time series. There were 37 runoff events at MW that captured both water chemistry (i.e. chloride and nitrate) and discharge continuously out of the 135 total runoff events.

Rainfall data was missing from 2012-02-10 to 2012-03-25. Missing rainfall data were estimated from the daily rainfall data from the Petzenkirchen meteorological station. Missing event runoff volume data at MW were estimated from a log-log linear regression

to the total rainfall associated with the event. Missing data of the rainfall and event runoff volumes did not overlap.

Missing data for baseflow parameters of any station (i.e. discharge and water chemistry) were estimated based on a normal linear regression to the outlet baseflow. Missing data for the runoff event parameters of any station were estimated based on a log-log linear regression to the event runoff volumes of the outlet. These differences in the type of regressions were used to ensure that the correlation had a relatively equal distribution throughout the range of the values.

4.4.2 Monthly Water and Nitrogen Input and Output Components

The primary water and nitrogen inputs and outputs of the catchment were estimated for the years 2011 and 2012. The water components include precipitation, evapotranspiration (ET), and surface water discharge. Other water components like deep groundwater seepage were not included due to lack of data. The nitrogen components include fertilizer applications, crop harvests, and surface water nitrogen load. Other nitrogen components like denitrification were not included due to lack of data.

Precipitation was measured using the precipitation gauges described in Sect. 4.4.1. Discharge was aggregated at the catchment outlet for the total volume of water leaving the catchment per month. Daily ET was estimated using the procedures developed by the Food and Agricultural Organization of the United Nations (FAO) for crop ET (ET_c) (*Food and Agriculture Organization of the United Nations*, 1998). Daily reference ET (ET_o) was estimated for 2011 and 2012 from the meteorological data of the Petzenkirchen station from Sect. 4.4.1 using the FAO procedures. A daily time series of crop coefficients (K_c) were assigned to each parcel of land within the catchment based on the land management data and the procedures outlined in the *Food and Agriculture Organization of the United Nations* (1998).

The event runoff volumes were separated from the complete hydrograph from 2011-2012 by constructing a straight line from the initial rise of the hydrograph to the inflection point at the trailing limb of the hydrograph on a semi-log plot (*Shaw*, 2011). Baseflow nitrate loads were estimated by assuming that the baseflow nitrate concentrations during the events were the same as the baseflow concentrations before the events. The prior baseflow nitrate concentrations were multiplied by the extracted baseflow discharges to estimate baseflow nitrate loads.

Fertilization and harvest data were gathered about the land management within the catchment and converted to kg of TN (*Wendland et al.*, 2011). Pig manure slurries were applied to the fields in addition to mineral fertilizers. The surface application of manure slurry as performed in the HOAL catchment volatilizes significant amounts of ammonia from the slurry into the atmosphere. Many studies have measured or estimated the ammonia volatilization from manure slurry and have found that there is a wide range in the rates (*Huijsmans et al.*, 2003; *Misselbrook et al.*, 2004; *Mkhabela et al.*, 2009; *Gordon et al.*, 2001; *Chantigny et al.*, 2004; *Moal et al.*, 1995). We decided to assume that 35% of the manure application was lost as ammonia volatilization based on both *Huijsmans et al.* (2003); *Misselbrook et al.* (2004), because the value is consistent and fairly average

throughout the literature. Ammonia volatilization losses were removed from the total fertilizer estimate presented in the manuscript.

Total nitrogen was measured for the manual grab samples, but only nitrate was measured continuously during the bulk of the rainfall events. The grab sample total nitrogen data was then correlated to nitrate using a normal linear regression. The resulting equation from the linear regression was used to estimate total nitrogen from the continuous nitrate data for rainfall events. The R^2 and normalized root mean square error (NRMSE) of the linear regression was 0.996 and 0.045 respectively. The mean ratio of nitrate load to total nitrogen in the grab samples was 0.93 from 58 samples.

4.4.3 Flowpath Input Assessment

The flowpaths were categorized by how the water physically flows into the stream. Some flowpath inputs are self-explanatory to the descriptions given in earlier sections (i.e. tile drainages, springs, surface waters, and the erosion gullies). The one additional stream input is the diffuse groundwater flowpath. The net diffuse groundwater input was defined as the residual difference of the total discharge from the outlet (MW) to the sum of all the point inputs to the stream. The net diffuse input calculation makes the assumption that no water is flowing from the stream to the groundwater.

Mean yearly concentrations were estimated for all of the inputs by dividing the total yearly loads by the total yearly discharge. The seasonal flowpath input contribution assessment used grab samples from 2010-2013 for all input locations and an estimated baseflow time series extracted and smoothed from the continuously monitored discharge at MW.

In both the yearly lumped baseflow assessment and the seasonal flowpath input contribution assessment, water samples were taken at locations directly before these inputs would enter the stream. As the stream is approximately 620 m long, some inputs may spend longer or shorter periods of time in the stream than others. For example, Sys4 is the initial inflow to the stream and subsequently the water from Sys4 spends the longest period in the stream, while A1 and A2 enter at approximately halfway. Past tracer experiments within the stream (unpublished) and much scientific literature has shown that streams frequently exchange water between the groundwater and the stream water itself (*Covino et al.*, 2011; *Harvey and Bencala*, 1993; *Payn et al.*, 2009; *Lowry et al.*, 2007; *Covino and McGlynn*, 2007; *Briggs et al.*, 2012; *Westhoff et al.*, 2007b). Consequently, the pathway assessment may sum all of the masses at the input locations and subtract that from the total mass at the outlet to determine a net diffuse groundwater input to the stream, but in reality the true proportions of the input pathways to the outlet will be lower in proportion to the distance the water has traveled. The diffuse groundwater input contribution to the outlet on the other hand will be higher due to the losses of the other pathways and the gains from the groundwater.

Tile drainages are typically installed in the shallow subsurface, consequently in our catchment they would normally drain the shallow aquifer water. This appears to be true at all locations except one. Although the water at Sys1 flows out of a drain pipe, the water flowing out of Sys1 is chemically and dynamically water from the deep aquifer rather

than the shallow aquifer. Likewise, not all springs are from the deep aquifer. Chemically and dynamically, the water from K1 is distinct from the shallow aquifer. From the historic maps, the location of K1 has a corresponding drainage system associated with it. The original outflow drainage pipe of K1 may have either collapsed or had been removed in the past, nevertheless flow is still routed to the original outlet location and currently manifests as a spring. A1 and A2 appear to be chemically and dynamically a combination of both the shallow and deep aquifer.

4.4.4 Baseflow Source Separation Assessment

The end member mixing analysis (EMMA) performed on the outlet baseflow used mass balance equations for a two end member EMMA (*Exner-Kittridge et al.*, 2014). The aggregated nitrate concentrations of known deep aquifer inputs (i.e. Q1 and Sys1) and the perennial tile drainages (i.e. Sys4 and Sys2) were used as the two end-member concentrations for the deep aquifer and the shallow aquifer respectively.

$$Q_{DA} = Q_{MW}\left(\frac{C_{MW} - C_{SA}}{C_{DA} - C_{SA}}\right) \tag{4.1}$$

where Q_{DA} is the deep aquifer water contribution at MW in l/s, C_{MW} is the concentration of nitrate at MW in mg-N/l, C_{SA} is the end-member concentration of nitrate of the shallow aquifer water in mg-N/l defined above as the aggregated flow proportional concentration of the perennial tile drainages, and C_{DA} is the end-member concentration of nitrate of the deep aquifer water in mg-N/l defined above as the aggregated flow proportional concentration of the deep aquifer point discharges. Equation (4.1) was applied at every time period when grab sample data with discharges and nitrate concentrations were available.

4.4.5 Uncertainty Estimations

Uncertainty in yearly and monthly rainfall aggregates are due primarily to the spatial heterogeneity of rainfall distribution (*Grayson and Blöschl*, 2001). Assuming that the available rainfall gauges are distributed evenly throughout the catchment, a basic estimate of spatial uncertainty in rainfall distribution is the standard deviation of the yearly totals of the individual precipitation gauges. As described in Sect. 4.4.1, the missing rainfall data was filled from rainfall data from the Petzenkirchen weather station. As the amount of missing data was a little over a month, the uncertainty estimates associated with the Petzenkirchen data was determined by aggregated monthly comparisons of the HOAL data to the Petzenkirchen data for 2012. The root mean square error (RMSE) between the HOAL data and the Petzenkirchen data of these months was used for the uncertainty values.

ET_c uncertainty was estimated by comparing the yearly and monthly ET_c and ET aggregates from estimates of an eddy covariance station (ET_{eddy}) installed within the catchment. The eddy covariance station was not installed until August 2012, so ET_c and ET_{eddy} could be compared for the end of 2012 through 2013. The RMSE between

the monthly totals of the ET_c and ET_{eddy} for the available months were used for the uncertainty values.

The discharge uncertainty for the monthly aggregations was estimated from duplicate continuous water level measurements acquired at MW. The estimated discharge from the pressure sensor water level was compared to the ultrasonic sensor estimated discharge, and the average normalized difference between the estimates of the two devices was used as the value of uncertainty.

The uncertainty for the continuous measurements of nitrate were estimated by comparing the field calibrated measurements of nitrate to the periodic grab sample nitrate concentrations from laboratory measurements. Differences in the concentrations were made at all grab sample times and linear interpolations were performed during the periods between the grab sample times to create a continuous series of nitrate concentration differences. These differences were normalized to the continuous nitrate measurements from the ISE devices and aggregated monthly to estimate the monthly nitrate concentration uncertainty.

Uncertainty for the fertilizer applications and crop uptake were not estimated due to a lack of information on the uncertainty of the associated data.

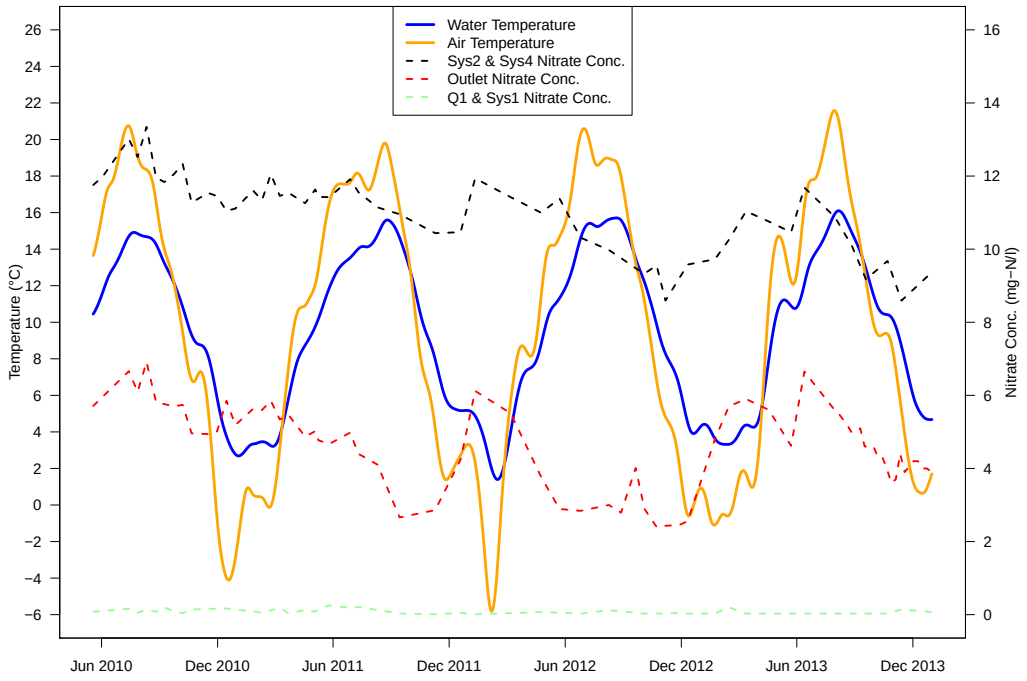

Figure 4.4: Air and stream water temperature overlaid with the nitrate concentrations of the end-members and MW during mid-2010 to the end of 2013.

4.5 Results

The air temperature at the Petzenkirchen weather stations and the outlet water temperature from mid-2010 to the end of 2013 are shown in Figure 4.4. Superimposed onto the temperatures are the nitrate concentrations of the deep aquifer point inputs (i.e. Q1 and Sys1), the shallow aquifer point inputs (i.e. Sys2 and Sys4), and the catchment outlet (i.e. MW). The outlet discharge during the summer and winter periods are about 1.0 and 4.5 l/s respectively, and the nitrate concentrations are about 2.7 and 6.0 mg-N/l. The yearly cycles of temperature are clearly seen and are consistent throughout the several years and range from 2 to 16 °C. Linear regressions of nitrate concentrations to discharge and water temperature for all available data from mid-2010 to the end of 2013 are shown in Figure 4.4. A smaller subset of the data is also illustrated for the nitrate to water temperature regression from early 2011 to April 2013.

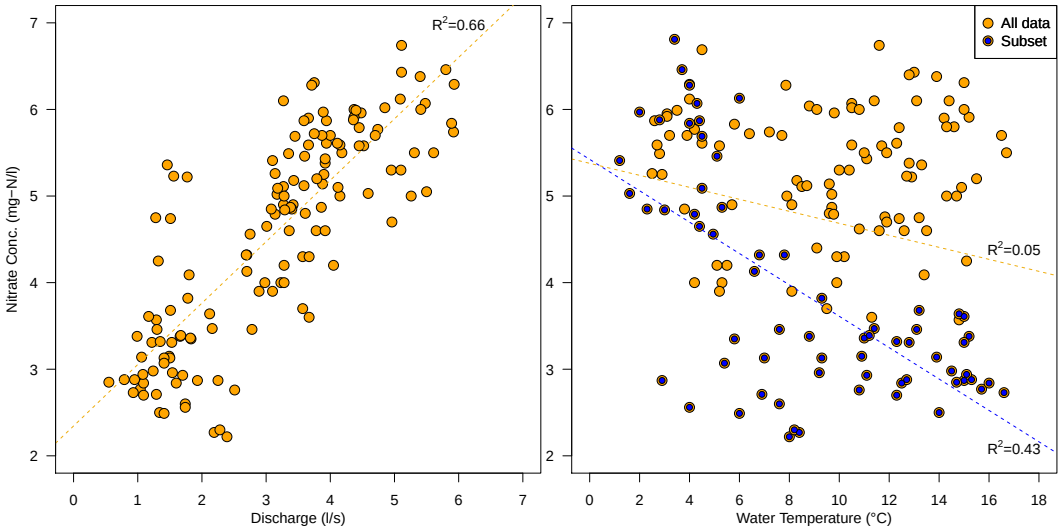

Figure 4.5: Linear regressions of nitrate concentrations to discharge and water temperature. All data includes the years from mid-2010 to the end of 2013, while the Subset includes only data from early 2011 to April 2013 represented by Fig. (4.4).

The monthly totals of the main water budget components are shown in Figure 4.6. Precipitation is generally distributed around the summer months, but winter months can also provide significant amounts of precipitation. Baseflow dominated the total surface water outflow from 2011-2012 with 82% as compared to event flow from 2011-2012. Two rainfall events in mid-January of both years accounted for 56% of total event flow volume for both years. ET_c tends to follow the incoming solar radiation intensity and the number of sunshine hours throughout the year. Discharge on the other hand is highest around winter and spring when ET is low and precipitation is moderate and slowly diminishes through to autumn.

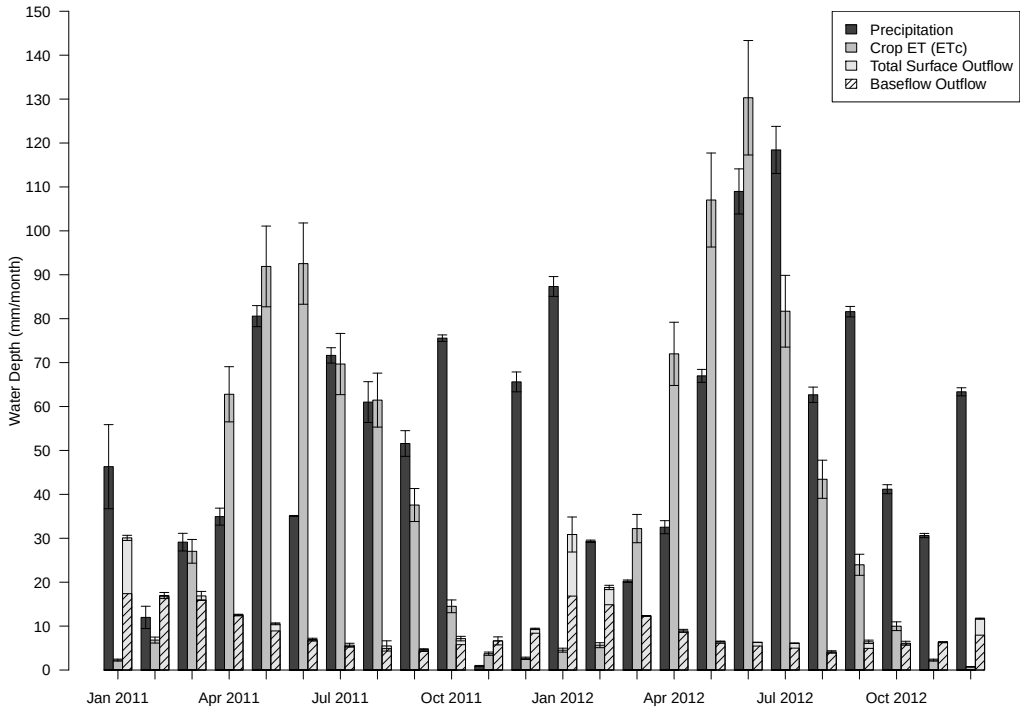

Figure 4.6: The monthly totals of the water budget components (i.e. precipitation, crop ET, and surface water outflow) to the contributing area above the catchment outlet (MW). The bracketed lines at the top of each monthly bar are the uncertainties in the form of standard deviations.

Figure 4.7 shows the three main nitrogen components that were aggregated monthly. Fertilizer applications primarily occur in spring and autumn and crop nitrogen uptake follows the pattern of ET_c. Similarly, the total monthly outlet nitrogen load followed the seasonal pattern of the total monthly runoff volume. Similar to the baseflow water volume contribution, the contribution of the baseflow TN load was 73% compared to event TN load from 2011-2012. During most of the year, the baseflow accounts for nearly all of the total discharge and nitrate load.

The yearly pathway nitrogen concentrations and contributions to the outlet for 2011 and 2012 are shown in Table 4.1. For both years, the net diffuse discharge has the highest contribution to the outlet with about 38%, while the perennial tile drainages and the deep aquifer point discharges contribute an equal amount to the outlet and most of the remaining water (i.e. about 26%). The perennial tile drainages contribute most of the TN load to the outlet (i.e. about 60%) followed by the diffuse discharge (i.e. about 26%). The high contribution of the perennial tile drainages are attributed to the relatively high TN concentrations of over 11 mg/l compared to the other water pathways.

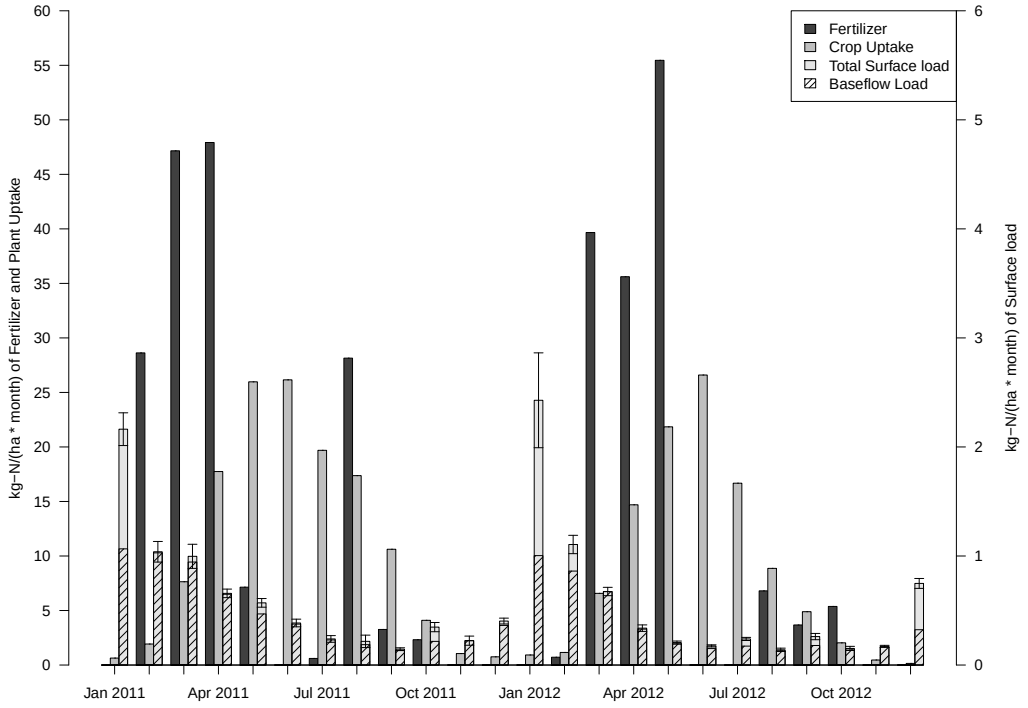

Figure 4.7: The monthly totals of the nitrogen budget components that could be estimated on a monthly basis (i.e. fertilization, crop nitrogen uptake, and surface water load outflow) to the contributing area above the catchment outlet (MW). The bracketed lines at the top of the surface load bar are the uncertainties in the form of standard deviations.

The outlet baseflow dynamics from mid-2010 to the end of 2013 is shown in Figure 4.8. As can be inferred from the discharge in Figure 4.8, the summers of 2010 and 2013 were substantially wetter than 2011 and 2012. The precipitation amounts from the Petzenkirchen meteorological station for 2009, 2010, and 2013 were 1020, 735, and 930 mm. While 2009 and 2013 were exceptionally wet years, 2010 had approximately the same amount of precipitation as 2012 only distributed differently within both years. The nitrate concentration at the outlet oscillates closely to the rise and fall of the baseflow during these years. The nitrate concentrations of the tile drainages and deep aquifer point pathways (i.e. Q1 and Sys1) do not show a similar distinctive oscillation. Although the input pathway nitrate concentrations do not show a seasonal trend, the baseflow contributions of these input pathways do show a change associated with the magnitude of the outlet baseflow. Both the tile drainages and the net diffuse discharge input dominate the baseflow contribution changes over the years. While the contribution of the tile drainages to the total discharge changes very little throughout the year (i.e. 25-

Table 4.1: The baseflow contributions of the various input pathways to the outlet for 2011-2012. Additionally, the yearly average concentrations of nitrate, total nitrogen, and chloride are listed for each pathway category. The ratio values are the yearly loads of the input types normalized to the yearly load of MW (unitless). The concentrations are in mg/l-N. Other Point discharges include all of the point inputs to the stream excluding Sys2 and Sys4.

			MW	Sys2+Sys4	Deep Aq	Other Point Inputs	Diffuse
2011	Ratios	Flow	1.00	0.26	0.27	0.10	0.39
		NO_3	1.00	0.60	0.01	0.12	0.27
		TN	1.00	0.59	0.03	0.12	0.27
	Conc	NO_3	4.81	11.09	0.11	5.44	3.36
		TN	5.00	11.40	0.48	5.82	3.49
2012	Ratios	Flow	1.00	0.25	0.28	0.10	0.38
		NO_3	1.00	0.62	0.01	0.11	0.26
		TN	1.00	0.61	0.03	0.11	0.26
	Conc	NO_3	4.46	10.81	0.12	5.00	3.00
		TN	4.64	11.09	0.49	5.30	3.19

30%), the contribution of the diffuse input has a substantially larger range (i.e. 0-50%).

The results of the baseflow EMMA from the perennial tile drainages and the deep aquifer point pathways end-member concentrations are shown in Figure 4.9. The deep aquifer diffuse water, contrary to the deep aquifer point pathways, does follow a similar pattern to the overall baseflow, but the pattern is less pronounced than the shallow aquifer water. Most of the additional deep aquifer water originates in the net diffuse discharge, while the additional shallow aquifer water originates from both the other point discharges and the net diffuse discharge. In the baseflow of the summers of 2011 and 2012, the deep aquifer constitutes almost all of the other point discharges including the net diffuse discharge. The deep aquifer water typically contributes 75% of the total outlet discharge in the summer and 50% in the winter.

4.6 Discussion

Agricultural land management could impact the seasonal nitrogen concentrations and loads by fertilization flowing directly from the soil surface shortly after application. Direct discharge of fertilizer from the unsaturated zone into the surface waters occurs mainly by heavy rain events shortly after fertilizer applications. Catchments that have flashy hydrographs and have little to no baseflow throughout the year would have the majority of the yearly nitrogen load from runoff events and subsequently the fertilizer discharge into the surface waters may have a significant contribution (*David et al.*, 1997; *Cirmo and McDonnell*, 1997). Although runoff events directly after fertilizer applications do occasionally occur in the HOAL, runoff events do not contribute the majority

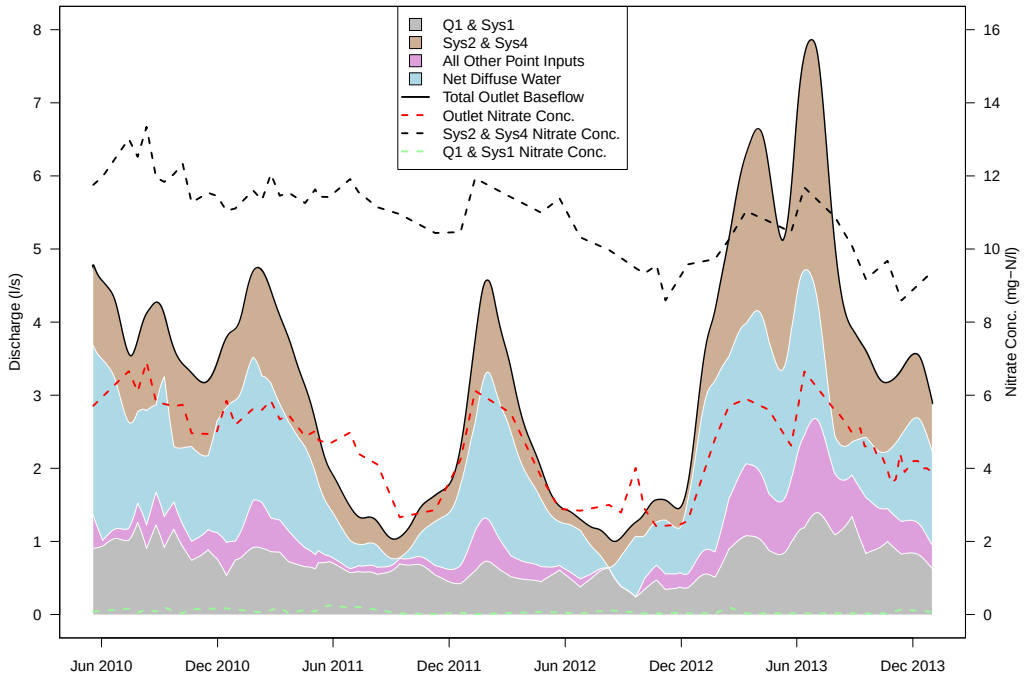

Figure 4.8: The baseflow input pathways as a proportion of the total outlet baseflow. Strong seasonal dynamics are shown in the surface, tile drainage, and net diffuse waters. Q1 and Sys1 have less pronounced seasonal dynamics. The dominant end member nitrate concentrations of the perennial tile drainages and deep aquifer point discharges bound the outlet concentration.

of the TN load to the outlet, and the seasonality of the fertilizer applications do not fully coincide with the nitrogen loads (Figure 4.7). Rather in the HOAL, the fertilizer applications supply the long term load into the solute reservoirs, and only multi-year reductions in the fertilizer applications would gradually reduce the solute mass in the reservoirs and subsequently the load into the stream.

If in-stream and/or seasonal biochemical reactions would be a source or sink for the nitrogen, then the seasonal temperature and vegetation growth should be the primary factors for these biochemical reactions. The summers of 2010 and 2013 were unusually wet, but they were not unusually cool (Figure 4.4) and had normal crop and riparian growth patterns. Nevertheless, the summers of 2010 and 2013 did have relatively high nitrate concentrations more closely associated with the typical winter periods. In-stream denitrification has been shown to be dominant in streams with very low nitrate concentrations (e.g. less than 0.1 mg/l), while in-stream biochemical reactions in agricultural streams with elevated nitrate concentrations (e.g. greater than 1 mg/l) would have a

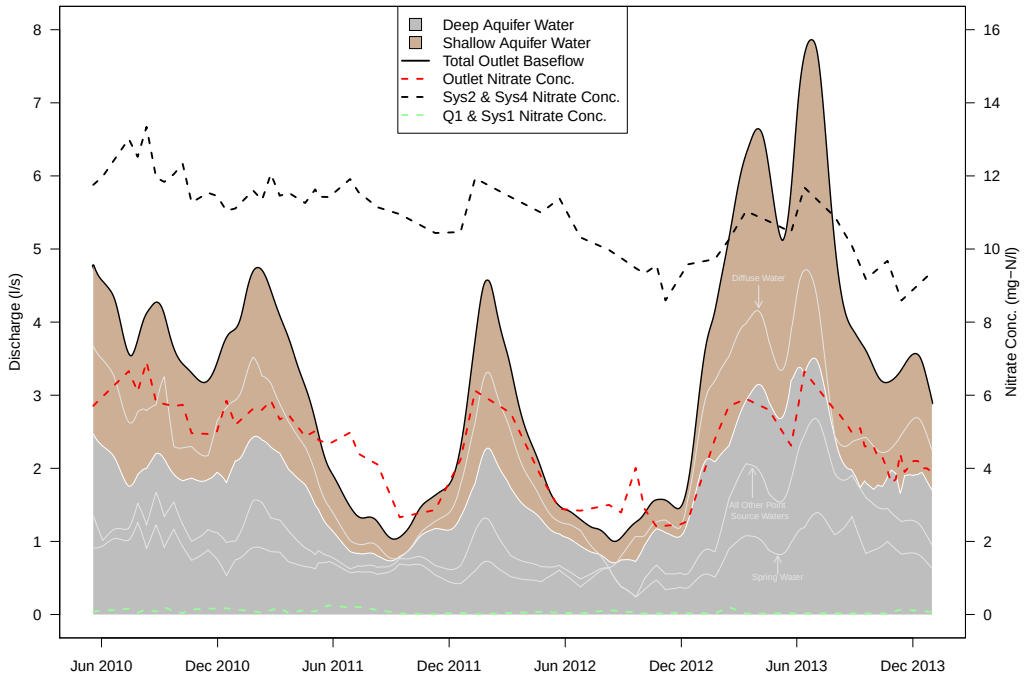

Figure 4.9: The baseflow source components of the outlet assuming that the perennial tile drainage concentrations define the shallow aquifer concentration and the deep aquifer point discharges define the deep aquifer concentration. The outlines of the input pathways from Fig. (4.8) are shown in light gray for reference.

substantially lower impact on the total nitrogen load and subsequently the in-stream nitrate concentrations (*Peterson et al.*, 2001; *Mulholland et al.*, 2008).

The seasonal baseflow dynamics from mid-2010 to the end of 2013 are dominated by changes in the contributions by the tile drainage water and the net diffuse water (Figure 4.8). The deep aquifer point discharges show little seasonal changes other than a slight increase in mid-2013. Although the pathway contributions change seasonally, the concentrations of the perennial tile drainages and the deep aquifer point discharges have little seasonality.

The evidence indicates that the seasonal volatility of the outlet nitrate concentration is attributed primarily to the changing input pathway and source contributions rather than the earlier explanations (e.g. fertilizer applications, in-stream denitrification, biochemical reactions, etc.). This is especially clear from the wet summers of 2010 and 2013. 2011 and 2012 had relatively normal seasonal patterns of temperature and precipitation, which caused a more typical pattern of high baseflow discharges in the winter and spring and low baseflow discharges in summer and autumn. 2010 and especially 2013 had ex-

ceptionally wet summers, yet the outlet nitrate concentrations were similarly high as they were in the winters of 2011/2012 and 2012/2013.

Linear regressions of nitrate concentrations to discharge and water temperature for all available data from mid-2010 to the end of 2013 show a clear positive correlation of nitrate concentration to discharge (R^2 of 0.66) and practically no correlation to water temperature (R^2 of 0.05) (Figure 4.5). Although, if the period of data was from early 2011 to mid 2013 associated with Figure 4.4 then the correlation of temperature to nitrate concentration would be more prominent with an R^2 of 0.43. During years with typical seasonal patterns, discharge and water temperature can have a strong relationship, but at least in our catchment this correlation does not equate to causation.

It is important to emphasize that the net diffuse input was estimated as the residual amount of water and solute load from the total input pathways to the stream. These pathway results assume that diffuse discharge and solutes are only entering the stream as opposed to both diffuse discharge entering the stream and stream water exiting the stream into the groundwater. Based on unpublished tracer tests performed on this stream and from numerous studies on other streams, stream water is also flowing into the groundwater to some extent that changes throughout the year (*Covino et al.*, 2011; *Payn et al.*, 2009; *Westhoff et al.*, 2007b; *Briggs et al.*, 2012; *Lowry et al.*, 2007). One consequence of this interaction is that the gross diffuse groundwater input to the stream is higher than the net diffuse value published here and that the other point inputs have a lower gross contribution to the stream as a function of distance from the outlet. The other consequence is that any biochemical reactions that do occur in the stream that reduce the nitrogen loads are manifested in the net diffuse load estimation.

The two end-member mixing analysis performed on the catchment outlet differentiates the two primary baseflow source components (i.e. deep and shallow aquifer). The results from Figure 4.9 show that most of the contents of the net diffuse water is deep aquifer water. This can also be seen in the yearly average nitrate concentration of the net diffuse water in Table 4.1. Although we did not expect such substantial volatility in the deep aquifer water from our experience with the known point discharges of the deep aquifer water along the stream (i.e. Q1 and Sys1), the EMMA results do show that the total deep aquifer discharge throughout the year does change relative to the total baseflow. We do see some increases in the discharge of Q1 and Sys1 over the years, but significantly lower volatility than the estimated deep aquifer discharge from the EMMA. This result should not be surprising as a higher hydrostatic pressure exerted by the shallow aquifer on the deep aquifer should increase the discharge from the deep aquifer. Indeed, a correlation using a normal regression between the total baseflow and the estimated deep aquifer water component has a very high positive correlation with an R^2 and a NRMSE of 0.98 and 0.06 respectively.

If the solute concentrations at the outlet of the catchment are primarily due to the changing source and pathway contributions, then the traditional hydrologic conceptual model of catchments that have large distinct reservoirs of contributing water is consistent with the low solute concentration fluctuations of the source waters. If the catchment source water reservoirs are large enough, then the impact of individual rainfall events,

fertilization applications, and seasons on the total solute concentration of the entire reservoir should be minimal. In order to reduce the overall nitrogen load to the surface waters in these headwater agricultural catchments, long-term reductions in fertilizer applications would be needed rather than changes in the seasonal application rates.

The major source of uncertainty in interpretation is related to the impact of the riparian zone. In addition to some of the above studies related to the seasonal nitrate concentrations and loads, many studies have also found that riparian zones contribute significant amounts of water to the total surface water outflow (*McGlynn and McDonnell*, 2003; *Hooper et al.*, 1998; *Burns et al.*, 2001). Although, these studies tend to have study areas in more natural environments with well-developed riparian zones rather than agricultural areas with limited riparian zones. Water samples from within the piezometers installed within the riparian zone indicate that the riparian zone water has similar nitrate and dissolved oxygen concentrations as the deep aquifer water. From this nitrate concentration similarity, the identification of the source contributions of the net diffuse water from the deep aquifer or the riparian zone would be uncertain. A mixture of riparian zone water and deep aquifer water could explain the contradiction between the lack of significant seasonality in the measured deep aquifer point discharges and the clear seasonality of the estimated deep aquifer water from the EMMA. Nevertheless, other solutes measured in the riparian piezometers do not coincide with those of the estimated net diffuse water concentrations. For example, the average concentrations of TP and dissolved silica were 0.40 mg/l and 19.9 mg/l for the riparian piezometers, 0.04 mg/l and 30.0 mg/l for the net diffuse water, and 0.05 mg/l and 35.5 mg/l for the deep aquifer point discharges. Consequently, the contribution of the riparian water in the soil matrix to the stream water appears to be minimal.

4.7 Conclusions

The monthly nitrogen loads were dominated by the total monthly runoff volumes. The diffuse groundwater discharge into the stream had the highest contribution to the total yearly flow with 38% and was followed by the perennial tile drainages and deep aquifer point discharges with about 26% each. However, the majority of the nitrogen load contribution (60%) came from the perennial tile drainages due to their high nitrogen concentrations.

The monthly water and nitrogen volumes, the pathway contributions, and the source contributions indicate that the seasonality in the nitrate concentration is primarily due to the alternating input pathway contributions and ultimately the source contributions throughout the year. In-stream denitrification, biochemical reactions, and fertilizer application timings were not found to be the significant processes in the seasonality of the surface water nitrogen concentrations and loads.

Chapter 5

The source and flowpath contribution dynamics of runoff events in an Austrian headwater agricultural catchment

5.1 Abstract

The goal of this study is to determine the representative source and flowpath dynamics of water and solute load during runoff events in a two year period in a headwater agricultural catchment. Hydrochemical analyses using end-member mixing analysis (EMMA) and hydrologic modeling at a surface water gauge and a tile drainage were used to identify and estimate the source water contributions at both locations. The two largest runoff events during the two years contributed over 50% to the total event runoff volume, nitrate load, and chloride load. Four source waters were identified to contribute to the surface water outlet during runoff events, while three were identified for the tile drainage. Both the shallow aquifer water (Q_{SA}) and the rain event water (Q_{Rain}) contributed over 80% of the event runoff flow at the outlet with the majority of the remainder contributed by the upper unsaturated soil (Q_{Soil}). The majority of the tile drainage event runoff flow volume (68%) came from Q_{Rain}, but the majority of the nitrate load (61%) came from Q_{Soil}. The variability in the source water contributions primarily occurred in Q_{Soil}. The largest 10% of runoff events had significantly more Q_{Soil} (17%) than smaller events (3%), and due to the high nitrate concentrations of Q_{Soil} half of the nitrate load came from Q_{Soil} along with Q_{SA} in the large events. The large runoff events tended to have Q_{SA} occurring earlier in events and Q_{Soil} tended to occur later in events as compared to the bulk of smaller events, while Q_{Rain} occurred in the center of events regardless of size. The input flowpaths to the stream of the small events consisted of almost entirely point inputs to the stream (e.g. tile drainages and springs), while the larger events had an increasing flowpath contribution of diffuse groundwater and overland flow. The results

from this study has shown that there is significant variability in the source contributions depending on the size and prior conditions of rainfall events. Each source water has a distinct contribution dynamic to downstream surface waters depending on the source location, hydrologic condition, and flowpaths that each take to the stream.

5.2 Introduction

Runoff from diffuse sources (e.g. agricultural lands) with tile drainages can contribute the majority of certain types of pollutant loads to surface waters (e.g. fertilizer nutrients) (*Drury et al.*, 1993; *Tan et al.*, 1998). The excess of nutrients in surface water environments negatively impact both the riverine ecosystems and human health (*Romstad et al.*, 1997; *Walling et al.*, 2002). The eutrophication of lakes, rivers, and coastal zones is a major issue facing environmental policy (*Clercq*, 2001). Understanding the underlying hydrologic and chemical transport processes that contribute to the solute load of agricultural catchments is crucial to finding and targeting effective measures to reduce pollutant loads. There are still significant issues related to hydrologic and solute transport that need to be addressed.

In catchments, the cumulative water and solute loads throughout the year can be dominated by either baseflow or runoff events. Although, even if a catchment is dominated by baseflow, runoff events still generally have a significant contribution. The estimation of yearly baseflow in typical monitoring procedures of weekly or biweekly sampling can accurately estimate the cumulative water and solute loads. On the other hand, runoff events are both unpredictable in occurrence and in the flow and solute load response (*Aulenbach*, 2013). Due to cost and labor restrictions, event monitoring is sporadic and can lead to significant inaccuracies when attempting to estimate the cumulative flow and load from several events (*Preston et al.*, 1989). Much work has been performed to optimize the sample collection for runoff events (*Aulenbach and Hooper*, 2006; *Aulenbach*, 2013), but on-site measurement devices for various solutes that can continuous capture a large proportion of events would be optimal to ensure representativeness for any subsequent analyses performed in catchments.

One major influence on the release of pollutants from agricultural lands are upstream source water reservoirs and the processes that contribute to the downstream surface waters during runoff events. Source water reservoirs in the environment are conceptually understood as large water reservoirs that store both water and solutes for a period of time and due to the size of the reservoir the solute concentrations remain relatively stable. These can include groundwater aquifers of various types, lakes, and rain water. In surface water hydrology, one of the more widespread analysis methods to extract source water reservoirs from runoff events is hydrograph separation. The most basic conceptual model for hydrograph separation is the separation of baseflow from the hydrograph water mobilized from a particular rainfall event utilizing only the hydrograph itself. This does not necessarily equate to specific source waters, but only accounts for a rise in the hydrograph above a prior baseflow associated with a rainfall event (*Beven*, 2011). As hydrologic models grew in complexity and began to focus on more detailed

hydrologic processes within catchments, water flows within the hydrologic system were separated into multiple reservoirs. Consequently, hydrograph separation became more used to separate water source reservoirs in order to calibrate and/or validate hydrologic models (*Beven*, 2011). Catchment scale solute transport models require knowledge of the dominant dynamic source reservoirs and flowpaths of the solutes to be modeled.

The use of hydrograph separation from both the flow and the solutes can provide detailed information about the sources and flowpaths of water and solutes in catchments. One of the more prominent methods to separate the source water contribution of a downstream surface water measurement station is end-member mixing analysis (EMMA). EMMA assumes that a downstream hydrograph is composed of upstream source reservoirs with distinct and homogeneous chemical or isotopic concentrations (*Christophersen et al.*, 1990). Typically, EMMA has been applied on small sets of runoff event hydrographs and used to separate the hydrographs into two distinct source reservoirs (e.g. pre-event water and rain event water) (*Klaus and McDonnell*, 2013). Two source reservoirs are assumed due in part to the limited data at downstream gauges and limited data about the catchment hydrologic conditions. Other studies have increased the number of source reservoirs to three or four in locations where the catchment has been well studied and water chemistry data at gauges are available (*Iwagami et al.*, 2010; *Klaus and McDonnell*, 2013). In both cases, studies generally analyze only a small subset of the total runoff events during a particular year and consequently may not be completely representative of the total runoff events at a catchment. Larger solute transfer models will benefit the most from studies that are representative both of typical catchments and of the runoff events throughout all seasons of the year.

Isotope EMMA is typically considered the most accurate method to separate source waters due to the isotopes being truly conservative (*Klaus and McDonnell*, 2013). Unfortunately, the cost and time required to measure dozens of runoff events over years is prohibitive until commercial on-site devices are readily available. Additionally, isotopes may not be the most appropriate tracer to use for differentiating some solute reservoirs as they may not have significant differences between solute reservoirs and may not provide the same source and flowpath information for solute transport (*Ladouche et al.*, 2001). Electrical conductivity (EC) has been used frequently as a surrogate for conservative solutes to separate the rainfall event water from pre-event water (*Cey et al.*, 1998; *Muñoz-Villers and McDonnell*, 2012; *Laudon and Slaymaker*, 1997; *Pellerin et al.*, 2008). Due to the chemically lumped nature of EC, it may not be representative of a single conservative solute (e.g. chloride, sodium, silicate) (*Obradovic and Sklash*, 1986; *Pearce et al.*, 1986).

The flowpaths that the water takes to enter the stream also affect the type and amount of source waters that contribute to the surface waters (e.g. tile drainages, diffuse groundwater flow, etc.) (*Schilling and Helmers*, 2008; *Klaus and McDonnell*, 2013). In certain agricultural catchments, tile drainages can contribute the majority of the flow and solute load to the surface waters (*Tan et al.*, 2002a; *Macrae et al.*, 2007). As preferential flowpaths have been found to increase the conveyance of rainfall water and any mobilizable material on the soil surface, tile drainages as even larger conduits

can also increase the contribution of rainfall water and other surface material to the stream (*Geohring et al.*, 1998; *Jaynes et al.*, 2001; *Tan et al.*, 1998). Utilizing the tile drainage input information combined with EMMA can improve the interpretation of source separation results.

For our investigation, we have chosen the existing experimental catchment called the Hydrologic Open Air Laboratory (HOAL) in Petzenkirchen, Austria (Figure 5.1). The HOAL is a headwater agricultural catchment with typical soils, land use, and precipitation characteristics for the region. The HOAL has been thoroughly studied hydrologically and has been instrumented with many measurement devices for the acquisition of various types of physical, chemical, and biologic data (*Blöschl et al.*, 2016).

The goal of the study is to capture a representative sample of the runoff events for flow and solute load, identify the primary source waters that contribute to the runoff flow and solute load, estimate and summarize the source water contributions that are representative of the runoff events during a two year period, and determine the dominance of different flowpaths as they relate to the source water contributions. Source and flowpath analyses of a large number of runoff events during a two year period will provide a valuable representative understanding of the internal hydrologic conditions and processes that dominate the storage and transfer of water and solutes in a typical Austrian headwater agricultural catchment. The results will be more generalizable for the catchment itself as well as similar catchments.

5.3 Field site

The study area was the HOAL catchment. The HOAL is located in Petzenkirchen in Lower Austria, approximately 100 km west of Vienna (Figure 5.1). It has a first order stream that runs about 620m through the southern part of the catchment and the total catchment area is approximately 66 hectares. The land cover is about 82% of arable land, 3% riparian forest, 5% planted trees with grass undergrowth, 8% grassland, and 2% impermeable surfaces (e.g. paved roads, buildings, etc.).

The study period was from 2011 to 2012 and during this time 631 mm and 742 mm of precipitation fell on the catchment respectively. The total surface runoff during these two years were 133 mm and 124 mm with average discharge at 2.8 l/s and 2.6 l/s respectively. There are 10 known point inputs into the stream. These include six tile drainages (i.e. Sys1, Sys2, Sys3, Sys4, Frau1, and Frau2) and four springs (i.e. Q1, K1, A1, and A2). Additionally, the surface water outlet that defines the contributing area of the catchment is called MW. Sys4 has the highest single point contribution to the total baseflow of MW (*Exner-Kittridge et al.*, 2016) and both MW and Sys4 will be primary data sources for this study.

The soils in the catchment down to 0.7m below the surface are generally classified as silt loam or more specifically as Cambisols that have 7.2% sands (0.51 coefficient of variation (CV)), 68.7% silts (0.11 CV), and 24.1% clays (0.30 CV) (*Deckers et al.*, 2002). Due to the high clay and silt content of the upper soil, cracking of the soil occurs frequently during the dry summer months. A detailed geologic survey has not been

performed in this catchment, but based on core samples from piezometers placed in and around the riparian area and production wells installed by the local farmers the silt loam extends down approximately 5 to 7 m below the surface where it meets a fractured siltstone unit. There is neither information about the thickness of the fractured siltstone unit nor what geologic units are below it. The catchment has general characteristics that are typical throughout the extent of catchments of the prealpine area alongside the eastern Alps with intensive agriculture associated with the seasonality of rainfall, runoff, and drainage density (*Merz and Blöschl*, 2007).

More detailed descriptions of the HOAL catchment can be found in *Exner-Kittridge et al.* (2016) and *Blöschl et al.* (2016).

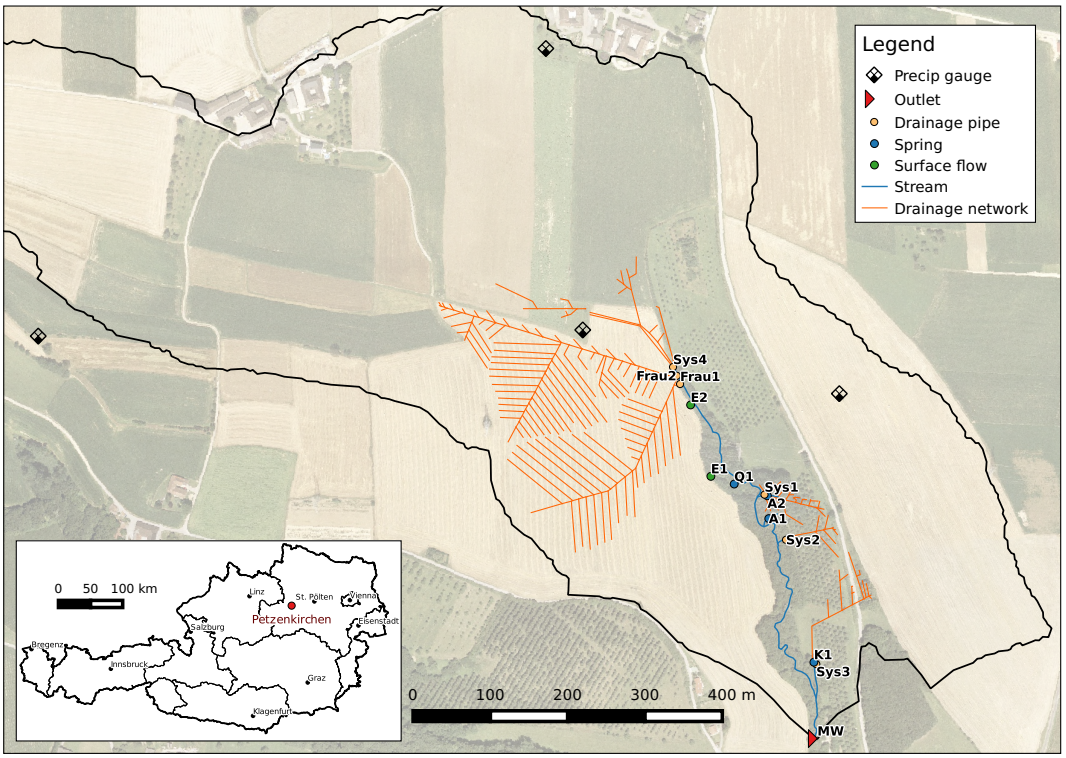

Figure 5.1: Site map for the Hydrologic Open Air Laboratory (HOAL) in Petzenkirchen, Austria.

5.4 Methods

5.4.1 Available data

All of the point input flowpaths along the stream were measured continuously for water level which was then used to estimate discharge in l/s at 1 min intervals. Two springs (Q1 and K1) were installed with V-notch weirs, while the other point input locations

had H-flumes. Both systems used the measurement of water level from pressure sensors to estimate discharge based on calibrated water level to discharge relationships (*Shaw*, 2011). The measurement of water level at MW also included an ultrasonic water level sensor for redundancy and improved uncertainty estimation. In addition to discharge, MW and Sys4 had other physical and chemical water parameters measured continuously at 5 min intervals. The relevant continuously measured parameters were chloride and nitrate using Ion Sensitive Electrodes (ISE). Sys4 used the Water Monitoring Enclosure to house the sensors (*Exner-Kittridge et al.*, 2013). Sys1, Sys2, Sys4, and Q1 flow at least 0.01 l/s throughout the year, while all of the other stations run dry or below 0.01 l/s for some time during the year.

Manual grab samples were collected at all flowing locations along the stream including MW. These water samples were collected once every 1-4 weeks during 2011-2012 and were analyzed for many physical and chemical parameters including chloride, nitrate and discharge. Two 24-bottle autosamplers were installed at MW to collect samples of flow during rainfall events and was utilized in this study to correct the ISE values as needed. An additional autosampler was installed at Sys4 in early 2012 for the same purpose.

Three precipitation gauges are located within the catchment and use precision weighting systems to measure precipitation. The precipitation gauges are distributed equally throughout the catchment and measure near real-time (nRT) precipitation at 1 minute intervals. No post-processed corrections of the precipitation data was performed. A meteorological station is located within the town of Petzenkirchen less than 1 km from the catchment and is maintained by the Federal Agency for Water Management, Institute for Land and Water Management Research (IKT).

5.4.2 Flow and solute load assessment

For the runoff event assessment, the continuous discharge and water chemistry data were used for MW and Sys4. Due to the very low flows of many stations (less than 0.1 l/s), discharge data and water chemistry was not always available at all stations throughout the year. Gaps in the individual rainfall events within the HOAL were filled by Petzenkirchen meteorological station.

As mentioned in the introduction, traditional hydrograph separation utilizing only the flow assumes that the separated runoff event water is the water mobilized as a consequence of the short term rainfall event. As long as all events are separated consistently, the estimates of these runoff flow and solute load volumes can be compared between all runoff events (*Beven*, 2011). For the estimation of total event runoff flow volume and solute load, we also performed simple hydrograph separation for comparisons to the total yearly baseflow and to the individual source water contributions. The runoff event volumes were separated from the hydrograph by interpolating a straight line from the initial rise of the hydrograph to the inflection point at the trailing limb of the hydrograph on a semi-log plot (*Shaw*, 2011). Baseflow nitrate and chloride loads were estimated and removed from the total event load by assuming that the baseflow nitrate concentrations during the events was the same as the baseflow concentrations before the events. The prior baseflow concentrations were multiplied by the extracted baseflow discharges to

estimate baseflow solute loads.

To get a better understanding of the flow contribution of the point inputs to the stream (e.g. tile drainages and springs) as compared to the diffuse and overland flow inputs, we accumulated all available discharge data from the point sources and compared them to the total discharge at MW. As described in section 5.4.1, a total of nine point input stations contribute to the flooding volume during rainfall events. Due to the low flows at many stations and the difficulties of accurately measuring water levels and estimating discharge, the other input stations to the stream other than Sys4 had intermittent periods of discharge data availability. We took all events that have the criteria of having at least six stations available that also must include Sys4 as one of these (as it is the dominant point source). In total, there were 14 available runoff events that matched this criteria and uncertainty values were propagated using standardize methods (*BIPM et al.*, 2008).

5.4.3 Source separation (EMMA)

Water sources can be separated using standard EMMA equations derived from basic conservation of mass equations (*Exner-Kittridge et al.*, 2014) and methodology is described in section 5.4.5. The main assumption of the EMMA equations is the conservative mixing of the solute sources before reaching the measurement point. EMMA can be applied at any particular point along a stream, but only represents the proportions of the sources at that particular point. EMMA can also be applied over time on a hydrograph during a runoff event. If EMMA is applied in this way, then the source reservoir concentrations must be fixed during the entire event hydrograph. Fixing the source concentrations over time may be appropriate for some sources (i.e. rainfall and aquifer water), but may be inaccurate for others (i.e. unsaturated zone) (*McCallum et al.*, 2010). Few studies have attempted to vary the end-member concentrations over time due to the difficulty of reliably estimating the end-members over time (*Harris et al.*, 1995; *McGlynn and McDonnell*, 2003). Unfortunately, some of these assumptions cannot be avoided in practice when attempting to apply EMMA over a large catchment with limited data (*Klaus and McDonnell*, 2013).

5.4.4 End-member identification

A previous study within the HOAL catchment determined that the outlet baseflow is composed primarily of two end-member reservoirs (*Exner-Kittridge et al.*, 2016). These two are the shallow and deep aquifers (Q_{SA} and Q_{DA} respectively). During rainfall events, these two flow sources must also be present at the outlet, but additional sources may also appear. The rain water (Q_{Rain}) is an obvious possible source as it is a large newly introduced and chemically distinct water volume and has been used as a source water in most source separation studies (*Klaus and McDonnell*, 2013). Other water sources may not be as obvious. Additional sources found in other studies include riparian water, unsaturated soil water, and water from additional distinct geologic units (*Guinn Garrett et al.*, 2012; *McGlynn and McDonnell*, 2003).

Sys2 and Sys4 flow perennially and most of the inorganic solute concentrations measured at these tile drainages are very similar (e.g. a mean difference of 10% and 12% between nitrate and chloride concentrations respectively). As most of the tile drainages in the catchment are installed between 1 to 1.5 m below the surface and that Sys2 and Sys4 drain opposite sides of the catchment, the relevant inorganic chemistry presented in this study for the shallow aquifer is represented by the baseflow concentrations from the mean values of Sys2 and Sys4 (Figure 5.2). As the tile drainages are installed in the shallow soil, tile drainage effluent water during runoff events could only consist of the shallow aquifer water, the rain water, and the unsaturated zone water.

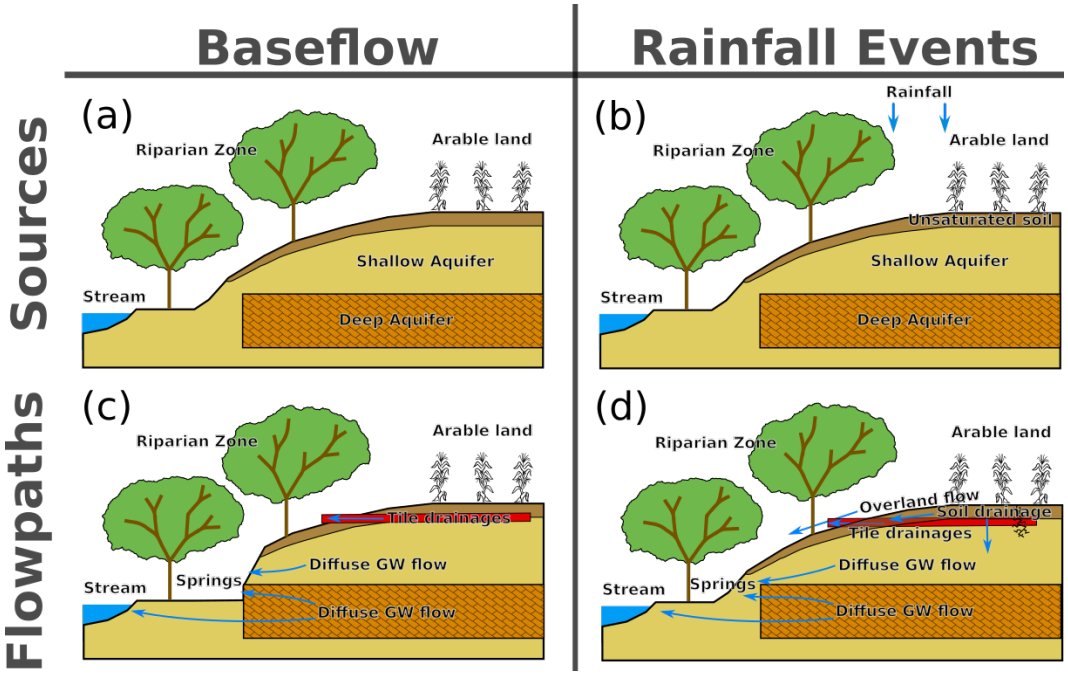

Figure 5.2: Conceptual diagrams of the sources and pathways that occur during the two hydrologic states of the catchment. During baseflow, only the shallow aquifer and the deep aquifer contribute to the stream flow. During rainfall events, the unsaturated soil and the rainfall itself in addition to the shallow and deep aquifers contribute to the stream.

The spring Q1 originates at the fractured siltstone unit and the water at Q1 has distinct chemical characteristics from Sys2 and Sys4. Comparing Q1 to Sys2 and Sys4, the differences include much lower nitrate concentrations (0.1 compared to 10.1 mg/l), generally higher chloride concentrations (27.9 compared to 22.6 mg/l), much lower dissolved oxygen concentrations (1.2 compared to 9.1 mg/l), higher dissolved silica concentrations (35.3 compared to 22.0 mg/l), and higher ammonium concentrations (0.25 compared to 0.01 mg/l). The other distinct difference between Q1 and the tile drainages is that Q1 has a lack of hydrograph dynamics during rainfall events. Most input flowpaths have a pronounced runoff hydrograph associated with rainfall events. Sys1 also has the same

physical and chemical characteristics as Q1. Q1 and Sys1 has been assumed to represent the relevant solute concentrations for the deep aquifer and have similar representativeness to Sys2 and Sys4 with the shallow aquifer as both Q1 and Sys1 drain areas from the opposite sides of the stream.

Observations of the dilution patterns of chloride and nitrate during runoff events provided an initial qualitative assessment for a fourth end-member. The dilution pattern of chloride during runoff events always dilute the chloride concentration at MW as if the rainfall was diluting a single reservoir or reservoirs with relatively similar chloride concentrations. No abnormal increases or decreases of the chloride concentration were ever observed during a runoff event to indicate an introduction of another source reservoir with a significantly different chloride concentration. On the other hand, the nitrate concentration during runoff events did not show a simple dilution of rainfall on a single reservoir, rather there were increases in the nitrate concentration during periods when the chloride concentration would continue to decrease. The increase in the nitrate concentration during the runoff event would indicate the introduction of another source water with a higher concentration of nitrate as compared to the other three source waters. As another qualitative comparison of the solute concentrations, top soil samples were collected using vacuum pumps at specific areas within the catchment during different times of the year. The samples from the top soil had a chloride concentration similar to that of the shallow aquifer, but the top soil had a nitrate concentration significantly higher than the shallow aquifer (Table 5.1). During irrigation tests in an upland catchment, *Anderson et al.* (1997) found a significant contribution of water from the upper soil horizons. As the catchment is predominantly arable land with systematic fertilizer applications during the year, the upper unsaturated zone of the soil (soil water (Q_{Soil})) appeared to be the likely candidate as others have also used in similar studies (*Bazemore et al.*, 1994; *Casper et al.*, 2003; *Liu et al.*, 2004; *DeWalle and Pionke*, 1994).

As has been used in many other source separation studies, chloride was found to have distinct characteristics between the rain water and the other sources (Table 5.1). Due to the frequent fertilizer applications to the top soil, nitrate was found to be distinct between the soil water, the shallow aquifer, and the other two sources (i.e. rain and deep aquifer water) (Table 5.1). Although nitrate may not be conservative over longer time periods of weeks and months, nitrate has been found to be conservative over the short periods of runoff events (*Hudak*, 2004) and has been used in EMMA studies (*Durand and Juan Torres*, 1996; *Soulsby et al.*, 2003).

Where there was no contribution from the deep aquifer (e.g. Sys4), chloride and nitrate were used as the solutes in the EMMA to identify the shallow aquifer, soil, and rainfall water during rain event conditions. At MW where the deep aquifer contributed to the flow in addition to the other three source waters, a reservoir cascade model was developed to model the dynamics of the deep aquifer water at the outlet as described in section 5.4.6. All samples collected within the catchment had concentration values that fell within the estimated source water solute concentrations (Table 5.1). Samples for water chemistry concentrations were collected or estimated for the end-members throughout the years. Consequently, a time series of end-member concentrations were

made for both years so that each runoff event would have a distinct set of end-member concentrations to take into account the variability of the end-member concentrations. Although, the variability throughout the year was only expected to be significant in the soil water nitrate concentration. Nevertheless, the end-member concentration would be fixed for the duration of each runoff event.

Representative samples for the end-member concentrations could be collected for the shallow aquifer water, the deep aquifer, and the rain water. Some samples of the top soil were collected using vacuum pumps at specific areas within the catchment during different times of the year, but these samples may not be representative of the actual aggregated unsaturated zone water that reaches the tile drainages and the catchment outlet due to solute concentration stratification (*Padilla et al.*, 1999). Based on the pattern of the chloride dilution during runoff events and from the similarity in the existing vacuum pump samples of the soil water chloride concentration, we decided to assign the chloride concentration of the soil water equal to the shallow aquifer. Others have also found that the shallow groundwater chloride concentration is very similar to the soil water concentration (*Bazemore et al.*, 1994). As the soil water nitrate concentration was significantly higher than the other source waters and due to the importance of nitrate in EMMA for the soil water, the soil water nitrate end-member was determined separately in the procedure described in section 5.4.5.

Table 5.1: Statistics of the four end-members identified in the HOAL. All rows excluding "CV" are concentrations in mg/l. CV is the coefficient of variation. The "EMMA model" category lists the statistics from the values used for the end-members in the EMMA. The "Vac" category lists the statistics from the values collected by the vacuum pump of the top soil.

	End-member	Min	Max	Mean	Median	CV
EMMA model	$C_{Rain,NO3}$	0.55	1.88	1.23	1.24	0.38
	$C_{SA,NO3}$	8.66	11.86	10.51	10.70	0.08
	$C_{Soil,NO3}$	15.69	27.01	22.18	24.13	0.18
	$C_{DA,NO3}$	0.01	0.25	0.07	0.04	0.82
	$C_{Rain,Cl}$	0.20	0.60	0.34	0.30	0.39
	$C_{SA+Soil,Cl}$	19.12	25.98	22.70	23.09	0.08
	$C_{DA,Cl}$	24.19	33.19	27.21	26.59	0.09
Vac	$C_{Soil,NO3}$	16.56	21.36	18.88	18.84	0.08
	$C_{Soil,Cl}$	15.40	20.60	18.18	18.20	0.09

5.4.5 EMMA equations

The basic form of EMMA uses two mass balance equations:

$$Q_{Tot}(x,t) = Q_1(x,t) + Q_2(x,t) + Q_3(x,t) + ... + Q_n(x,t) \tag{5.1}$$

$$Q_{Tot}(x,t)C_{Tot}(x,t) = Q_1(x,t)C_1 + Q_2(x,t)C_2 + Q_3(x,t)C_3 + ... + Q_n(x,t)C_n \quad (5.2)$$

where Q_{Tot} is the discharge at location x at time t, the other Q's are the contributing discharges of the specific n source waters at location x at time t, C_{Tot} is the concentration of a solute at location x at time t, and the other C's are the concentrations of the n sources (i.e. end-member concentrations) and are invariant in time and space. For this study, the locations of x will be MW and Sys4, and EMMA will be applied over all time series measurements t during each runoff event.

In most EMMA studies, the measurement location of Q_{Tot} is measured for discharge and the required solutes (or isotopes). Additionally, the end-member concentrations are either measured or estimated prior to the final separation. Consequently, only the contributing source waters (i.e. Q_n) are unknown. For example if only two sources were to be separated (i.e. Q_1 and Q_2) from a discharge location with measured flow and a single solute, then only equations (5.1) and (5.2) would need to be combined as long as the concentrations of the two source waters (i.e. C_1 and C_2) were known. With each added source water to be separated, an additional equation (5.2) with a different solute associated with C_{Tot} would need to be added to the previous equations. The different solutes would need to have significant concentration differences between some of the source waters or substantial estimation uncertainties will arise (*Barthold et al.*, 2011).

In our study, we have four source waters for MW and three for Sys4 (section 5.4.4). To estimate the source water contributions at Sys4, two sets of solutes (in our case nitrate and chloride) would need to be known for all three of the source waters. All three source water end-member concentrations will be known once the soil water nitrate end-member is estimated in section 5.4.5. MW has four source waters, so without an additional measured solute with associated end-members the EMMA for MW cannot be solved. To overcome this issue, we were able to model the Q_{DA} dynamics at MW independently of the EMMA and is described in section 5.4.6. With Q_{DA} and the associated end-members known, the EMMA equations can be solved.

Soil water nitrate end-member

Section 5.4.4 described how the end-members were identified and assigned for all except the soil water nitrate end-member. The assigned end-members are based on estimates that are independent of the EMMA itself. As stated earlier in section 5.4.4, samples of the soil water were taken, but may not be representative for the entire catchment throughout the two years. Consequently, the end-members for nitrate would need to be estimated through the initial EMMA of Sys4.

The initial set of derivations will be for Sys4. The only difference between Sys4 and the outlet, MW, is that Sys4 does not include the deep aquifer, which simplifies the equations and uncertainties. We first start with the essential mass balance equations from equations (5.1) and (5.2) for the three source waters:

$$Q_{Tot} = Q_{SA} + Q_{Soil} + Q_{Rain} \quad (5.3)$$

$$Q_{Tot}C_{Tot} = Q_{SA}C_{SA} + Q_{Soil}C_{Soil} + Q_{Rain}C_{Rain} \tag{5.4}$$

where Q_{Soil} is the part of Q_{Tot} from the soil water, Q_{Rain} is the part of Q_{Tot} from the rain water, C_{Soil} is the solute concentration of the soil water, and C_{Rain} is the solute concentration of the rain water.

Using the end-member assumptions mentioned earlier, equation (5.4) becomes the following when chloride is used as the solute with the assumption that $C_{SA,Cl} = C_{Soil,Cl}$:

$$Q_{Tot}C_{Tot,Cl} = [Q_{SA} + Q_{Soil}]C_{SA,Cl} + Q_{Rain}C_{Rain,Cl} \tag{5.5}$$

Combining equations (5.3) and (5.5) solves for Q_{Rain}:

$$Q_{Rain} = \frac{Q_{Tot}(C_{Tot,Cl} - C_{SA,Cl})}{C_{Rain,Cl} - C_{SA,Cl}} \tag{5.6}$$

Chloride was used to estimate Q_{Rain} and so nitrate would need to be used to determine the other two sources (i.e. Q_{SA} and Q_{Soil}). Unfortunately, we do not have reasonable estimates of $C_{Soil,NO3}$ which likely changes throughout the year. Due to this lack of information, the multiple equations of equation (5.4) for nitrate becomes underdetermined. If we are going to estimate $C_{Soil,NO3}$, then we need to make another assumption to solve the equations. A number of assumptions could be made. In the end, we chose to make an assumption about Q_{SA} at one specific point during the flood hydrograph. The combined nitrate loads of Q_{SA} and Q_{Soil} can be estimated using the available information:

$$Q_{SA}C_{SA,NO3} + Q_{Soil}C_{Soil,NO3} = Q_{Tot}C_{Tot,NO3} - Q_{Rain}C_{Rain,NO3} \tag{5.7}$$

We can rename the combined nitrate loads of Q_{SA} and Q_{Soil} in the following form:

$$Q_{SA+Soil}C_{SA+Soil,NO3} = Q_{SA}C_{SA,NO3} + Q_{Soil}C_{Soil,NO3} \tag{5.8}$$

and

$$Q_{SA+Soil} = Q_{SA} + Q_{Soil} \tag{5.9}$$

Combining equations (5.3), (5.7), (5.8), and (5.9) we can solve for $C_{SA+Soil,NO3}$:

$$C_{SA+Soil,NO3} = \frac{Q_{Tot}C_{Tot,NO3} - Q_{Rain}C_{Rain,NO3}}{Q_{Tot} - Q_{Rain}} \tag{5.10}$$

All of the equations listed in this section are applied at one specific location at all time steps during a flood hydrograph associated with a rainfall event. Subsequently, there is a $C_{SA+Soil,NO3}$ at every time step in the flood hydrograph. Our assumption about Q_{SA} is that at the time step of the maximum value of $C_{SA+Soil,NO3}$ the value of Q_{SA} at that point is the linear interpolation between the baseflow values of Q_{SA}. This linear interpolation was estimated from the traditional hydrograph separation method by constructing a straight line from the initial rise of the hydrograph to the inflection

point at the trailing limb of the hydrograph on a semi-log plot (*Shaw*, 2011). As the peak value of $C_{Soil,NO3}$ and subsequently $C_{SA+Soil,NO3}$ tends to be after the peak discharge due to the slower overall response of the soil water, Q_{SA} should be relatively close to this assumption. Consequently as we only fix one point, the dynamics of Q_{SA} during the rest of the flood hydrograph should still be reflected in the analysis.

The solution for $C_{Soil,NO3}$ combines equations (5.8) and (5.9) and becomes:

$$C_{Soil,NO3} = \frac{Q^{mp}_{SA+Soil} C^{mp}_{SA+Soil,NO3} - Q^{mp}_{SA} C_{SA,NO3}}{Q^{mp}_{SA+Soil} - Q^{mp}_{SA}} \tag{5.11}$$

where the ^{mp} symbol represents the maximum value of $C_{SA+Soil,NO3}$ along the flood hydrograph. Note that, unlike the other end-member concentrations, $C_{Soil,NO3}$ is derived at a specific discharge point. As Sys4 is defined as not containing the deep aquifer end-member and was used to create the seasonal end-member concentrations for the shallow aquifer, the above procedure to estimate $C_{Soil,NO3}$ was performed on Sys4 to assign the seasonally variable end-member of $C_{Soil,NO3}$.

5.4.6 Original stream water pulse

As mentioned in section 5.4.4, the identified deep aquifer end-member inputs to the stream (i.e. Q1 and Sys1) do not dynamically respond to rainfall events. The discharge remains steady into the stream during runoff events. The constant discharge input may apply to the locations along the stream where deep aquifer water is flowing into the stream, but due to the in-stream hydraulic dynamics of the stream during runoff events a constant deep aquifer discharge may not apply at MW. Consequently, Q_{DA} is assumed to be dynamic during runoff events as with the other source waters. Due to the limited solute concentrations monitored continuously at MW, Q_{DA} would need to be estimated independently from the EMMA. We determined that complex hydraulic routing models would be unnecessary due to the introduction of additional uncertainty and potential incompatibility with the EMMA methodology. We decided to use a simple instantaneous reservoir cascade model to estimate the impact of the original stream water volume from prior baseflow conditions and the continuous constant input of Q_{DA} to the stream.

Conceptually, the model includes a reservoir with one constant inflow and an inflow that varies with time. The outflow is also composed of the same two input components except that both outflow components vary with time. For our example, the constant inflow is the deep aquifer water, while all other components (i.e. Q_{SA}, Q_{Rain}, and Q_{Soil}) will be lumped into a single term called Q_{Other}. We start with the basic water mass balance equations for a single reservoir:

$$Q^{Out}_{Tot} = Q^{Out}_{DA} + Q^{Out}_{Other} \tag{5.12}$$

$$Q^{Out}_{Tot} = Q^{In}_{DA} + Q^{In}_{Other} + \frac{\Delta V_{DA}}{\Delta t} + \frac{\Delta V_{Other}}{\Delta t} \tag{5.13}$$

$$\Delta V_{Tot} = \Delta V_{DA} + \Delta V_{Other} \tag{5.14}$$

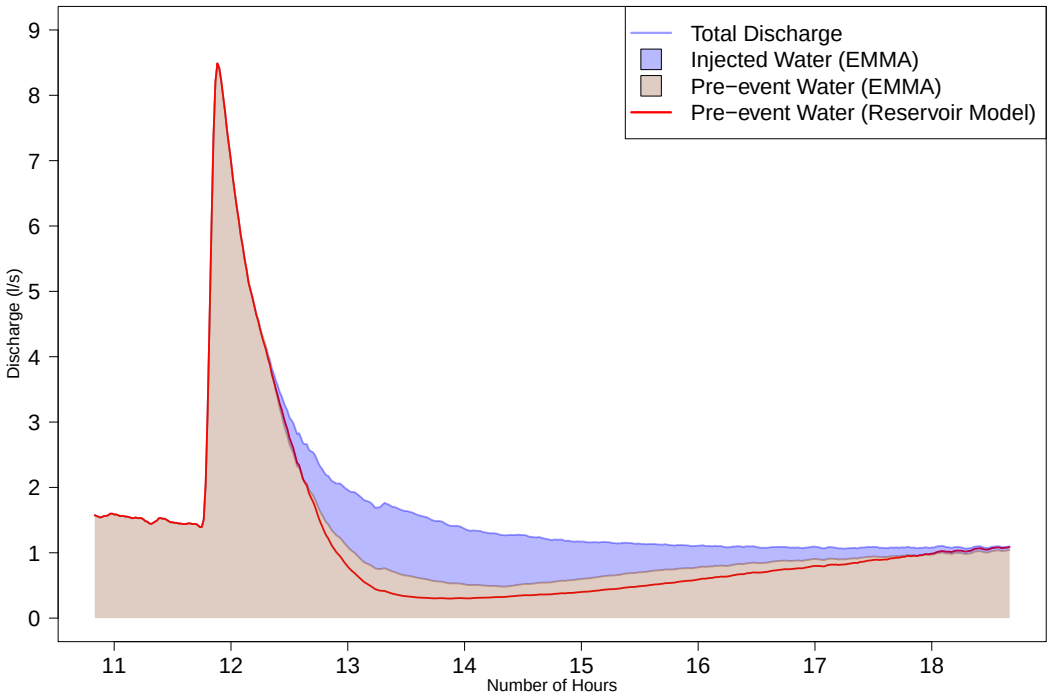

Figure 5.3: The first flooding test hydrograph of MW comparing the results from the EMMA and the reservoir model. The pre-event water was estimated from EMMA utilizing bromide from the injected water at Sys4.

where Q_{Tot}^{Out} is the total discharge at MW in l/s, Q_{DA}^{Out} is the discharge of the deep aquifer water component at MW in l/s, Q_{Other}^{Out} is the discharge of the water at MW excluding the deep aquifer water in l/s, ΔV_{DA} is the change in the volume of the deep aquifer water stored in the stream in liters, ΔV_{Other} is the change in the volume of water stored in the stream excluding the deep aquifer water in liters, and ΔV_{Tot} is the change in the total volume of water in the stream in liters.

We transformed the equations to be solved numerically by separating the change in storage terms:

$$Q_{Tot}^{Out} = Q_{DA}^{In} + Q_{Other}^{In} + \frac{V_{DA,i-1}}{\Delta t} - \frac{V_{DA,i}}{\Delta t} + \frac{V_{Other,i-1}}{\Delta t} - \frac{V_{Other,i}}{\Delta t} \tag{5.15}$$

$$V_{Tot} = V_{DA} + V_{Other} \tag{5.16}$$

where the i designates the current time step and $i-1$ designates that previous time step. Equation (5.16) is valid at any time step.

One assumption that we need to make to solve the linear equations is the sequence and type of mixing in the reservoir. We assume that at each time step the inflow components enter the reservoir, mix completely with the existing water in the reservoir, then the water exits the reservoir as the outflow components. With this in mind, combining

equations (5.15) and (5.16) and with some rearrangement, we get the following equation for the inflow ratios:

$$1 = \frac{\frac{V_{DA,i-1}}{\Delta t} + Q_{DA}^{In}}{\frac{V_{Tot}}{\Delta t} + Q_{Tot}^{Out}} + \frac{\frac{V_{Other,i-1}}{\Delta t} + Q_{Other}^{In}}{\frac{V_{Tot}}{\Delta t} + Q_{Tot}^{Out}} \tag{5.17}$$

and the following for the outflow ratios from equation (5.12):

$$1 = \frac{Q_{DA}^{Out}}{Q_{Tot}^{Out}} + \frac{Q_{Other}^{Out}}{Q_{Tot}^{Out}} \tag{5.18}$$

Based on our previous mixing assumption, the inflow ratios for each component would be equal to the respective outflow component ratio. As we want to solve for Q_{DA}^{Out}, the final equation would be the following:

$$Q_{DA}^{Out} = Q_{Tot}^{Out} \frac{\frac{V_{DA,i-1}}{\Delta t} + Q_{DA}^{In}}{\frac{V_{Tot}}{\Delta t} + Q_{Tot}^{Out}} \tag{5.19}$$

We decided to have V_{Tot} vary between runoff events, but not within the events. We did this rather than vary the V_{Tot} within runoff events due to the change in V_{Tot} being ill defined as a function of Q_{Tot}^{Out} and that we did not expect that varying V_{Tot} within an event would significantly change the resulting Q_{DA}^{Out}. The V_{Tot} for each event was a function of the initial baseflow discharge. Subsequently, if ΔV_{Tot} is zero, then Q_{Other}^{In} would be simply estimated from equation (5.13) rather than having to rely on an upstream measurement or estimate of discharge.

Equation (5.19) is for a single reservoir. As the propagation of a flood wave does not completely mix with the existing water in a stream, we decided to include a linear cascade of many reservoirs in series to simulate incomplete mixing (*Beven*, 2011). Q_{DA}^{In} and Q_{Other}^{In} would be inputs for the first reservoir, and the outputs of each reservoir would be the inputs of the successive reservoirs. The mixing cascade of reservoirs would be instantaneous and not time dependent, so the estimation of Q_{Other}^{In} would still be the same as with one reservoir. Although the V_{Tot} for the entire stream would stay the same for the cascade of reservoirs, each reservoir in series would have a volume equal to $\frac{V_{Tot}}{n_{res}}$. Where n_{res} is the number of reservoirs in the model. Q_{DA}^{Out} does appear to converge to a fixed limit when n_{res} is greater than 100. For this reason, we used a value of 200 for n_{res}.

With this model, all input data are known except for V_{Tot}, which as mentioned before is assumed to be constant during a runoff event. V_{Tot} is then the only parameter that can be modified to adjust the output of the model.

To calibrate this reservoir cascade model, we compared the model results to results from two artificial flooding tests performed in the catchment in autumn 2011 (*Eder et al.*, 2014). Two flooding experiments were performed by quickly injecting a large amount of water at the most upstream point (i.e Sys4) of the stream and monitoring the downstream discharge and other parameters. Bromide was dissolved into the injected water at Sys4 and subsequently measured downstream at MW. As the natural baseflow

water has a concentration that is several magnitudes lower than the injected water, a single end-member EMMA from equations (5.1) and (5.2) could be applied at MW to separate the injected water from the original baseflow water.

5.4.7 Timing surveys

A center of mass timing survey was conducted for the overall hydrograph and the source components by taking a discharge weighted average of the times during each runoff event. The times for the source components were then categorized into "Early", "Center", and "Late" based on the overall hydrograph. When a source component occurred within 5 minutes of the center of mass of the overall hydrograph, then the component was considered "Center". If the component occurred earlier than 5 minutes before the hydrograph the component was considered "Early", and if the component occurred later than 5 minutes after the hydrograph the component was considered "Late". The decision for the 5 minute window for the "Center" is due to the measurement resolution of the input chemistry data. When the volumes of specific source waters were lower than the estimated uncertainty, those source water were excluded from the survey and labeled "Minimal".

Additionally, a peak timing survey was performed to assess the internal progression of the source components during runoff events. Similar to the center of mass survey, the same categories were used to describe the timing as well as the 5 minute window. But instead of the center of mass, the discharge peaks associated with rainfall pulses were used for the timing points between the hydrograph and the source components. Only six events out of the 40 captured runoff events had a single hydrograph peak, so most events had multiple rain and discharge peaks to provide information about the timing progression of runoff events. When no discernible hydrograph pulse of a source water could be identified associated with a rainfall pulse, the source water was given the label "No Peak" for that specific peak.

5.4.8 Uncertainty assessment

The primary sources of uncertainty are from the continuously measured data (i.e. discharge and water chemistry) and the input parameters of the end-member concentrations for the mass balance equations (*Barthold et al.*, 2011). Model structure uncertainty is considered negligible as compared to the above model input uncertainty. All uncertainties will be estimated from a normal distribution based on an error function associated with each parameter. The determination of the error functions for the parameter uncertainty distribution curves are described in section 5.4.8. With the uncertainty distributions, Monte-Carlo simulations were performed based on random sampling of each parameter uncertainty distribution. 5,000 simulations were performed. The final results include distributions of source component estimates at every time step for every flooding event.

Parameter uncertainty estimations

Discharge uncertainty was defined as a fixed percentage of the discharge magnitude. The mean absolute normalized error (MANE) of the manual grab measurements of discharge to the estimates of discharge used in the continuous time series was used for the discharge uncertainty percentage. To estimate the uncertainty distribution for the Monte-Carlo simulations, the MANE was used as the standard deviation in the random normal distribution.

Based on laboratory testing and grab samples at MW, the uncertainty for the continuous solute measurements from the ISE devices had a large percentage of uncertainty for the low concentrations, but significantly lower as the concentration increased. The function of parameter uncertainty with concentration magnitude was not linear, but the mean of chloride and nitrate ranged from 230% for a concentration of 0.5 mg/l, to 91% at 1 mg/l, to 15% at 5 mg/l, and to 8% at 20 mg/l. As with the discharge uncertainty, an uncertainty function dependent on the concentration was used as the standard deviation for the random normal distribution.

The uncertainties for the end-member concentrations were estimated from the grab measurements of the designated end-members. The standard deviation for the uncertainty distribution for the rainfall end-members was estimated from the standard deviation of the monthly sample set of the rainfall end-member concentrations. Both the uncertainty for the Q_{SA} and Q_{DA} end-members were estimated from the difference between the representative grab measurement locations (i.e. Sys2 and Sys4 for the shallow aquifer and Q1 and Sys1 for the deep aquifer) divided by the mean at each sample period.

As the chloride end-member concentrations of the soil water were assumed to be the same as the shallow aquifer water, the uncertainty was also assumed to be the same. The $C_{Soil,NO3}$ uncertainty was determined by first estimating the maximum realistic $C_{Soil,NO3}$ concentration from equation (5.11). $C^{max}_{Soil,NO3}$ was estimated by assuming that $Q^{mp}_{SA} = 0$. As both $Q^{mp}_{SA+Soil}$ and $C^{mp}_{SA+Soil,NO3}$ are always larger than Q^{mp}_{SA} and $C_{SA,NO3}$, $C^{max}_{Soil,NO3}$ should be the maximum realistic concentration when $Q^{mp}_{SA} = 0$. To obtain the standard deviation for use in generating the normal distribution, the midpoint value ($C^{mid}_{Soil,NO3}$) was calculated between $C_{Soil,NO3}$ and $C^{max}_{Soil,NO3}$ and the ratio of the difference between $C_{Soil,NO3}$ and $C^{mid}_{Soil,NO3}$ was used as the standard deviation.

5.5 Results

5.5.1 Water and solute loads

During the period from 2011-2012, there were 122 runoff event hydrographs captured at MW that exceeded a rise in discharge above baseflow of 2 l/s. There were an additional 7 flooding events that were not captured at MW due to equipment failure and identified based on the rainfall time series. Of the 129 runoff events hydrographs, there were 40 runoff events at MW that captured both water chemistry (i.e. chloride and nitrate) and discharge at a 1 min intervals. These included the top 5 largest runoff events. At Sys4,

72 flooding event hydrographs were captured for flow and 25 events for both flow and solutes. Unfortunately, the top 5 runoff events for Sys4 were neither captured for flow nor solutes. Although the majority of both the flow and the solute load during the two years was from baseflow rather than the runoff events (i.e. 83% compared to 17%), the runoff events still supplied a significant part of the total flow and solute loads (Table 5.2). The runoff coefficients for the runoff events of MW were very low with a range of 0.002 to 0.033 and a mean of 0.008. The runoff coefficient summary excluded the rain-on-snow events.

Table 5.2: The ratios of the flow condition (i.e. baseflow and event runoff flow) to the total yearly flow volumes and solute loads. Q_{DA} only has a net contribution during baseflow, while Q_{Soil} and Q_{Rain} only contribute during runoff events.

	Flow Type	Flow	NO_3-N Load	Cl Load	Q_{SA}
2011	Baseflow	0.85 (±0.04)	0.78 (±0.07)	0.92 (±0.04)	0.87 (±0.10)
	Runoff events	0.15 (±0.01)	0.22 (±0.04)	0.08 (±0.03)	0.13 (±0.06)
2012	Baseflow	0.78 (±0.04)	0.70 (±0.06)	0.87 (±0.04)	0.75 (±0.08)
	Runoff events	0.22 (±0.01)	0.30 (±0.06)	0.13 (±0.04)	0.25 (±0.12)
Total	Baseflow	0.83 (±0.04)	0.76 (±0.07)	0.90 (±0.04)	0.82 (±0.09)
	Runoff events	0.17 (±0.01)	0.24 (±0.04)	0.10 (±0.04)	0.18 (±0.08)

The two largest events, both in terms of maximum discharge and total volume, occurred in mid-January of both years and accounted for over half of the total runoff event water volume and solute load for both years (Table 5.3). Both events were rain-on-snow events with soils at field capacity. The five largest events, which was about 3.7% of the total number of events, accounted for 70% to 80% of the runoff event water volume and solute load. The top 10% of the largest runoff events accounted for over 80% of the flow and load and over 90% for the nitrate load and Q_{Soil}. Excluding the top 5 largest events, Sys4 on average contributed about 35% of the event runoff flow volume and nitrate load and over half of Q_{Rain} to MW (Table 5.3). Approximately a third of the event flow and nitrate load at MW was from Sys4, and although Q_{SA} from Sys4 was low both the Q_{Soil} and Q_{Rain} contribution from Sys4 was substantial.

Log-log regressions of event runoff flow volumes to solute loads and source components showed very high correlations (i.e. R^2 of over 0.95) for MW, but only moderate correlations were found for Sys4 (i.e. R^2 of about 0.65). The mean bulk event nitrate concentration for the lower 90% of runoff events was 2.85 mg/l with a CV of 0.14, while the top 10% of events had a mean concentration of 11.07 mg/l with a CV of 0.41. Sys4 had a wider distribution with a mean of 4.79 mg/l and CV of 0.95 for the lower 90% and a mean of 10.04 mg/l and CV of 0.41 for the top 10%.

The results from the flowpath contribution assessment from the 14 events are shown in Table 5.4. The total contribution ratio includes all point inputs to the stream and excludes the diffuse groundwater input and the overland flow input. The ratios of the sum of all of the point input stations into the stream to MW ranged from 0.57 to 1.10.

Table 5.3: Mean flow ratios of the contribution of the top largest runoff events to the total event runoff volume at MW. The percentages next to the number of events is the percentage of the events to the total number of events for the two year measurement period. "Sys4 to MW" is the contribution ratio of the runoff events of Sys4 to MW, but exclude the top 5 events as they were not captured by Sys4.

Events	Flow	NO_3-N Load	Cl Load	Q_{SA}	Q_{Soil}	Q_{Rain}
All Events	1.00	1.00	1.00	1.00	1.00	1.00
Top 2 (1.5%)	0.56	0.57	0.55	0.53	0.59	0.58
Top 5 (3.7%)	0.71	0.80	0.73	0.67	0.84	0.70
Top 10 (7.5%)	0.80	0.89	0.84	0.79	0.93	0.77
Top 13 (10.0%)	0.84	0.91	0.87	0.82	0.96	0.81
Sys4 to MW	0.35	0.37	0.21	0.12	0.43	0.55

During small events, the point inputs can supply all of the flow to MW. As the runoff events grow larger, the point input contribution decreased steadily. The event volume sum of the point input stations is very well correlated with total event volume at MW with a log-log correlation R^2 and MANE of 0.99 and 0.06.

5.5.2 Original stream water pulse

The results of the bromide EMMA of the flooding experiment show that much of the event peak hydrograph is composed of original pre-event water stored in the stream (Figure 5.3). The injected water appears significantly later than the runoff peak and accounts for approximately 80% of the runoff event volume. The reservoir cascade model fit well the bromide EMMA with a V_{Tot} of 16500 liters. This value of V_{Tot} is equivalent to an earlier cross-section survey of the stream that estimated the baseflow volume of the stream at approximately 22000 liters with an outlet baseflow discharge of 6.3 l/s. As the discharge during the flooding test was approximately 1.5 l/s, a lower value of V_{Tot} for the flooding test is reasonable. These two sets of relationships between baseflow discharge and V_{Tot} were used to create the linear function to estimate a V_{Tot} given an initial baseflow discharge.

5.5.3 Source components

The results from the EMMA for MW are illustrated in Figures 5.4 and 5.5, and the results for Sys4 are shown in Figure 5.6. Figure 5.4 presents the representative top 10% of runoff events by volume, and Figure 5.5 presents the representative lower 90% of runoff events. The figure for Sys4 has a mixture of events from the two MW figures. On average for MW, Q_{SA} and Q_{Rain} contributed approximately an equal amount to the total flow volume (i.e. 0.43 and 0.42 respectively) with a substantially lower contribution of water from Q_{Soil} (i.e. 0.15) (Table 5.5). The only difference between the top 10% and the lower 90% for MW is a lower contribution of Q_{Soil} to the total flow volume for the smaller events, while the other two components still contribute an equal share to the

Table 5.4: Flowpath contribution ratios during runoff events with sufficient discharge data from the point inputs to the stream. "Other Tiles" include all of the tile drainage systems without Sys4 (i.e. Sys2, Sys3, Frau1, and Frau2). "Springs" include all of the shallow dynamic springs (i.e. A1, A2, and K1). The "Total Pts." column is the sum of the stream point input ratios, while the "MW" column is the water volume of the runoff event at MW in cubic meters. The ± values in parentheses are the uncertainty ratios associated with the specific stream inputs. The table is ordered by the MW event volume.

Date	Sys4	Other Tiles	Springs	Total Pts.	MW (m^3)
2011-10-12	0.27 (±0.02)	0.27 (±0.03)	0.10 (±0.01)	0.64 (±0.03)	790
2012-09-12	0.40 (±0.02)	0.30 (±0.03)	0.14 (±0.04)	0.84 (±0.06)	530
2012-07-28	0.34 (±0.02)	0.16 (±0.02)	0.17 (±0.02)	0.67 (±0.03)	470
2012-09-05	0.28 (±0.02)	0.19 (±0.02)	0.10 (±0.02)	0.57 (±0.03)	380
2011-08-04	0.52 (±0.03)	0.19 (±0.04)	0.11 (±0.01)	0.82 (±0.05)	250
2011-09-18	0.22 (±0.01)	0.34 (±0.03)	0.17 (±0.02)	0.73 (±0.04)	230
2011-12-07	0.48 (±0.03)	0.21 (±0.02)	0.15 (±0.02)	0.84 (±0.04)	198
2012-07-26a	0.32 (±0.02)	0.31 (±0.05)	0.28 (±0.05)	0.91 (±0.08)	69
2012-05-31	0.39 (±0.02)	0.29 (±0.05)	0.30 (±0.04)	0.98 (±0.07)	60
2012-07-26b	0.38 (±0.02)	0.37 (±0.06)	0.28 (±0.06)	1.03 (±0.09)	54
2011-09-08	0.27 (±0.02)	0.44 (±0.09)	0.32 (±0.04)	1.03 (±0.10)	44
2012-06-09	0.51 (±0.03)	0.40 (±0.07)	0.19 (±0.02)	1.10 (±0.08)	41
2012-08-04	0.53 (±0.03)	0.32 (±0.05)	0.24 (±0.02)	1.09 (±0.07)	40
2012-08-26	0.60 (±0.04)	0.33 (±0.06)	0.17 (±0.05)	1.10 (±0.08)	35

total flow volume. For the nitrate load in the large events, Q_{SA} and Q_{Soil} contributed approximately equal shares to the total load, while Q_{Rain} contributes little to the solute load. As the contribution of Q_{Soil} flow volume decreases in the smaller events, so does the nitrate load contribution and subsequently the dominant source of nitrate load in the lower 90% of events is Q_{SA}. The dominant source of chloride load is from Q_{SA}, and the contribution increases as the runoff event volume decreases. Compared to MW, the runoff events at Sys4 contained little Q_{SA}, had similar proportions of Q_{Soil} to the larger events of MW, and the majority of the flow was composed of Q_{Rain}. Consequently, the bulk of the nitrate load at Sys4 was from Q_{Soil} (Table 5.5).

5.5.4 Timing surveys

The component center of mass timing survey shows consistent recurring trends (Table 5.6). For all events, both Q_{SA} and Q_{Rain} consistently occur during the center of mass of the hydrograph, while Q_{Soil} either does not flow with appreciable amounts or if there is significant flow then Q_{Soil} occurs later in the hydrograph. The lower 90% of events have similar frequency trends for Q_{SA} and Q_{Rain} as all events, but with nearly no Q_{Soil}.

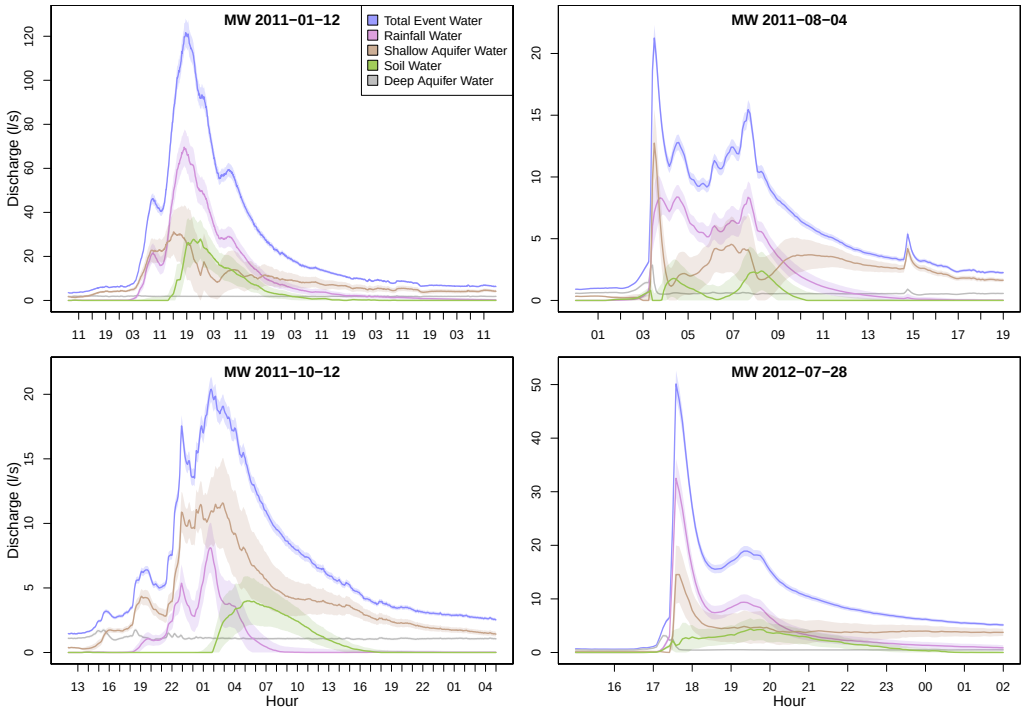

Figure 5.4: Four examples of the EMMA results for largest 10% of events at MW with soil water during 2011-2012.

The top 10% events have a higher tendency for Q_{SA} to occur early and a large majority of Q_{Soil} occurs later in the hydrograph. As with the lower 90% category, Q_{Rain} tends to occur during the center of the hydrograph.

The peak timing survey has some similarities to the center of mass timing survey, but the peak timing survey does have some differences and additional results (Table 5.7). The peaks of both Q_{SA} and Q_{Rain} do tend to occur at the same time as the overall hydrograph, but unlike the center of mass timing the peaks do not occur early very often. The peaks all tend to occur later more often than the center of mass. There is also a general increase in frequency that the component peak occurs at the same time as the hydrograph peak with the increasing number of peaks. Also, almost 40% of the time Q_{Rain} did not have a noticeable first peak with the associated hydrograph peak, while Q_{SA} had nearly all associated peaks.

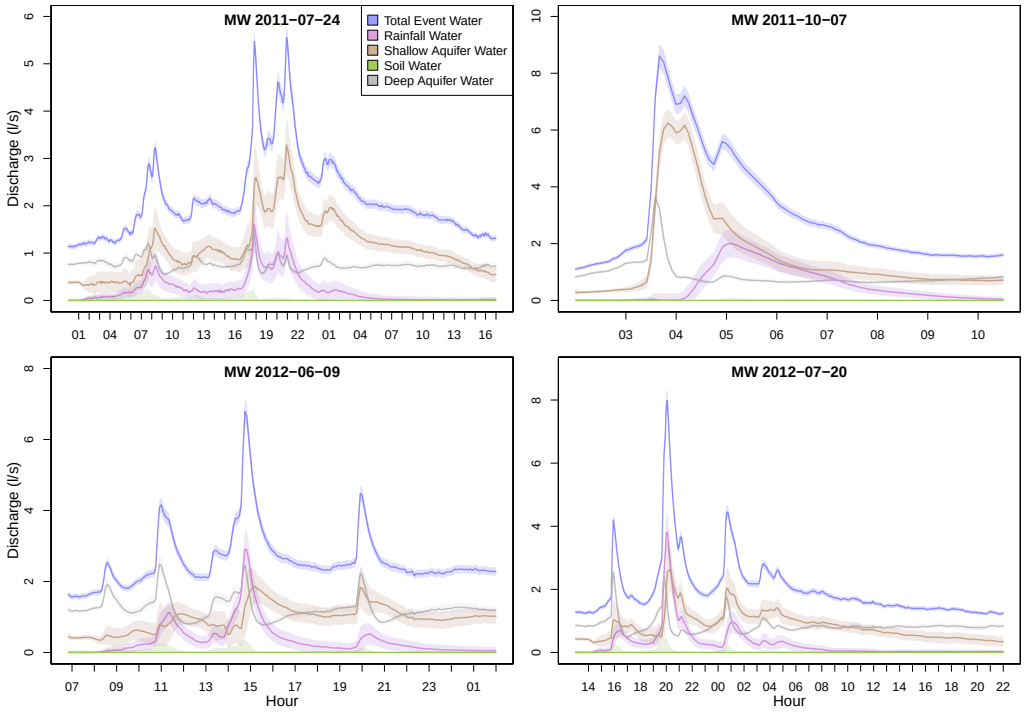

Figure 5.5: Four examples of the EMMA results for lower 90% of events at MW and are representative of most events during 2011-2012.

5.6 Discussion

5.6.1 Runoff event summary

The predominant catchment state for the transport of water, nitrogen, and chloride is baseflow. Nevertheless, event runoff does supply a significant amount of water and solute load that cannot be neglected in water and solute load budgets. In the HOAL, over half of the runoff water and solute load was supplied by only two winter events and up to 80% during five events. In most catchments, solute loads and water chemistry in general are not continuously monitored due to instrument maintenance requirements and cost. When runoff events are captured, they are typically opportunistic and may not be representative of the yearly distribution of runoff events.

Other studies have found substantial errors in the estimate of solute loads when only periodic sampling was performed (*Aulenbach*, 2013). Log-log regressions of runoff event volume to the solute loads and source components were quite high indicating that runoff event magnitude is a major factor for transport processes. Nevertheless, if the two largest runoff events were not captured and the solute loads would need to be estimated from the log-log regressions from the other captured events, then the nitrate and chloride loads for the total runoff would be overestimated by approximately 70% for

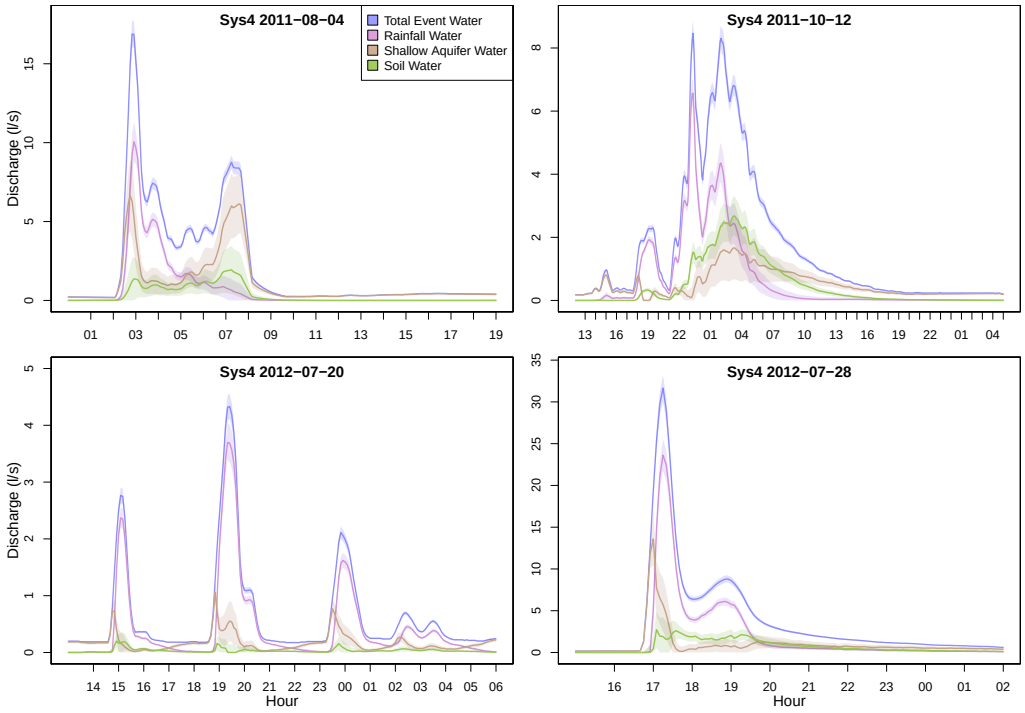

Figure 5.6: Four examples of the EMMA results at Sys4 from selected events illustrated in Figures 5.4 and 5.5.

both years. Although if the top five events were not captured, the nitrate load would only be overestimated by 17% due to the coincidence of some of the other large events compensating for the overestimation of the top two largest events. These estimates assume that discharge was measured for all top events unlike Sys4 where neither solutes nor discharge were captured. As the top two largest events were rain-on-snow events with a relatively small event rainfall, if the discharge and solute loads would need to be estimated from the rainfall alone then the flow and solute loads estimates would be substantially inaccurate.

5.6.2 Original stream water pulse - deep aquifer water

During normal small runoff events, the initial pulse of water originally stored in the stream can have a significant impact on the beginning of the hydrograph depending on the initial baseflow discharge and the magnitude of the runoff event. Other studies have observed large proportions of pre-event water in the initial rise of the hydrograph of some events (*Brown et al.*, 1999; *Caissie et al.*, 1996; *Gonzales et al.*, 2009; *McGlynn and McDonnell*, 2003; *Hinton et al.*, 1994), which could be interpreted at least partially as pre-event in-stream storage. During the large events, this pulse was insignificant to the hydrologic and chemical dynamics of the event. Other studies have found that the

Table 5.5: The mean ratios of the source components to the total event runoff flow volume, nitrate load, and chloride load for different event categories of runoff events at MW and Sys4 for 2011-1012. All events for Sys4 does not include the top 5 largest events during 2011-2012.

	Site	Category	Q_{SA}	Q_{Soil}	Q_{Rain}
Flow	MW	All Events	0.43	0.15	0.42
		Top 10%	0.42	0.17	0.40
		Lower 90%	0.47	0.03	0.50
	Sys4	All events	0.16	0.16	0.68
NO_3-N	MW	All Events	0.49	0.46	0.04
		Top 10%	0.47	0.49	0.04
		Lower 90%	0.74	0.19	0.07
	Sys4	All events	0.27	0.61	0.12
Cl	MW	All Events	0.71	0.26	0.03
		Top 10%	0.68	0.29	0.03
		Lower 90%	0.88	0.08	0.04
	Sys4	All events	0.44	0.46	0.09

initial water stored in or immediately surrounding the stream has a minimal impact on the total runoff event volume (*McDonnell*, 1990; *Waddington et al.*, 1993).

The pulse model was meant to model Q_{DA}, because the input of Q_{DA} into the stream was assumed to be constant due to observations of the deep aquifer point sources (i.e. Q1 and Sys1). The initial pulse of Q_{DA} is dependent on the volume of baseflow water stored in the stream prior to a runoff event and estimated from the initial baseflow discharge. Runoff events with a high initial baseflow compared to the peak discharge will have a more significant impact by the Q_{DA} pulse then large events with initial flows greatly exceeding the maximum possible Q_{DA} pulse of 4 to 5 l/s (Figure 5.5). Nevertheless, the assumption of a constant inflow into the stream of Q_{DA} entails that there is no net additional gain of Q_{DA} during runoff events above baseflow.

5.6.3 Source water contribution dynamics and associated flowpaths

Rainfall water

Rainfall water contribution from other studies has ranged from 1-100% of the total flow depending on the hydrologic properties of the catchment and the hydrologic conditions prior to runoff events (*Klaus and McDonnell*, 2013). In agricultural systems with tile drainages and overlaying preferential flowpaths, the contribution of rainfall water was between 11-54% (*Stone and Wilson*, 2006; *Cey et al.*, 1998; *Everts and Kanwar*, 1990). Typically, rainfall water contributed about 20-40% of the total flow with most water originating from within the catchment prior to the events. Our study with a mean of 42% rainfall water was not abnormal in the context of other studies, but Sys4 with a

Table 5.6: Component Timing Survey for the MW runoff events from 2011-2012. "Minimal" are component flow volumes are less than the component uncertainty flow volume, "Early" occurs when the component has a center of mass is before the total flow center of mass, "Center" occurs when the center of mass of the component is ±5 min of the total flow, and "Late" occurs when the component center of mass is after the total flow. The values are in frequency ratios where a value of 0.72 for Q_{SA} at "Center" means that 72% of the time Q_{SA} occurs at the center of mass of the total flow. All events include all measured events, the Top 10% include the events within the top 10% of runoff event volumes, and the Lower 90% includes all of the other runoff events.

	Timing	Q_{SA}	Q_{Soil}	Q_{Rain}
All Events	Minimal	0.00	0.75	0.00
	Early	0.17	0.00	0.26
	Center	0.72	0.08	0.67
	Late	0.11	0.17	0.08
Top 10%	Minimal	0.00	0.00	0.00
	Early	0.63	0.00	0.38
	Center	0.38	0.25	0.63
	Late	0.00	0.75	0.00
Lower 90%	Minimal	0.00	0.96	0.00
	Early	0.04	0.00	0.21
	Center	0.82	0.04	0.68
	Late	0.14	0.00	0.11

mean of 68% was on the higher end of the rainfall water contribution range. Although, some studies have estimated that the event rainfall contribution is primarily derived from rainfall directly falling onto the stream channel rather than passing through the subsurface (*Hogan and Blum*, 2003), but as we measured Sys4 which has a substantial amount of rainfall water volume and no open channel the amount of rainfall falling on the stream cannot be the dominant source of rainfall water.

For Q_{Rain} to appear in the surface waters during a runoff event, it must travel quickly to the stream and not flow into a large reservoir where Q_{Rain} would become diluted. Rainfall water can fall directly on the stream and would appear in the stream immediately. In certain catchments with very little overland and preferential flow, rain falling directly onto the stream can be the dominant pathway (*Hogan and Blum*, 2003). Others, including ourselves, have not found this processes to be dominant. Other than rain falling directly onto the stream, the primary flowpaths of Q_{Rain} would be overland and preferential flow. The dominance of one over the other appears to be dependent on the specific catchment conditions and the current hydrologic state of the catchment.

Antecedent soil moisture conditions has been found to play a role in the transmittance of rainfall water. Most studies have found an increase in the conveyance of the

Table 5.7: Component peak timing survey for the MW runoff events from 2011-2012. The analysis is similar to Table 5.6 except that this assesses the peak discharges during runoff events rather than the total component and hydrograph volumes. All runoff events are lumped together. The terminology is the same as Table 5.6 except "No Peak" means that no observable peak discharge response occurred. All results for each peak column required at least five events. Peaks with less than five events are listed as "NA". The peaks of Q_{Soil} did not consistently correspond to the hydrograph peaks and were not included in the survey.

		Timing	1st Peak	2nd Peak	3rd Peak	4th Peak
Q_{SA}	Top 10%	No Peak	0.00	0.00	0.00	NA
		Early	0.20	0.60	0.00	NA
		Center	0.60	0.40	0.75	NA
		Late	0.20	0.00	0.25	NA
	Lower 90%	No Peak	0.07	0.00	0.00	0.00
		Early	0.00	0.00	0.00	0.00
		Center	0.63	0.48	0.64	0.78
		Late	0.30	0.52	0.36	0.22
Q_{Rain}	Top 10%	No Peak	0.20	0.00	0.00	NA
		Early	0.00	0.20	0.00	NA
		Center	0.60	0.40	0.75	NA
		Late	0.20	0.40	0.25	NA
	Lower 90%	No Peak	0.41	0.00	0.00	0.00
		Early	0.00	0.05	0.00	0.11
		Center	0.30	0.75	0.79	0.67
		Late	0.30	0.20	0.21	0.22

event rainfall water with increasing soil moisture (*Huang et al.*, 2006; *Muñoz-Villers and McDonnell*, 2012; *McCartney et al.*, 1998; *Tan et al.*, 2002b; *Guinn Garrett et al.*, 2012; *Hogan and Blum*, 2003). The increase in conveyance with increased soil moisture was also found in agricultural catchments with tile drainages (*Stone and Wilson*, 2006; *Cey et al.*, 1998; *Everts and Kanwar*, 1990). On small runoff events and events with multiple rainfall pulses, we found that the initial rainfall pulse had a low runoff coefficient compared to events with a high rainfall intensity and/or the successive rainfall pulses. Additionally, Q_{Rain} sometimes did not respond to the initial rainfall pulse (Table 5.7). In our catchment, we found that the runoff coefficient and the contribution of Q_{Rain} was more dependent on the rainfall intensity and development of the rainfall pulses during runoff events.

When runoff coefficients for events are low, rainfall water contribution is high, and rainfall to hydrograph peak time has been short, this has indicated that shallow pref-

erential flow has been dominant in some catchments (*Brown et al.*, 1999; *Blume et al.*, 2008; *Casper et al.*, 2003; *McDonnell*, 1990) rather than overland flow. A high proportion of pre-event water (e.g. 80-90%) has indicated highly permeable soils that quickly infiltrate directly into the groundwater aquifer and are subsequently diluted by the large reservoir (*Muñoz-Villers and McDonnell*, 2012).

Cey et al. (1998) found that the tile drainage rainfall water contribution was significantly lower than the surface water outlet contribution. They interpreted the cause of this discrepancy to overland flow contributing significantly to the surface water volume, which should contain a substantial proportion of rainfall water. This is in contradiction to our study where the tile drainage had a significantly higher contribution of rainfall water. Where preferential flow is more dominant than overland flow for runoff events, the tile drainages would contain a higher proportion of rainfall water as compared to the outlet, while the surface water outlet would have a higher contribution of rainfall water when overland flow is more dominant.

Although we did observe increasing peak discharge response in successive rainfall pulses to rainfall intensity, no correlation was found between either total runoff event volume or rainfall volume/intensity and the component proportions. Some studies have found that Q_{Rain} increased with the rainfall event volume in addition to runoff coefficients (*James and Roulet*, 2009; *Segura et al.*, 2012), while others have observed the opposite effect (*Casper et al.*, 2003; *Blume et al.*, 2008).

Due to the heavy soils, the tile drainages, and little apparent overland flow, preferential flow is the dominant flowpath for Q_{Rain}. The major controls on the conveyance variability of Q_{Rain} is due to the antecedent soil moisture conditions and the rainfall intensity. As the tile drainages supply most of Q_{Rain} to the stream, these processes must take place within the top 1-1.5 m below the surface. Q_{Rain} tends to shape the center of the hydrograph as the timing is consistently at the center of mass of the overall hydrograph.

Soil water

The primary cause for the variability on the source components across the MW runoff events is the contribution of Q_{Soil}. The larger runoff events have a significant contribution of Q_{Soil}, while the smaller and more common events have little Q_{Soil}. As Q_{Soil} has a high concentration of nitrate and a moderate concentration of chloride, the associated solute load contributions reflect these differences. During the large events, Q_{Soil} contributed half of the nitrate load along with Q_{SA}, but the contribution of Q_{Soil} for the smaller events was much lower.

Amongst studies that have used soil water as an end-member, soil water generally does not contribute the majority of the flow volume, but does contribute a substantial proportion of the solute load (*Bazemore et al.*, 1994; *Casper et al.*, 2003; *Liu et al.*, 2004; *DeWalle and Pionke*, 1994). Those that have compared larger runoff events to smaller runoff events have also consistently seen a higher proportion of soil water in the larger events compared to the smaller events (*Bazemore et al.*, 1994; *Liu et al.*, 2004). *Hinton et al.* (1994) found that the soil water contribution increased later in the runoff events

and *Liu et al.* (2004) found that the bulk of the soil water occurs later in the larger runoff events. *Iwagami et al.* (2010) found that soil water contribution increased as the water table rose and intersected with the upper unsaturated zone during large runoff events. We also found that the larger events with higher soil saturation conditions increased the soil water contribution.

During irrigation experiments on tile drainages utilizing tracers, *Everts and Kanwar* (1990) found that preferential flow was more dominant earlier in the hydrograph and matrix flow was more dominant in the center and end of the hydrograph. As the macropores fill and increase the hydrostatic pressure on the surrounding matrix, more of the matrix water would be pressed out into the tile drains. Q_{Soil} occurring later in the hydrograph supports this hypothesis as the unsaturated soil water should be mainly held within the matrix.

The source water designated soil water appears to be matrix water stored within some zone of the upper 1-1.5 m of the soil as Sys4 contained a significant proportion of soil water. Due to excess saturation of the soil from large rainfall events, the soil water can be slowly mobilized from the matrix into the preferential flowpaths that can either use the tile drains to reach the stream or can directly reach the stream via the preferential flowpaths. Due to the high contribution of soil water in Sys4, the tile drains appear to be the dominant input of soil water to the stream.

Shallow aquifer water

Q_{SA} is the primary groundwater source that is equivalent conceptually to many other studies with a groundwater source and has been consistently found to be the dominant source water for both baseflow and event runoff flow in many catchments (*Klaus and McDonnell*, 2013). Q_{SA} is a dominant source of total event runoff flow volume with an equal contribution as Q_{Rain}, but Q_{SA} has a substantially higher nitrate and chloride load contribution and is the dominant source during the lower 90% of runoff events. From an earlier study, the Q_{SA} end-member concentrations were relatively stable over the two years which would indicate a large reservoir with some degree of internal mixing (*Exner-Kittridge et al.*, 2016).

There has been two flowpaths interpreted to transmit groundwater to streams: displacement/piston flow (*Ladouche et al.*, 2001) and preferential flow (*Waddington et al.*, 1993). The timing of the source water within the hydrograph has been an indication of the dominant flowpath as displacement flow can potentially occur earlier in the hydrograph due to water pressures transferring faster than the actual water. *Caissie et al.* (1996) found such an early response of the groundwater in the hydrograph as compared to the rainfall water. We found that it was dependent on the size of the event. The smaller and more common events had a timing similar to that of Q_{Rain}, while the larger events were more likely to have Q_{SA} occur early in the hydrograph (Tables 5.6 & 5.7). Irrigation experiments combined with EMMA have indeed found that the groundwater component can travel by both displacement and preferential flow *Everts and Kanwar* (1990).

Little Q_{SA} was found in Sys4 as compared to MW. In the smaller more common

events, significant amounts of Q_{SA} must enter the stream from other point inputs like the shallow springs as there is little to no diffuse groundwater entering the stream to compensate for the lack of Q_{SA} at Sys4. The large events could have more Q_{SA} entering the stream from both other point inputs and diffuse groundwater flowpaths as the diffuse component could contribute significant water volumes.

The groundwater source component has been studied in catchments utilizing EMMA extensively, but there are still many unknowns regarding the specifics on what part of the subsurface does Q_{SA} represent and what is the dominant flowpath to the surface waters. The end-member concentrations of Q_{SA} according to the baseflow sampling at the perennial tile drainages indicate a relatively stable concentration reservoir unlike Q_{Soil}. This would indicate a typical large groundwater aquifer. Nevertheless, the response of Q_{SA} indicates that Q_{SA} can quickly reach the stream and in the case of large events even faster than Q_{Rain}. Q_{SA} appears to be displaced into the stream from the increased hydrostatic pressure of the rainfall as well as travel through preferential flowpaths depending on certain conditions of the event (e.g. rainfall volume and intensity, antecedent soil moisture conditions, etc.). As Sys4 contains little Q_{SA} compared to MW, the source of the shallow aquifer could be from soil below the tile drainages at least partially in contrast to the soil water which is predominantly above the tile drainages.

5.6.4 Uncertainty analysis

Uhlenbrook and Hoeg (2003) described several sources of uncertainty in EMMA studies. These include uncertainties in: discharge and chemical measurements, inter-event variability in the end-member concentrations, solution of minerals from the solid phase of soils into the event water, and the spatial heterogeneity of end-member concentrations. The last source of uncertainty listed above equates to the representative estimate of the specific end-members and researchers have generally found this uncertainty to be one of the highest in EMMA studies (*Uhlenbrook and Hoeg*, 2003; *Genereux*, 1998; *Bazemore et al.*, 1994). This uncertainty source was partially included in this study through the baseflow sampling of some end-members from the appropriate point inputs from both sides of the stream. Nevertheless, not all of the catchment is covered by the point inputs and the soil water end-members did not have an easy to sample source. All end-members likely have a higher spatial heterogeneity and consequently a higher uncertainty than those given in this study. This is even more problematic for the soil water end-members as the captured variability of the nitrate end-member throughout the two years was higher than the others. Both *Genereux* (1998); *Bazemore et al.* (1994) also found a higher uncertainty in the soil water end-members than the other source water end-members.

The high variability in the nitrate soil water end-member creates another source of uncertainty. At certain periods, the nitrate soil water end-member had concentrations within 4-5 mg/l of the shallow aquifer nitrate end-member. When the concentrations of end-members are similar, then the EMMA results can have a high uncertainty (*Rice and Hornberger*, 1998). This is one of the causes for the high uncertainty of the soil and shallow aquifer waters as compared to the rainfall water which has very different

chloride and nitrate concentrations compared to the soil and shallow aquifer waters.

Capturing representative soil water end-member concentrations are difficult, because unlike the other source water end-members that either drain from the soil under field conditions (e.g. groundwater aquifer) or can be directly measured at several locations in a catchment (e.g. rain water) the soil water is attached to the soil matrix. Not only is the soil water difficult to extract, but the extracted soil water may not be representative of what actually gets flushed out during rainfall events. This issue of soil water representativeness was partially the reason for estimating the nitrate soil water end-member using the method presented in this study.

Even with the uncertainty, the final results show clear consistencies between events and the interpretations would not change. The knowledge of the specific sources that have high uncertainties allows us to better target the parameters that need to be more accurately measured and/or estimated to improve the reliability of the results. The improvements will include a better estimate of the soil water end-member independent of the EMMA process and an increase in the continuously measured solutes to validate the source contribution dynamics results.

5.7 Conclusions

Continuous monitoring of water chemistry in addition to discharge provides valuable information about the source water contributions and input flowpaths to surface waters, which can be utilized when developing more complex hydrologic and solute transport models for entire catchments. During the two year measurement period, baseflow contributed the majority of the total flow and load to the outlet, and two runoff events contributed over half of the event runoff water and solute load to the outlet. The tile drainage Sys4 contributed about 35% of the event runoff water and nitrate load to the outlet. These results reflect the necessity of continuous monitoring for the capture of representative and dominant runoff events.

Four source waters were identified to contribute to the surface water outlet. These included the deep aquifer, the shallow aquifer, the upper unsaturated zone of the soil, and the rain water. The deep aquifer water was found to discharge into the stream at a constant rate. Consequently, the hydrograph dynamics at the outlet could be effectively modeled utilizing a reservoir cascade model without the necessity of chemical tracers. The rain water on average contributed 42% of the total flow with an equal proportion of the shallow aquifer water. During the largest 10% of runoff events, the soil water contribution (17%) was significantly higher than the lower 90% of events (3%). As the soil water nitrate concentration is on average over twice the concentration of the shallow aquifer water, the contribution of the soil water to the nitrate load was approximately the same as the shallow aquifer water. On the other hand, most of the nitrate load during the smaller events came from the shallow aquifer. Most of the hydrograph at Sys4 came from the rain water, but Sys4 had a soil water contribution similar to the large events at the outlet. Consequently, most of the nitrate load at Sys4 came from the soil water.

The dominant flowpath of rain and soil water to reach the stream appeared to be via preferential flowpaths which can also be captured by the tile drainage. While both source waters travels via the preferential flowpaths, the soil water must first be mobilized by rain water saturating the upper soil, which has the consequence of the soil water occurring later in the hydrograph. The tile drainages appear to be the dominant input of soil water to the stream due to the high contribution of soil water in Sys4 as compared to the outlet. The shallow aquifer appears to travel by both matrix flow from displacement and preferential flowpaths. Other point inputs to the stream must contain a higher contribution of shallow aquifer water as compared to the outlet due to the low contribution of shallow aquifer water in Sys4. An increase in the antecedent soil moisture conditions also increases the conveyance of all the dynamic source waters.

The results from this study has shown that there is significant variability in the source contributions depending on the size and prior conditions of rainfall events. Each source water has a distinct contribution dynamic to downstream surface waters depending on the source location, hydrologic condition, and flowpaths that each take to the stream. Tile drainages provide additional valuable information about the contribution of source waters in the soil above the drain and the tile drainage contribution to the surface water outlet. The representativeness of the study allows the results of the internal hydrologic conditions and processes that dominate the storage and transfer of water and solutes to be generally applicable across other headwater agricultural catchments with similar properties.

Chapter 6

Conclusions

The overall goals of the thesis were to determine the major sources and flowpaths of water and solutes as well as the processes involved with the water and solute transport dynamics in the Hydrologic Open Air Laboratory (HOAL) catchment. The thesis included a sequence of chapters that furthered the above goals.

In Chapter 2, a new device to house water monitoring devices was presented and successfully deployed in the Hydrologic Open Air Laboratory (HOAL) catchment. The device was called the Water Monitoring Enclosure (WME) and it ensures a minimum internal water level which ensures that the enclosed water monitoring devices remain submerged even when there is no flow into the WME. The limited diameter of the inflow pipe buffers the flow velocity within the WME as some devices are sensitive to dramatic changes in flow velocity. The WME also conveys sediment through the system to ensure that the aggregation of sediment would not interfere with the internal water monitoring devices. The device is powered purely from natural hydraulic forces, so it requires no power source, and requires little additional maintenance beyond periodic cleaning. The functional assessments have shown that the WME has a minimal effect on the chemistry of the water and with the addition of a small magnet the WME can also measure discharge accurately up to 0.5l/s.

Chapter 3 presented a new methodology to estimate the stream to groundwater exchange (SGE) and associated groundwater solute concentrations, and a comparison to exciting methodologies. The newly developed method assumes that the inflowing and outflowing fluxes occur simultaneously and uniformly along the entire stream reach. Through the use of artificial stream simulations, the new method had the highest performance compared to the other methods and that all methods produced significantly different results depending on the flux distribution assumptions. Although this study found that the the new method performed better against the numerical simulations, estimating SGE using all three methods would be very valuable as minimum and maximum SGE values can provide information on the full range of realistic SGE values. For the same inputs, the different assumptions of each method can lead to values of gross stream gains and losses differing up to one order of magnitude between approaches. Estimating SGE using the proposed simple analytical method over numerical models solving full

hydrodynamic sets of partial differential equations has the clear advantages of much less parametrization.

Chapter 4 addressed the question of the seasonal variability of the nitrate concentration by analyzing the seasonal source and flowpath dynamics in additional to other seasonal biochemical explanations. The diffuse groundwater discharge into the stream had the highest contribution to the total yearly flow with 38% and was followed by the perennial tile drainages and deep aquifer point discharges with about 26% each. However, the majority of the nitrogen load contribution (60%) came from the perennial tile drainages due to their high nitrogen concentrations. The cause of the seasonal nitrate concentration was due to the alternating source aquifer contributions throughout the year with the deep aquifer typically contributing 75% of the water during the summer and 50% in the winter. In-stream denitrification, biochemical reactions, and fertilizer application timings were not found to be the significant processes in the seasonality of the surface water nitrogen concentrations and loads.

Building off of the previous chapters, Chapter 5 determined the representative source and flowpath dynamics of water and solute load during runoff events in the HOAL. The two largest runoff events contributed over 50% to the total event runoff flow and nitrate load. The main tile drainage contributed about 35% of the event runoff water and nitrate load to the outlet. The rain water on average contributed 42% of the total event runoff flow with an equal proportion of the shallow aquifer water. During the largest 10% of runoff events, the soil water contribution (17%) was significantly higher than the lower 90% of events (3%). As the soil water nitrate concentration is on average over twice the concentration of the shallow aquifer water, the contribution of the soil water to the nitrate load was approximately the same as the shallow aquifer water. On the other hand, most of the nitrate load during the smaller events came from the shallow aquifer. The dominant flowpath of rain and soil water to reach the stream appeared to be via preferential flowpaths. While both source waters travel via the preferential flowpaths, the soil water must first be mobilized by rain water saturating the upper soil, which has the consequence of the soil water occurring later in the hydrograph. The tile drainages appeared to be the dominant input of soil water to the stream due to the high contribution of soil water in the main tile drainage as compared to the outlet. The shallow aquifer appears to travel by both matrix flow from displacement and preferential flowpaths.

The thesis has advanced the knowledge of the source and flowpath dynamics of water and solutes in a typical Austrian headwater agricultural catchment. This thesis has provided several new advancements for the scientific community. This thesis provided a new device that will help other researchers more effectively monitor water properties continuously. This thesis has also provided a more accurate methodology to estimate stream to groundwater exchange in small streams to help in diffuse solute transport studies. With the knowledge of the internal processes of the source water and flowpaths that control the conveyance of solutes to the surface waters, the development of large comprehensive transport models will better identify and target significant pollutant sources and flowpaths that contribute to pollutant loads of surface waters.

References

Alexander, R. B., J. K. Böhlke, E. W. Boyer, M. B. David, J. W. Harvey, P. J. Mulholland, S. P. Seitzinger, C. R. Tobias, C. Tonitto, and W. M. Wollheim (2009), Dynamic modeling of nitrogen losses in river networks unravels the coupled effects of hydrological and biogeochemical processes, *Biogeochemistry*, *93*(1-2), 91–116, doi:10.1007/s10533-008-9274-8.

Anderson, J. K., S. M. Wondzell, M. N. Gooseff, and R. Haggerty (2005), Patterns in stream longitudinal profiles and implications for hyporheic exchange flow at the H.J. Andrews Experimental Forest, Oregon, USA, *Hydrological Processes*, *19*(15), 2931–2949, doi:10.1002/hyp.5791.

Anderson, S. P., W. E. Dietrich, R. Torres, D. R. Montgomery, and K. Loague (1997), Concentration-discharge relationships in runoff from a steep, unchanneled catchment, *Water Resources Research*, *33*(1), 211–225, doi:10.1029/96WR02715.

Arfken, G. B., and H. J. Weber (2005), *Mathematical Methods For Physicists International Student Edition*, Academic Press.

Arheimer, B., L. Andersson, and A. Lepistö (1996), Variation of nitrogen concentration in forest streams — influences of flow, seasonality and catchment characteristics, *Journal of Hydrology*, *179*(1–4), 281–304, doi:10.1016/0022-1694(95)02831-5.

Aulenbach, B. T. (2013), Improving regression-model-based streamwater constituent load estimates derived from serially correlated data, *Journal of Hydrology*, *503*, 55–66, doi:10.1016/j.jhydrol.2013.09.001.

Aulenbach, B. T., and R. P. Hooper (2006), The composite method: an improved method for stream-water solute load estimation, *Hydrological Processes*, *20*(14), 3029–3047, doi:10.1002/hyp.6147.

Barthold, F. K., C. Tyralla, K. Schneider, K. B. Vaché, H.-G. Frede, and L. Breuer (2011), How many tracers do we need for end member mixing analysis (EMMA)? A sensitivity analysis, *Water Resources Research*, *47*(8), W08,519, doi:10.1029/2011WR010604.

Bazemore, D. E., K. N. Eshleman, and K. J. Hollenbeck (1994), The role of soil water in stormflow generation in a forested headwater catchment: synthesis of natural tracer and hydrometric evidence, *Journal of Hydrology*, *162*(1), 47–75, doi: 10.1016/0022-1694(94)90004-3.

Beven, K. J. (2011), *Rainfall-Runoff Modelling: The Primer*, John Wiley & Sons.

BIPM, I., I. IFCC, I. IUPAC, and O. ISO (2008), *Evaluation of measurement data—guide for the expression of uncertainty in measurement. JCGM 100: 2008*, ed.

Blöschl, G., and M. Sivapalan (1995), Scale issues in hydrological modelling: A review, *Hydrological Processes*, *9*(3-4), 251–290, doi:10.1002/hyp.3360090305.

Blöschl, G., A. P. Blaschke, M. Broer, C. Bucher, G. Carr, X. Chen, A. Eder, M. Exner-Kittridge, A. Farnleitner, A. Flores-Orozco, P. Haas, P. Hogan, A. Kazemi Amiri, M. Oismüller, J. Parajka, R. Silasari, P. Stadler, P. Strauß, M. Vreugdenhil, W. Wagner, and M. Zessner (2016), The Hydrological Open Air Laboratory (HOAL) in Petzenkirchen: a hypotheses driven observatory, *Hydrology and Earth System Sciences*, *20*(1), 227–255, doi:10.5194/hess-20-227-2016.

Blume, T., E. Zehe, and A. Bronstert (2008), Investigation of runoff generation in a pristine, poorly gauged catchment in the Chilean Andes II: Qualitative and quantitative use of tracers at three spatial scales, *Hydrological Processes*, *22*(18), 3676–3688, doi:10.1002/hyp.6970.

Briggs, M. A., L. K. Lautz, and J. M. McKenzie (2012), A comparison of fibre-optic distributed temperature sensing to traditional methods of evaluating groundwater inflow to streams, *Hydrological Processes*, *26*(9), 1277–1290, doi:10.1002/hyp.8200.

Brown, V. A., J. J. McDonnell, D. A. Burns, and C. Kendall (1999), The role of event water, a rapid shallow flow component, and catchment size in summer stormflow, *Journal of Hydrology*, *217*(3–4), 171–190, doi:10.1016/S0022-1694(98)00247-9.

Burns, D. A., J. J. McDonnell, R. P. Hooper, N. E. Peters, J. E. Freer, C. Kendall, and K. Beven (2001), Quantifying contributions to storm runoff through end-member mixing analysis and hydrologic measurements at the Panola Mountain Research Watershed(Georgia, USA), *Hydrological Processes*, *15*(10), 1903–1924.

Burns, D. A., E. W. Boyer, E. M. Elliott, and C. Kendall (2009), Sources and transformations of nitrate from streams draining varying land uses: evidence from dual isotope analysis, *Journal of Environmental Quality*, *38*(3), 1149–1159.

Caissie, D., T. L. Pollock, and R. A. Cunjak (1996), Variation in stream water chemistry and hydrograph separation in a small drainage basin, *Journal of Hydrology*, *178*(1–4), 137–157, doi:10.1016/0022-1694(95)02806-4.

Carrasco, M., J. Bautista, and J. Mateo (2007), Automated sequential monitoring of ammonium, phosphate and nitrite in wastewater by multi-commutated peristaltic and solenoid pumped flow system - A comparative study, *Chemia Analityczna*, *52*(5), 757–770.

Casper, M. C., H. N. Volkmann, G. Waldenmeyer, and E. J. Plate (2003), The separation of flow pathways in a sandstone catchment of the Northern Black Forest using DOC and a nested Approach, *Physics and Chemistry of the Earth, Parts A/B/C*, *28*(6–7), 269–275, doi:10.1016/S1474-7065(03)00037-8.

Castro, N. M., and G. M. Hornberger (1991), Surface-subsurface water interactions in an alluviated mountain stream channel, *Water Resources Research*, *27*(7), 1613–1621.

Cey, E. E., D. L. Rudolph, G. W. Parkin, and R. Aravena (1998), Quantifying groundwater discharge to a small perennial stream in southern Ontario, Canada, *Journal of Hydrology*, *210*(1–4), 21–37, doi:10.1016/S0022-1694(98)00172-3.

Chantigny, M. H., P. Rochette, D. A. Angers, D. Massé, and D. Côté (2004), Ammonia Volatilization and Selected Soil Characteristics Following Application of Anaerobically Digested Pig Slurry, *Soil Science Society of America Journal*, *68*(1), 306, doi:10.2136/sssaj2004.3060.

Christophersen, N., C. Neal, R. P. Hooper, R. D. Vogt, and S. Andersen (1990), Modelling streamwater chemistry as a mixture of soilwater end-members — A step towards second-generation acidification models, *Journal of Hydrology*, *116*(1–4), 307–320, doi:10.1016/0022-1694(90)90130-P.

Cirmo, C. P., and J. J. McDonnell (1997), Linking the hydrologic and biogeochemical controls of nitrogen transport in near-stream zones of temperate-forested catchments: a review, *Journal of Hydrology*, *199*(1–2), 88–120, doi:10.1016/S0022-1694(96)03286-6.

Clercq, P. (2001), *Nutrient management legislation in European Countries*, Department of Soil Management and Soil Care Faculty of Agricultural and Applied Biological Sciences, Wageningen.

Covino, T., B. McGlynn, and J. Mallard (2011), Stream-groundwater exchange and hydrologic turnover at the network scale, *Water Resources Research*, *47*(12), doi:10.1029/2011WR010942.

Covino, T. P., and B. L. McGlynn (2007), Stream gains and losses across a mountain-to-valley transition: Impacts on watershed hydrology and stream water chemistry, *Water Resources Research*, *43*(10), doi:10.1029/2006WR005544.

David, M. B., L. E. Gentry, D. A. Kovacic, and K. M. Smith (1997), Nitrogen balance in and export from an agricultural watershed, *Journal of Environmental Quality*, *26*(4), 1038–1048.

Deckers, J. A., P. M. Driessen, F. O. Nachtergaele, and O. C. Spaargaren (2002), World reference base for soil resources, in *Encyclopedia of Soil Science*, pp. 1446–1451, Marcel Dekker, New York.

DeWalle, D. R., and H. B. Pionke (1994), Streamflow generation on a small agricultural catchment during autumn recharge: II. Stormflow periods, *Journal of Hydrology*, *163*(1–2), 23–42, doi:10.1016/0022-1694(94)90020-5.

Drury, C. F., W. I. Findlay, J. D. Gaynor, and D. J. McKenney (1993), Influence of tillage on nitrate loss in surface runoff and tile drainage, *Soil Science Society of America Journal*, *57*(3), 797–802.

Durand, P., and J. L. Juan Torres (1996), Solute transfer in agricultural catchments: the interest and limits of mixing models, *Journal of Hydrology*, *181*(1–4), 1–22, doi:10.1016/0022-1694(95)02922-2.

Eder, A., M. Exner-Kittridge, P. Strauss, and G. Blöschl (2014), Re-suspension of bed sediment in a small stream – results from two flushing experiments, *Hydrol. Earth Syst. Sci.*, *18*(3), 1043–1052, doi:10.5194/hess-18-1043-2014.

Ensign, S., and H. Paerl (2006), Development of an unattended estuarine nutrient monitoring program using ferries as data-collection platforms, *Limnology and Oceanography: Methods*, *4*, 399–405.

Everts, C. J., and R. S. Kanwar (1990), Estimating preferential flow to a subsurface drain with tracers, *Transactions of the ASAE*, *33*(2), 451.

Exner-Kittridge, M., R. Niederreiter, A. Eder, and M. Zessner (2013), A simple and flexible field-tested device for housing water monitoring sensors at point discharges, *Water Science & Technology*, *67*(5), 1026, doi:10.2166/wst.2013.655.

Exner-Kittridge, M., J. L. Salinas, and M. Zessner (2014), An evaluation of analytical stream to groundwater exchange models: a comparison of gross exchanges based on different spatial flow distribution assumptions, *Hydrol. Earth Syst. Sci.*, *18*(7), 2715–2734, doi:10.5194/hess-18-2715-2014.

Exner-Kittridge, M., P. Strauss, G. Blöschl, A. Eder, E. Saracevic, and M. Zessner (2016), The seasonal dynamics of the stream sources and input flow paths of water and nitrogen of an Austrian headwater agricultural catchment, *Science of The Total Environment*, *542, Part A*, 935–945, doi:10.1016/j.scitotenv.2015.10.151.

Food and Agriculture Organization of the United Nations (1998), *Crop evapotranspiration: guidelines for computing crop water requirements*, no. 56 in FAO irrigation and drainage paper, Food and Agriculture Organization of the United Nations, Rome.

Genereux, D. (1998), Quantifying uncertainty in tracer-based hydrograph separations, *Water Resources Research*, *34*(4), 915–919, doi:10.1029/98WR00010.

Geohring, L. D., P. E. Wright, and T. S. Steenhuis (1998), Preferential flow of liquid manure to subsurface drains, *Drainage in the 21st Century: Food Production and the Environment*, pp. 8–10.

Gonzales, A. L., J. Nonner, J. Heijkers, and S. Uhlenbrook (2009), Comparison of different base flow separation methods in a lowland catchment, *Hydrol. Earth Syst. Sci.*, *13*(11), 2055–2068, doi:10.5194/hess-13-2055-2009.

Gordon, R., R. Jamieson, V. Rodd, G. Patterson, and T. Harz (2001), Effects of surface manure application timing on ammonia volatilization, *Canadian Journal of Soil Science*, *81*(4), 525–533.

Grayson, R., and G. Blöschl (Eds.) (2001), *Spatial patterns in catchment hydrology: observations and modelling*, Cambridge University Press, Cambridge, U.K. ; New York.

Grimaldi, C., V. Viaud, F. Massa, L. Carteaux, S. Derosch, A. Regeard, Y. Fauvel, N. Gilliet, and F. Rouault (2004), Stream Nitrate Variations Explained by Ground Water Head Fluctuations in a Pyrite-Bearing Aquifer, *Journal of Environment Quality*, *33*(3), 994, doi:10.2134/jeq2004.0994.

Guinn Garrett, C., V. M. Vulava, T. J. Callahan, and M. L. Jones (2012), Groundwater–surface water interactions in a lowland watershed: source contribution to stream flow, *Hydrological Processes*, *26*(21), 3195–3206, doi:10.1002/hyp.8257.

Harmel, R., R. Cooper, R. Slade, R. Haney, and J. Arnold (2006), Cumulative uncertainty in measured streamflow and water quality data for small watersheds, *Transactions of the ASABE*, *49*(3), 689–701.

Harris, D. M., J. J. McDonnell, and A. Rodhe (1995), Hydrograph Separation Using Continuous Open System Isotope Mixing, *Water Resources Research*, *31*(1), 157–171, doi:10.1029/94WR01966.

Harvey, J., and K. Bencala (1993), The effect of streambed topography on surface-subsurface water exchange in mountain catchments, *Water Resources Research*, *29*(1), 89–98.

Harvey, J. W., and B. J. Wagner (2000), 1 - Quantifying Hydrologic Interactions between Streams and Their Subsurface Hyporheic Zones, in *Streams and Ground Waters*, edited by Jeremy B. Jones and Patrick J. Mulholland, pp. 3–44, Academic Press, San Diego.

Hinton, M. J., S. L. Schiff, and M. C. English (1994), Examining the contributions of glacial till water to storm runoff using two-and three-component hydrograph separations.

Hogan, J. F., and J. D. Blum (2003), Tracing hydrologic flow paths in a small forested watershed using variations in 87Sr/86Sr, [Ca]/[Sr], [Ba]/[Sr] and δ18O, *Water Resources Research*, *39*(10), 1282, doi:10.1029/2002WR001856.

Holloway, J. M., and R. A. Dahlgren (2001), Seasonal and event-scale variations in solute chemistry for four Sierra Nevada catchments, *Journal of Hydrology*, *250*(1–4), 106–121, doi:10.1016/S0022-1694(01)00424-3.

Hooper, R. P., B. T. Aulenbach, D. A. Burns, J. Mcdonnell, J. Freer, C. Kendall, and K. Beven (1998), Riparian control of stream-water chemistry : implications for hydrochemical basin models, in *IAHS-AISH publication*, pp. 451–458, International Association of Hydrological Sciences.

Huang, Y., B. P. Wilcox, L. Stern, and H. Perotto-Baldivieso (2006), Springs on rangelands: runoff dynamics and influence of woody plant cover, *Hydrological Processes*, *20*(15), 3277–3288, doi:10.1002/hyp.6332.

Hudak, P. F. (2004), *Principles of Hydrogeology, Third Edition*, CRC Press.

Huijsmans, J., J. Hol, and G. Vermeulen (2003), Effect of application method, manure characteristics, weather and field conditions on ammonia volatilization from manure applied to arable land, *Atmospheric Environment*, *37*(26), 3669–3680.

Iwagami, S., M. Tsujimura, Y. Onda, J. Shimada, and T. Tanaka (2010), Role of bedrock groundwater in the rainfall–runoff process in a small headwater catchment underlain by volcanic rock, *Hydrological Processes*, *24*(19), 2771–2783, doi:10.1002/hyp.7690.

James, A. L., and N. T. Roulet (2009), Antecedent moisture conditions and catchment morphology as controls on spatial patterns of runoff generation in small forest catchments, *Journal of Hydrology*, *377*(3–4), 351–366, doi:10.1016/j.jhydrol.2009.08.039.

Jaynes, D. B., S. I. Ahmed, K.-J. S. Kung, and R. S. Kanwar (2001), Temporal Dynamics of Preferential Flow to a Subsurface Drain, *Soil Science Society of America Journal*, *65*(5), 1368, doi:10.2136/sssaj2001.6551368x.

Kaelin, D., L. Rieger, J. Eugster, K. Rottermann, C. Bänninger, and H. Siegrist (2008), Potential of in-situ sensors with ion-selective electrodes for aeration control at wastewater treatment plants, *Water Science and Technology: A Journal of the International Association on Water Pollution Research*, *58*(3), 629–637, doi:10.2166/wst.2008.433.

Kalbus, E., F. Reinstorf, and M. Schirmer (2006), Measuring methods for groundwater – surface water interactions: a review, *Hydrol. Earth Syst. Sci.*, *10*(6), 873–887, doi:10.5194/hess-10-873-2006.

Kestel, S., M. Gray, and G. Lee (2010), Effect of Ionic Strength on Ion Selective Electrodes in the Activated Sludge Process, *Proceedings of the Water Environment Federation*, pp. 6955–6960, doi:10.2175/193864710798207134.

Kilpatrick, F. A., and E. D. Cobb (1985), *Measurement of discharge using tracers*, Department of the Interior, US Geological Survey.

Kim, H.-J., K. A. Sudduth, and J. W. Hummel (2009), Soil macronutrient sensing for precision agriculture, *J. Environ. Monit.*, *11*(10), 1810–1824, doi:10.1039/B906634A.

Klaus, J., and J. J. McDonnell (2013), Hydrograph separation using stable isotopes: Review and evaluation, *Journal of Hydrology*, *505*, 47–64, doi:10.1016/j.jhydrol.2013.09.006.

Ladouche, B., A. Probst, D. Viville, S. Idir, D. Baqué, M. Loubet, J. L. Probst, and T. Bariac (2001), Hydrograph separation using isotopic, chemical and hydrological approaches (Strengbach catchment, France), *Journal of Hydrology*, *242*(3–4), 255–274, doi:10.1016/S0022-1694(00)00391-7.

Laudon, H., and O. Slaymaker (1997), Hydrograph separation using stable isotopes, silica and electrical conductivity: an alpine example, *Journal of Hydrology*, *201*(1–4), 82–101, doi:10.1016/S0022-1694(97)00030-9.

Legnerová, Z., P. Solich, H. Sklenářová, D. Šatínský, and R. Karlíček (2002), Automated simultaneous monitoring of nitrate and nitrite in surface water by sequential injection analysis, *Water Research*, *36*(11), 2777–2783.

Liu, F., M. W. Williams, and N. Caine (2004), Source waters and flow paths in an alpine catchment, Colorado Front Range, United States, *Water Resources Research*, *40*(9), W09,401, doi:10.1029/2004WR003076.

Lowry, C. S., J. F. Walker, R. J. Hunt, and M. P. Anderson (2007), Identifying spatial variability of groundwater discharge in a wetland stream using a distributed temperature sensor, *Water Resources Research*, *43*(10), doi:10.1029/2007WR006145.

Macrae, M. L., M. C. English, S. L. Schiff, and M. Stone (2007), Capturing temporal variability for estimates of annual hydrochemical export from a first-order agricultural catchment in southern Ontario, Canada, *Hydrological processes*, *21*(13), 1651–1663.

Malard, F., K. Tockner, M.-J. DOLE-OLIVIER, and J. V. Ward (2002), A landscape perspective of surface–subsurface hydrological exchanges in river corridors, *Freshwater Biology*, *47*(4), 621–640.

Martin, C., L. Aquilina, C. Gascuel-Odoux, J. Molénat, M. Faucheux, and L. Ruiz (2004), Seasonal and interannual variations of nitrate and chloride in stream waters related to spatial and temporal patterns of groundwater concentrations in agricultural catchments, *Hydrological Processes*, *18*(7), 1237–1254, doi:10.1002/hyp.1395.

McCallum, J. L., P. G. Cook, P. Brunner, and D. Berhane (2010), Solute dynamics during bank storage flows and implications for chemical base flow separation, *Water Resources Research*, *46*(7), W07,541, doi:10.1029/2009WR008539.

McCartney, M. P., C. Neal, and M. Neal (1998), Use of deuterium to understand runoff generation in a headwater catchment containing a dambo, *Hydrol. Earth Syst. Sci.*, *2*(1), 65–76, doi:10.5194/hess-2-65-1998.

McDonnell, J. J. (1990), A rationale for old water discharge through macropores in a steep, humid catchment, *Water Resour. Res*, *26*(11), 2821–2832.

McGlynn, B. L., and J. J. McDonnell (2003), Quantifying the relative contributions of riparian and hillslope zones to catchment runoff, *Water Resources Research*, *39*(11), 1310, doi:10.1029/2003WR002091.

Merz, R., and G. Blöschl (2007), Saisonalität von Niederschlag und Abfluss, Karte 5.3, Hydrologischer Atlas Österreich. Österreichischer Kunst und Kulturverlag und Bundesministerium für Land-und Forstwirtschaft, *Umwelt und Wasserwirtschaft, Wien.*

Misselbrook, T., M. Sutton, and D. Scholefield (2004), A simple process-based model for estimating ammonia emissions from agricultural land after fertilizer applications, *Soil Use and Management*, *20*(4), 365–372.

Mkhabela, M., R. Gordon, D. Burton, E. Smith, and A. Madani (2009), The impact of management practices and meteorological conditions on ammonia and nitrous oxide emissions following application of hog slurry to forage grass in Nova Scotia, *Agriculture, Ecosystems and Environment*, *130*(1-2), 41–49.

Moal, J.-F., J. Martinez, F. Guiziou, and C.-M. Coste (1995), Ammonia volatilization following surface-applied pig and cattle slurry in France, *The Journal of Agricultural Science*, *125*(02), 245–252, doi:10.1017/S0021859600084380.

Molenat, J., C. Gascuel-Odoux, L. Ruiz, and G. Gruau (2008), Role of water table dynamics on stream nitrate export and concentration in agricultural headwater catchment (France), *Journal of Hydrology*, *348*(3–4), 363–378, doi:10.1016/j.jhydrol.2007.10.005.

Muñoz-Villers, L. E., and J. J. McDonnell (2012), Runoff generation in a steep, tropical montane cloud forest catchment on permeable volcanic substrate, *Water Resources Research*, *48*(9), W09,528, doi:10.1029/2011WR011316.

Mulholland, P. J., A. M. Helton, G. C. Poole, R. O. Hall, S. K. Hamilton, B. J. Peterson, J. L. Tank, L. R. Ashkenas, L. W. Cooper, C. N. Dahm, W. K. Dodds, S. E. G. Findlay, S. V. Gregory, N. B. Grimm, S. L. Johnson, W. H. McDowell, J. L. Meyer, H. M. Valett, J. R. Webster, C. P. Arango, J. J. Beaulieu, M. J. Bernot, A. J. Burgin, C. L. Crenshaw, L. T. Johnson, B. R. Niederlehner, J. M. O'Brien, J. D. Potter, R. W. Sheibley, D. J. Sobota, and S. M. Thomas (2008), Stream denitrification across biomes and its response to anthropogenic nitrate loading, *Nature*, *452*(7184), 202–205, doi:10.1038/nature06686.

Mwakanyamale, K., L. Slater, F. Day-Lewis, M. Elwaseif, and C. Johnson (2012), Spatially variable stage-driven groundwater-surface water interaction inferred from time-frequency analysis of distributed temperature sensing data, *Geophysical Research Letters*, *39*(6), n/a–n/a, doi:10.1029/2011GL050824.

Newman, I. A. (2001), Ion transport in roots: measurement of fluxes using ion-selective microelectrodes to characterize transporter function, *Plant, Cell & Environment*, *24*(1), 1–14, doi:10.1046/j.1365-3040.2001.00661.x.

Obradovic, M. M., and M. G. Sklash (1986), An isotopic and geochemical study of snowmelt runoff in a small arctic watershed, *Hydrological Processes*, *1*(1), 15–30, doi:10.1002/hyp.3360010104.

Ocampo, C. J., M. Sivapalan, and C. E. Oldham (2006), Field exploration of coupled hydrological and biogeochemical catchment responses and a unifying perceptual model, *Advances in Water Resources*, *29*(2), 161–180, doi:10.1016/j.advwatres.2005.02.014.

Padilla, I. Y., T.-C. J. Yeh, and M. H. Conklin (1999), The effect of water content on solute transport in unsaturated porous media, *Water Resources Research*, *35*(11), 3303–3313, doi:10.1029/1999WR900171.

Payn, R. A., M. N. Gooseff, D. A. Benson, O. A. Cirpka, J. P. Zarnetske, W. B. Bowden, J. P. McNamara, and J. H. Bradford (2008), Comparison of instantaneous and constant-rate stream tracer experiments through non-parametric analysis of residence time distributions, *Water Resources Research*, *44*(6), n/a–n/a, doi:10.1029/2007WR006274.

Payn, R. A., M. N. Gooseff, B. L. McGlynn, K. E. Bencala, and S. M. Wondzell (2009), Channel water balance and exchange with subsurface flow along a mountain headwater stream in Montana, United States, *Water Resources Research*, *45*(11), doi:10.1029/2008WR007644.

Pearce, A. J., M. K. Stewart, and M. G. Sklash (1986), Storm Runoff Generation in Humid Headwater Catchments: 1. Where Does the Water Come From?, *Water Resources Research*, *22*(8), 1263–1272, doi:10.1029/WR022i008p01263.

Pellerin, B. A., W. M. Wollheim, X. Feng, and C. J. Vörösmarty (2008), The application of electrical conductivity as a tracer for hydrograph separation in urban catchments, *Hydrological Processes*, *22*(12), 1810–1818, doi:10.1002/hyp.6786.

Peterson, B. J., W. M. Wollheim, P. J. Mulholland, J. R. Webster, J. L. Meyer, J. L. Tank, E. Martí, W. B. Bowden, H. M. Valett, A. E. Hershey, and others (2001), Control of nitrogen export from watersheds by headwater streams, *Science*, *292*(5514), 86–90.

Pionke, H. B., W. J. Gburek, R. R. Schnabel, A. N. Sharpley, and G. F. Elwinger (1999), Seasonal flow, nutrient concentrations and loading patterns in stream flow draining an agricultural hill-land watershed, *Journal of Hydrology*, *220*(1–2), 62–73, doi:10.1016/S0022-1694(99)00064-5.

Preston, S. D., V. J. Bierman, and S. E. Silliman (1989), An evaluation of methods for the estimation of tributary mass loads, *Water Resources Research*, *25*(6), 1379–1389, doi:10.1029/WR025i006p01379.

R Development Core Team (2011), R: A Language and Environment for Statistical Computing.

Rice, K. C., and G. M. Hornberger (1998), Comparison of hydrochemical tracers to estimate source contributions to peak flow in a small, forested, headwater catchment, *Water Resources Research*, *34*(7), 1755–1766, doi:10.1029/98WR00917.

Rieckermann, J., M. Borsuk, P. Reichert, and W. Gujer (2005), A novel tracer method for estimating sewer exfiltration, *Water Resources Research*, *41*(5), W05,013, doi:10.1029/2004WR003699.

Rieckermann, J., V. Bareš, O. Kracht, D. Braun, and W. Gujer (2007), Estimating sewer leakage from continuous tracer experiments, *Water Research*, *41*(9), 1960–1972, doi:10.1016/j.watres.2007.01.024.

Romstad, E., J. Simonsen, and A. Vatn (1997), *Controlling Mineral Emissions in European Agriculture; Economics, Policies and the Environment*, CAB International, Wallingford.

Roser, D., J. Skinner, C. LeMaitre, L. Marshall, J. Baldwin, K. Billington, S. Kotz, K. Clarkson, and N. Ashbolt (2002), Automated event sampling for microbiological and related analytes in remote sites: a comprehensive system, *Water science and technology: water supply*, *2*(3), 123–130.

Ruehl, C., A. Fisher, C. Hatch, M. L. Huertos, G. Stemler, and C. Shennan (2006), Differential gauging and tracer tests resolve seepage fluxes in a strongly-losing stream, *Journal of Hydrology*, *330*(1–2), 235–248, doi:10.1016/j.jhydrol.2006.03.025.

Runkel, R. L. (1998), *One-dimensional transport with inflow and storage (OTIS): A solute transport model for streams and rivers*, US Department of the Interior, US Geological Survey.

Scanlon, B. R., R. W. Healy, and P. G. Cook (2002), Choosing appropriate techniques for quantifying groundwater recharge, *Hydrogeology Journal*, *10*(2), 347–347, doi:10.1007/s10040-002-0200-1.

Schilling, K. E., and M. Helmers (2008), Tile drainage as karst: Conduit flow and diffuse flow in a tile-drained watershed, *Journal of Hydrology*, *349*(3–4), 291–301, doi:10.1016/j.jhydrol.2007.11.014.

Schmidt, C., M. Bayer-Raich, and M. Schirmer (2006), Characterization of spatial heterogeneity of groundwater-stream water interactions using multiple depth streambed temperature measurements at the reach scale, *Hydrology and Earth System Sciences Discussions*, *10*(6), 849–859.

Segura, C., A. L. James, D. Lazzati, and N. T. Roulet (2012), Scaling relationships for event water contributions and transit times in small-forested catchments in Eastern Quebec, *Water Resources Research*, *48*(7), W07,502, doi:10.1029/2012WR011890.

Shaw, E. M. (Ed.) (2011), *Hydrology in practice*, 4th ed ed., Spon, London ; New York.

Slater, L. D., D. Ntarlagiannis, F. D. Day-Lewis, K. Mwakanyamale, R. J. Versteeg, A. Ward, C. Strickland, C. D. Johnson, and J. W. Lane (2010), Use of electrical imaging and distributed temperature sensing methods to characterize surface water–groundwater exchange regulating uranium transport at the Hanford 300 Area, Washington, *Water Resources Research*, *46*(10), n/a–n/a, doi:10.1029/2010WR009110.

Soulsby, C., J. Petry, M. J. Brewer, S. M. Dunn, B. Ott, and I. A. Malcolm (2003), Identifying and assessing uncertainty in hydrological pathways: a novel approach to end member mixing in a Scottish agricultural catchment, *Journal of Hydrology*, *274*(1–4), 109–128, doi:10.1016/S0022-1694(02)00398-0.

Stenholm, Å., E. Eriksson, O. Lind, and B. Wigilius (2008), Comparison of continuous flow analysis including photometric detection and ion-selective electrode potentiometry for the measurement of ammonium nitrogen in wastewater, *International Journal of Environmental Analytical Chemistry*, *88*(3), 165–176, doi:10.1080/03067310701627777.

Stone, W. W., and J. T. Wilson (2006), Preferential flow estimates to an agricultural tile drain with implications for glyphosate transport, *Journal of Environmental Quality*, *35*(5), 1825–1835.

Szeftel, P., R. (Dan) Moore, and M. Weiler (2011), Influence of distributed flow losses and gains on the estimation of transient storage parameters from stream tracer experiments, *Journal of Hydrology*, *396*(3–4), 277–291, doi:10.1016/j.jhydrol.2010.11.018.

Tan, C. S., C. F. Drury, M. Soultani, I. J. Van Wesenbeeck, H. Y. F. Ng, J. D. Gaynor, and T. W. Welacky (1998), Effect of controlled drainage and tillage on soil structure and tile drainage nitrate loss at the field scale, *Water Science and Technology*, *38*(4), 103–110.

Tan, C. S., C. F. Drury, W. D. Reynolds, P. H. Groenevelt, and H. Dadfar (2002a), Water and nitrate loss through tiles under a clay loam soil in Ontario after 42 years of consistent fertilization and crop rotation, *Agriculture, ecosystems & environment*, *93*(1), 121–130.

Tan, C. S., C. F. Drury, J. D. Gaynor, T. W. Welacky, and W. D. Reynolds (2002b), Effect of tillage and water table control on evapotranspiration, surface runoff, tile drainage and soil water content under maize on a clay loam soil, *Agricultural Water Management*, *54*(3), 173–188, doi:10.1016/S0378-3774(01)00178-0.

Uhlenbrook, S., and S. Hoeg (2003), Quantifying uncertainties in tracer-based hydrograph separations: a case study for two-, three- and five-component hydrograph separations in a mountainous catchment, *Hydrological Processes*, *17*(2), 431–453, doi:10.1002/hyp.1134.

Waddington, J. M., N. T. Roulet, and A. R. Hill (1993), Runoff mechanisms in a forested groundwater discharge wetland, *Journal of Hydrology*, *147*(1), 37–60, doi:10.1016/0022-1694(93)90074-J.

Wagner, B. J., and J. W. Harvey (1997), Experimental design for estimating parameters of rate-limited mass transfer: Analysis of stream tracer studies, *Water Resources Research*, *33*(7), 1731–1741, doi:10.1029/97WR01067.

Walling, D., M. Russell, R. Hodgkinson, and Y. Zhang (2002), Establishing sediment budgets for two small lowland agricultural catchments in the UK, *Catena*, *47*(4), 323–353.

Ward, A. S., R. A. Payn, M. N. Gooseff, B. L. McGlynn, K. E. Bencala, C. A. Kelleher, S. M. Wondzell, and T. Wagener (2013), Variations in surface water-ground water interactions along a headwater mountain stream: Comparisons between transient storage and water balance analyses, *Water Resources Research*, *49*(6), 3359–3374, doi:10.1002/wrcr.20148.

Wendland, M., M. Diepolder, and P. Capriel (2011), *Leitfaden für die Düngung von Acker-und Grünland*, Bayerische Landesanst. für Bodenkultur und Pflanzenbau.

Westhoff, M. C., H. H. G. Savenije, W. M. J. . Luxemburg, G. S. Stelling, N. C. van de Giesen, J. S. Selker, L. Pfister, and S. Uhlenbrook (2007a), A distributed stream temperature model using high resolution temperature observations, *Hydrology and Earth System Sciences*, *11*(4), 1469–1480, doi:10.5194/hess-11-1469-2007.

Westhoff, M. C., H. H. G. Savenije, W. M. J. . Luxemburg, G. S. Stelling, N. C. van de Giesen, J. S. Selker, L. Pfister, and S. Uhlenbrook (2007b), A distributed stream temperature model using high resolution temperature observations, *Hydrology and Earth System Sciences*, *11*(4), 1469–1480, doi:10.5194/hess-11-1469-2007.

Winter, T. C. (1998), *Ground water and surface water: a single resource*, no. 1139 in U.S. Geological Survey circular, U.S. Geological Survey, Denver, Colo.

Wondzell, S. M. (2005), Effect of morphology and discharge on hyporheic exchange flows in two small streams in the Cascade Mountains of Oregon, USA, *Hydrological Processes*, *20*(2), 267–287.

Workshop, S. S. (1990), Concepts and Methods for Assessing Solute Dynamics in Stream Ecosystems, *Journal of the North American Benthological Society*, *9*(2), 95–119, doi:10.2307/1467445.

Zellweger, G. W., R. J. Avanzino, and K. E. Bencala (1989), *Comparison of tracer-dilution and current-meter discharge measurements in a small gravel-bed stream, Little Lost Man Creek, California*, Department of the Interior, US Geological Survey.

Appendix A

Derivation of the inflowing groundwater concentration (C_{gain}) from stream tracer tests

The derivation of C_{gain}, the tracer concentration of the inflowing groundwater, is different than that of the SGE equations. The derivation of C_{gain} is actually more similar to the initial derivation from the conceptual model starting from Eq. (3.40) in Sect. 3.5.2. Figure 3.11 represents this conceptual model quite well. The exception to Fig. 3.11 is that for the derivation of C_{gain} we are not interested in end-members above Q_{up}. Consequently, the location of Q_{up} becomes the upper end-member and the mass balance for total Q_{loss} becomes:

$$Q_{loss} = Q_{loss,up} + Q_{loss,GW} \tag{A.1}$$

and

$$Q_{loss}C_{loss} = Q_{loss,up}C_{up} + Q_{loss,GW}C_{gain} \tag{A.2}$$

where $Q_{loss,up}$ is the loss of water from the stream reach specifically from the original upstream water, $Q_{loss,GW}$ is the loss of water from the stream reach specifically from the inflowing groundwater, and C_{gain} is the groundwater concentration of the tracer (denoted C_{GW} in Sect. 3.5.2).

As we are only interested in C_{gain} and not the gross gains and losses for this derivation, we can collect the gross groundwater terms together as net groundwater similarly to Eq. (3.40). We get the following mass balance equations by including Eq. (A.2) with Eq. (3.1) and Eq. (A.1) with Eq. (3.2):

$$\begin{aligned} & Q_{up}C_{up} + (Q_{gain,GW} - Q_{loss,GW})C_{gain} = \\ = \; & Q_{down}C_{down} + Q_{loss,up}C_{up} \end{aligned} \tag{A.3}$$

and

$$Q_{gain,GW} - Q_{loss,GW} = Q_{down} - Q_{up} + Q_{loss,up} \tag{A.4}$$

With these two equation alone, we cannot solve for C_{gain} as we still have too many unknown variables. A stream tracer test with a conservative tracer (e.g. chloride salt) will provide us with the additional equation. As described in the paragraph prior to Eq. (3.26), the required assumptions are $Q_{gain,GW} > 0$ and that quasi-steady-state conditions apply before and after the tracer injection when the water samples are taken. By measuring the tracer concentrations before and after the tracer injection, we can form two distinct equations from Eq. (A.3):

$$\begin{aligned} & Q_{up}C_{up,prior} + (Q_{gain,GW} - Q_{loss,GW})C_{gain} = \\ = \;& Q_{down}C_{down,prior} + Q_{loss,up}C_{up,prior} \end{aligned} \tag{A.5}$$

$$\begin{aligned} & Q_{up}C_{up,post} + (Q_{gain,GW} - Q_{loss,GW})C_{gain} = \\ = \;& Q_{down}C_{down,post} + Q_{loss,up}C_{up,post} \end{aligned} \tag{A.6}$$

where the notation of the before and after tracer injection concentrations is the same to that of Eq. (3.27). Combining Eqs. (A.4), (A.5), and (A.6) and solving for C_{gain}, we get the final result:

$$C_{gain} = \frac{C_{up,prior}C_{down,post} - C_{down,prior}C_{up,post}}{C_{up,prior} - C_{up,post} - C_{down,prior} + C_{down,post}} \tag{A.7}$$

As mentioned earlier in this appendix section, Eq. (A.7) does not require a spatial distribution assumption to derive the equation and consequently can be applied with any of the SGE methods listed in this manuscript.

To solve for C_{gain}, we took one stream reach with two different states in time. These two states of the same stream reach allowed the creation of two equations from Eq. (A.2), because several concentration variables changed significantly due to the tracer injection. Instead of taking the same stream reach at different time states, we can also take two adjacent stream reaches under the same time state to create two equations from Eq. (A.2) if we can assume that the two adjacent stream reaches have the same C_{gain}. Each of the two adjacent stream reaches would have an equation and the derivation would be similar to that for Eq. (A.7). Although this is possible conceptually and mathematically, in practice the result may prove to be highly uncertain as the differences in the concentration values in the adjacent reaches may be very similar. This is the advantage of the tracer injection procedure described above. The larger the difference between the background concentration of the tracer in the stream and the tracer concentration in the stream due to the tracer injection will increase the accuracy of the estimate of C_{gain}.

Appendix B

Additional methods associated with the SGE methods

Although the following methods were not used directly in this study, they can provide useful complementary information for SGE studies.

There might be a need to estimate the groundwater concentration of other chemical solutes entering the stream in addition to the conservative tracer used to estimate the SGE. If other in-stream gains and losses in the new chemical solute can be neglected (e.g. without biochemical transformations), the only additional information needed would be the concentration of the new compound at the locations of Q_{up} and Q_{down}. The C_{gain} of the new chemical solute can be estimated using the following rearrangement of Eq. (3.21):

$$C_{gain,new} = \frac{(\frac{Q_{down}}{Q_{up}})^{(\frac{Q_{gain,Sim}}{Q_{up}-Q_{down}})} C_{up,new} - C_{down,new}}{(\frac{Q_{down}}{Q_{up}})^{(\frac{Q_{gain,Sim}}{Q_{up}-Q_{down}})} - 1} \tag{B.1}$$

where $C_{gain,new}$ is the concentration of the new solute entering the stream from the groundwater, $C_{up,new}$ is the upstream concentration of the new solute, and $C_{down,new}$ is the downstream concentration of the new solute. Any of the three SGE methods can be rearranged to calculate $C_{gain,new}$ and they will all produce the same result.

Following on the same spatial flow distribution assumption as the SIM method, an additional mass removal rate can be integrated to potentially represent a relevant physical, chemical, or biological process (e.g. ammonia removal by microorganisms). The assumptions are simultaneous and uniform losses throughout the stream reach and stationary in time. The derivation would require a mass removal term per unit stream length n_{rem} to be added to the right side of Eq. (3.14):

$$\begin{aligned} & \dot{m}(x) + C_{gain} q_{gain} dx = \\ = \quad & \left(\dot{m}(x) + \frac{\partial \dot{m}(x)}{\partial x} dx\right) + C(x) q_{loss} dx + n_{rem} dx \end{aligned} \tag{B.2}$$

The derivation would follow similarly to that of the SIM method derivation, and the final result solving for Q_{gain} is the following:

$$Q_{gain,Sim} = (Q_{up} - Q_{down}) \frac{ln[\frac{C_{down} - C_{gain} - \frac{N_{rem}}{Q_{gain,Sim}}}{C_{up} - C_{gain} - \frac{N_{rem}}{Q_{gain,Sim}}}]}{ln[\frac{Q_{down}}{Q_{up}}]} \tag{B.3}$$

where N_{rem} is the total mass removal (mass per time) within the stream reach and C_{up}, C_{down}, and C_{gain} in this case would be solute concentrations associated with N_{rem} (i.e ammonia concentrations for ammonia mass removal). Solving for N_{rem}, we get the following:

$$N_{rem} = \frac{Q_{gain,Sim}}{1 - D_{dis}} [D_{dis}(C_{up} - C_{gain}) - C_{down} + C_{gain}] \tag{B.4}$$

with

$$D_{dis} = e^{\frac{Q_{gain,Sim}}{Q_{up} - Q_{down}} ln[\frac{Q_{down}}{Q_{up}}]} \tag{B.5}$$

$Q_{gain,Sim}$ would need to be estimated from Eq. (3.21) using a conservative tracer. C_{gain} could again be estimated using Eq. (B.1) if we can safely assume that mass removal rates do not change over time before and after the tracer injection of the new solute. The key assumption limitation in this conceptual model is that over the short period of time of the solute tracer application the removal rate is not dependent on changes in concentration, which is certainly not true for many processes over long periods of time and also may not be true over short periods of time for certain processes. Although other mass removal models may be a more realistic assumption in many cases (e.g. Michaelis-Menten kinetics, first order removal, etc.), C_{gain} could not be estimated from Eq. (B.1) using other more complicated assumptions and furthermore would require more measurements and/or parameter estimation techniques to include the additional necessary terms (*Workshop*, 1990). A thorough analysis on the analytical derivations of solute dynamics in stream ecosystems including first order and non-linear removal can be found in *Workshop* (1990).

Appendix C

Authorship

Chapter 2 of this thesis is based on the publication "A simple and flexible field-tested device for housing water monitoring sensors at point discharges" by Michael Exner-Kittridge, Richard Niederreiter, Alexander Eder, and Matthias Zessner (*Exner-Kittridge et al.*, 2013).
The contribution of Michael Exner-Kittridge to this paper was:

- Literature review
- Concept development
- Device design
- Device testing
- Data collection
- Data analyses and summaries
- Results interpretation
- Figure and table creation
- Paper writing

Chapter 3 of this thesis is based on the publication "An evaluation of analytical stream to groundwater exchange models: a comparison of gross exchanges based on different spatial flow distribution assumptions" by Michael Exner-Kittridge, Jose Luis Salinas, and Matthias Zessner (*Exner-Kittridge et al.*, 2014).
The contribution of Michael Exner-Kittridge to this paper was:

- Literature review
- Concept development
- Simulation model development

- Data analyses and summaries
- Results interpretation
- Figure and table creation
- Paper writing

Chapter 4 of this thesis is based on the publication "The seasonal dynamics of the stream sources and input flowpaths of water and nitrogen of an Austrian headwater agricultural catchment" by Michael Exner-Kittridge, Peter Strauss, Günter Blöschl, Alexander Eder, Ernis Saracevic, and Matthias Zessner (*Exner-Kittridge et al.*, 2016).
The contribution of Michael Exner-Kittridge to this paper was:

- Literature review
- Concept development
- Data collection
- Data analyses and summaries
- Results interpretation
- Figure and table creation
- Paper writing

Chapter 5 of this thesis is based on the publication "The source and flowpath contribution dynamics of runoff events in an Austrian headwater agricultural catchment" by Michael Exner-Kittridge, Günter Blöschl, Alexander Eder, Peter Strauss, and Matthias Zessner. Submitted to Water Resources Research journal.
The contribution of Michael Exner-Kittridge to this paper was:

- Literature review
- Concept development
- Data collection
- Data analyses and summaries
- Results interpretation
- Figure and table creation
- Paper writing